GENETIC BACKGROUND EFFECTS

ELUCIDATING THE MECHANISMS UNDERLYING GENETIC BACKGROUND EFFECTS UTILZING *DROSOPHILA MELANOGASTER* WING TISSUE

By

BRANDON MCINTYRE, B.Sc. (Hons)

A Thesis Submitted to the School of Graduate Studies in Partial Fulfillment of the Requirements for the Degree Master of Science

Descriptive Note

McMaster University   MASTER OF SCIENCE (2023)

Hamilton, Ontario   (Biology)

TITLE: Elucidating the Mechanisms Underlying Genetic Background Effects
                    Utilizing *Drosophila melanogaster* Wing Tissue

AUTHOR: Brandon McIntyre B.Sc. (Hons) (Brock University)

SUPERVISOR: Dr. I. Dworkin

PAGES: i-xiv, 1-115

Lay Abstract

When investigating the roles of genes on phenotype it may seem intuitive that a mutation affecting gene function would display a consistent change in phenotype. Increasing evidence has asserted that this may not always be the case and genetic background effects may affect the genotype-phenotype relationship affecting experimental design, disease treatment and evolutionary trajectories. Here, we investigate the mechanisms involved in these genetic background effects utilizing *Drosophila melanogaster* wing tissue. We outline a change from the typically observed non-linear relationship between genotype and phenotype and for the first time quantify shape change effects by the *miniature* mutation.

Abstract

When investigating the developmental roles of genes on phenotypic expression it may seem reasonable to assume that a mutation would result in consistent phenotypic change. However, increasing evidence has shown this is not often the case, and the "wild-type" genetic background of an individual plays a large role in phenotypic expression of mutations and severity of genetic mediated diseases. Previous work has demonstrated that degree of genetic background effects shows a non-linear relationship with severity of mutational effects. This relationship is characterized by alleles of moderate phenotypic expressivity showing the relatively greatest degree of background dependence and between genotype variability in comparison with alleles of severe and modest phenotypic expressivity. Our previous work has shown this relationship for *Drosophila melanogaster* wing size through a *scalloped* (*sd*) allelic series crossed to naturally derived strains from the Drosophila Genetics Reference Panel (DGRP). I explored these effects with a *miniature* (*m*) allelic series where the results from our experiment suggest a vastly different response. *m* when compared to *sd* is characterized by a more linear relationship, whereby alleles of moderate phenotypic effect do not show increased background dependence nor increased variability within and between strains. Furthermore, our results suggest a strong correlation across DGRP strains with respect to *m* mutational severity and that the effect *m* has on wing shape is not largely due to wing size. Our working hypotheses for why this might be occurring is due to the increased interaction of *sd* with other aspects of wing development relative to that of *m*, the differences in when the genes are playing active roles in wing development, or the effects the mutations have on the wing to affect size. To add to our previous results employing *sd*, I am beginning to elucidate the non-linear relationship of genetic background effects with severity of mutational effects at a gene expression level. I am

accomplishing this through crossing a *sd* allelic series to six naturally derived DGRP strains used in previous experiments involving wing size. Preliminary results agree with previous work on genetic background effects, displaying a non-linear relationship with the severity of mutational effect. I aim to continue to explore this relationship including more genotypes and investigating more genes to better elucidate the mechanistic causes of genetic background effects.

<u>Acknowledgements</u>

I would like to begin by thanking my mentor and supervisor Dr. Ian Dworkin for his patience, support, encouragement, and motivation to push me to become both a better scientist and individual. The opportunity he has provided me to grow as an individual and the memories created doing so have brought a sense of fulfillment and pride which I will look back on my time at McMaster with fondness. I would like to thank my supervisory committee members Dr. Roger Jacobs and Dr. Lesley MacNeil for their insightful perspectives, welcoming demeanor, and beneficial suggestions.

Thank you to my fellow lab members Tyler Audet, Amanda Neves, Katie Pelletier, and Arteen Torabi-Marashi for their support, camaraderie, and suggestions. Thank you to Francesco Ruso who assisted in shape data collection, Meera Chopra who assisted in sample collection and imaging, Yun Bo Xi who assisted in sample collection, and Richard Saint-Laurent who assisted in sample collection, data collection, and data analysis.

Finally, I would like to thank my family Donald, Tammy, and Alyssa McIntyre who's support, love, and encouragement would not have allowed me to complete this degree. I would like to thank my friends; both old and new, who have stood by my side throughout this degree. Ronnie and her family for the encouragement, love, and support especially in the final stretch of this degree. My work and immediate supervisors for understanding when I needed days off to complete an experiment that ran late. I would not have been able to complete this research without the immense amount of support of everyone around me.

Table of Contents

List of Figures

List of Tables

List of Equations

Declaration of Academic Achievement

I declare that this thesis titled "Elucidating the Mechanisms Underlying Genetic Background Effects Utilizing *Drosophila melanogaster* Wing Tissue" is a bonafide record of research work done by me under the supervision of Dr. Ian Dworkin, Professor of Biology, McMaster University, Canada. I further declare that this thesis has not previously formed the bases of the award of a degree, diploma, associateship, fellowship, or other similar title of recognition. I declare Dr. Ian Dworkin assisted greatly in data analysis, Francesco Ruso assisted greatly in shape data collection, Meera Chopra assisted in sample collection and imaging, Yun Bo Xi assisted in sample collection, and Richard Saint-Laurent assisted in sample collection, data collection, and data analysis.

1. <u>Introduction</u>

1.1 Genetic Background Effects

Considerable effort has been placed in elucidating genetic pathways influencing trait expression in a variety of model organisms. While building this understanding, strict control of an organisms' wild-type genetic background through use of isogenic (or near isogenic) strains is necessary to avoid inferences from confounding variables. While powerful in its ability to identify genetic mechanisms governing many biological processes, it may provide incomplete or potentially even incorrect inferences, as no pathway operates in a void (Chandler et al., 2014). These pathways operate in the context of all the genes in a genome which typically varies on an individual level. Evidence has demonstrated that the influence of varying wild-type genetic backgrounds influences the phenotypic outcomes of mutations across many taxa, including yeast, worms flies, mice and humans (Chandler et al., 2013, 2017; Chen et al., 2016; De Belle & Heisenberg, 1996; Dorman et al., 2016; Dowell et al., 2010; Dworkin et al., 2009; Kammenga, 2017; Montagutelli, 2000; Mullis et al., 2018; Percival et al., 2017; Vu et al., 2015; Yoshiki & Moriwaki, 2006). This influence on phenotypic outcome, described as genetic background effects, can be defined as "the genotype at all other genes that may interact with the gene of interest, and therefore potentially influence the specific phenotype" (Yoshiki & Moriwaki, 2006). These genetic background effects are typically thought of and represent higher order epistatic genetic interactions between the effects of a focal allele of interest (the direct target of study), and alleles throughout the rest of the genome, that modify the effect of the focal allele of interest. One example of these epistatic interactions is the non-additive interaction between the *doc* allele with *miniature* and *dumpy* alleles in *Drosophila melanogaster* leading to enhanced phenotypes generated from mutations in both alleles (Kandasamy et al., 2021). Another example of these higher order epistatic interactions is the presence of shadow enhancers throughout the genome of

organisms which are redundant remote *cis*-regulatory elements that control gene expression patterns and levels of specific genes alongside a more proximal primary enhancer (Frankel et al., 2010; Hong et al., 2008). These higher order interactions were found to influence *ultrabithorax (ubx)* activity resulting highly variable expression of *ubx* alleles as well as enhancer silencing that depended on the genetic background (Crickmore et al., 2009). A final example of these interactions can be observed through the cooperative binding of different transcription factors (Domingo et al., 2019). This cooperative binding can lead to the activity of one transcription factor, compensating or interacting with other transcription factors on the same gene of interest, influencing phenotypic outcomes. An example of this can be observed with Hepatocyte nuclear factor 1α and Hepatocyte nuclear factor 4α synergistically binding to many of the same genes, with their synergistic effects differing on a gene by gene basis (Boj et al., 2010; Domingo et al., 2019).

The result of such higher-order genetic interactions is a change in phenotype, which manifests in a variety of ways including changes in penetrance, expressivity, dominance, and pleiotropy each affecting how we interpret genotype-phenotype relationships (Nadeau, 2001). One example of genetic background effects influencing phenotypic outcomes can be observed in *D. melanogaster* in a study by Dworkin and Gibson (2006). In this study the authors examined the roles of genes in the epidermal growth factor (EGFR), transforming growth factor-β, and hedgehog signaling pathways on wing shape in two laboratory backgrounds, Oregon-R (ORE) and Samarkand (SAM) (Dworkin & Gibson, 2006). The authors found significant differences of mutation expressivity in wing shape between the two backgrounds, of which the mutation for $scalloped^{E3}$ was particularly divergent, resulting in further study (Dworkin et al., 2009; Dworkin & Gibson, 2006). A second example of genetic background effects can be observed in a

study involving *deaf waddler (dfw)* (Street et al., 1995)*. dfw* is a neuroepithelial recessive

mutation in mice, that phenotypically presents with hesitant wobbly gait, head bobbing, and

deafness in homozygotes (Street et al., 1995). This trait is typically recessive, but in the

BALB/cBy "wild-type" mouse strain, heterozygotes for the dfw^{2J} mutation presents with

hearing loss. However, in the CAST/Eij wild-type genetic background, the same heterozygotes

do not present with hearing loss, representing a change in dominance due to genetic background

effects (Noben-Trauth et al., 1997). A third example of genetic background effects can be seen

by changes of pleiotropy with the *mushroom body miniature (mbm)* gene (De Belle &

Heisenberg, 1996). *mbm* affects *D. melanogaster* brain structure and olfactory learning in the

original *mbm* strain (De Belle & Heisenberg, 1996). However, when the same mutations in *mbm*

were introduced into a separate Canton Special (CS) wild-type strain, the mutant effects on brain

structure were rescued, while the effects on odorant learning remained (De Belle & Heisenberg,

1996). A final example of genetic background effects can be observed in a study on Mendelian

disorders (monogenic diseases or diseases assumed to be controlled by a single locus) in humans;

where researchers screened 874 defined highly penetrant, early onset, disease-causing genes in

589 306 genomes and discovered 13 adults with mutations for 8 severe mendelian conditions

with no reported clinical symptoms (Chen et al., 2016; Kammenga, 2017). This study

exemplifies changes in penetrance of monogenic disorders due to genetic background effects.

Though examples of genetic background effects are abundant the question of how these

alleles function as modifiers and how commonplace they are in natural populations is not well

understood. In a study by Mullis et al. (2018), the authors sought to characterize genetic

interactions between mutations and standing polymorphisms, that influence phenotypic traits of

interest in yeast. To accomplish this the authors crossed 1411 wild-type and mutant strains, with

7 gene knockout strains (Mullis et al., 2018). The authors discovered each knockout had between 73 to 543 interactions with 89% involving higher-order interactions between a knockout and multiple loci (Mullis et al., 2018). This work demonstrates the large number of alleles segregating in natural populations that can act as modifier loci for genes of interest. The influence of genetic background effects on phenotype have also been investigated at the level of enzymatic function. Yang et al. (2019) studied the effect of genetic background on the evolution of Methyl-Parathion Hydrolase (MPH), an enzyme that allows for the degradation and use of methyl-parathion as a source of phosphate and carbon in bacteria. MPH is an enzyme that was first isolated from bacteria in polluted soil near a methyl-parathion producing factory and through horizontal gene transfer, and has since disseminated to many bacterial strains through horizontal transmission, providing them with the capacity to utilize xenobiotic organophosphates for nutrients (Liu et al., 2005; Sun et al., 2004; Yang et al., 2019). From this study, the authors discovered five mutations that were necessary and sufficient for the evolution of MPH, and these mutations form complex interaction networks that constrained the adaptive pathways to allow for the evolution of MPH (Yang et al., 2019). In a study on chickens, the authors sought to investigate genetic interactions on long term selection responses for body weight on two different divergently selected chicken lines (Pettersson et al., 2011). From these lines, the authors investigated interactions between six modifier loci, and how they interacted with each other as well as the two genetic backgrounds used in the study (Pettersson et al., 2011). The authors demonstrated that these loci interact with each other and the background in a biologically relevant way and the stability of these interactions over time shows their lasting effect on phenotypic change within the two populations (Pettersson et al., 2011). Within mice and yeast authors sought to examine if genetic interactions on the effect of an allele is altered by the global

genetic ancestry proportion from distinct progenitors (Rau et al., 2020). Within mice 49 genotype-by-ancestry interactions across 14 phenotypes and 1400 Bonferroni-corrected genotype-by-ancestry interaction were observed (Rau et al., 2020). Within yeast 92 genotype-by-ancestry interactions across 38 phenotypes were observed (Rau et al., 2020). These results provide further evidence of the existence of diverse genetic background effects, and that heterogeneous modifier loci and single nucleotide polymorphism effects due to different ancestries are pervasive.

1.2 Phenotypic Trait Robustness

While genetic background effects are ubiquitous and influence genetic parameters (expressivity, dominance, pleiotropy, and penetrance), we still lack an understanding of the proximate mechanisms that govern them. In particular, the reductionist approach of biology to knock out one gene to infer the causal phenotypic effect of that gene, without consideration of genetic background that can affect phenotypic outcomes, is being challenged (N. Williams, 1997). The casual assumption of gene knockouts prompting a phenotypic effect can be especially problematic when the knockout results in low to little change in phenotype. The cause of this lack of phenotypic change may be due to the mechanisms involved in genetic background effects, one of which is the phenotypic robustness of traits (Marie Anne Félix & Barkoulas, 2015; Siegal & Leu, 2014). Phenotypic trait robustness is characterized by low levels of phenotypic variation despite environmental variance or genetic perturbation (Marie Anne Félix & Barkoulas, 2015). The idea of trait robustness stems from canalization which can be defined as "a process by which the phenotypic variance of a trait is reduced when faced with a given perturbation" and is often used interchangeably in the literature (Marie Anne Félix & Barkoulas, 2015). Work on canalization began with Waddington (1952) where he exposed a population *D. melanogaster* to heat stress during development, resulting in a crossveinless wing phenotype. He

continued artificially selecting on this environmentally induced phenotype for several

generations. Eventually it was observed that the phenotype persisted even when the perturbation

was no longer present (Waddington, 1952). This "canalization" took advantage of plasticity

within a population suggesting the alleles needed for this inheritance were within the population

but not displayed until perturbation (Waddington, 1952). This implies that canalization depends

on a trait's ability to vary, where decanalized traits have increased variability (Marie Anne Félix

& Barkoulas, 2015; Green et al., 2017; Waddington, 1942, 1952).

Like genetic background effects, robustness is a phenomenon observed across phyla and

there are many examples in development where the system responds to mitigate perturbations

ensuring proper development of organisms. One example of this is cell competition which was

first observed in *D. melanogaster* developing wing discs (Morata & Ripoll, 1975). The

researchers employed mutations in the *minute* genes which encode for ribosomal proteins that

are recessively lethal but dominantly growth inhibiting (Morata & Ripoll, 1975; Neto-Silva et al.,

2009). When heterozygous cells for the mutation were placed in wild-type discs the slower

growing heterozygote clones were outcompeted and eliminated from the growing wing disc

(Martin et al., 2009; Morata & Ripoll, 1975; Neto-Silva et al., 2009). Notably this phenomenon

is not only observed in *minute* cells but can also be seen with viable low insulin activity cells and

low *dmyc* (*Drosophila* equivalent proto-oncogene, contributing to growth proliferation and cell

competition) expressing cells (Böhni et al., 1999; De La Cova et al., 2004; Martin et al., 2009;

Moreno & Basler, 2004). Cell competition has been found to impact most if not all developing

adult tissues and can act as a tumor-suppression and tumor-promoting mechanism impacting

both robustness and cancer initiation and development (van Neerven & Vermeulen, 2022).

Another example of developmental robustness can be seen in redundancy at the genome level in

plants. Plants display this robustness through whole genome duplication and hybridization where many genes are maintained in duplicate and integration of related species genomes allows for trait robustness in the presence of mutations and robustness to environmental clines (Lachowiec et al., 2016). Likewise, members of closely related gene families can compensate for loss of gene function, though as paralogs diverge from one another in function trait robustness and compensation is reduced (Lachowiec et al., 2016). Redundancy is also observed regarding enhancers. Osterwalder et al. (2014) used mice limb development to investigate the role of ten embryonic enhancers that were previously shown to be evolutionarily conserved and responsible for robust limb activity in mice reporter assays (Attanasio et al., 2013; Osterwalder et al., 2014, 2018; Pennacchio et al., 2006; Rosin et al., 2013; Visel et al., 2007). The authors show that individual deletions of enhancers caused no discernable phenotypic change but double knockout resulted in discernable phenotypic change with functional redundancy attributed through additive effects of enhancers on gene expression levels (Osterwalder et al., 2018). The authors further sought to characterize how commonly enhancer redundancy occurs in the mammalian genetic landscape through a genome wide analysis integrating epigenetic and transcriptomic data on 12 different mouse tissues at two or three embryonic or perinatal time points per tissue (Osterwalder et al., 2018). From this the authors found genes are commonly associated with multiple enhancers with similar spatiotemporal activity and through systematic investigation of limb, heart, and forebrain tissues elucidated 1058 genes associated with five or more enhancers with redundant activity patterns (Osterwalder et al., 2018). These results show that redundancy is a ubiquitous feature of biology and a method to buffer perturbations to systems.

1.3 Robustness Considerations

To investigate robustness two considerations must first be addressed. First, what is the trait of interest (M. A. Félix & Wagner, 2008)? This is an important consideration as depending

on the focal phenotype conclusions about trait robustness can change (M. A. Félix & Wagner, 2008; Marie Anne Félix & Barkoulas, 2015). For example, when investigating the level of a specific protein in a biochemical pathway for *Drosophila* wing development or investigating the development of the wing itself, different conclusions of robustness while applying the same mutation in both investigations can be reached. In this example, a mutation could cause a significant decrease in the specific protein levels but have no change in overall wing development. If our focal trait was the specific protein levels, the conclusion would be the trait is not robust to the perturbation. If our focal trait was overall wing development the opposite conclusion would be reached (M. A. Félix & Wagner, 2008; Marie Anne Félix & Barkoulas, 2015). The second consideration is what are we testing the trait is robust to, as perturbations to robustness come in three forms. The first is microenvironmental, or noise, which is the stochastic variation that occurs in any biological system. The second is macroenvironmental, or environmental variation, which is variation due to changes in environment such as heat or ultraviolet radiation. The final form is genetic variation caused not just by d*e novo* mutations, but also recombination or introgression of specific alleles (M. A. Félix & Wagner, 2008; Marie Anne Félix & Barkoulas, 2015; Masel & Siegal, 2009; O'Neill, 2009). Addressing these questions is important as it will inform us on experimental design and the conclusions that can be drawn regarding the effects of trait robustness with the genotype-phenotype relationship.

1.4 Genotype-Phenotype Maps

A tool to help to conceptualize trait robustness and the genotype-phenotype relationship is the use of a genotype-phenotype map (Figure 1.1). This conceptual tool was outlined by Lewontin (1974), in his book "The genetic basis of evolutionary change", which contained a G space for all possible genotypes, and a P space for all possible phenotypes. This map can be further extended to include multiple components within each space (Lewontin, 1974). Examples

of this include the focal allele space and genetic background as components of the genotypic space or intermediate phenotypic spaces and trait spaces within the phenotypic space (Chandler et al., 2013; M. A. Félix & Wagner, 2008; Houle et al., 2010; Orgogozo et al., 2015) (Figure 1.1). These intermediate phenotypic spaces contain intermediate phenotypes (endophenotypes), which are measurable, intermediate developmental traits that can be used as indicators of other biological processes. (Chandler et al., 2013; Marie Anne Félix & Barkoulas, 2015; Houle et al., 2010) It is in these spaces that genetic background effects act to influence the robustness of the phenotypic trait of interest. The result of this is variance of both endophenotypes and the phenotypic trait of interest. This is important as both heritable disorders such as phenylketonuria, hypertension, and colorectal cancer as well as disorders frequently involving *de novo* mutations including schizophrenia, autism, and congenital heart disease are affected by genetic background effects. (Cooper et al., 2013; Fromer et al., 2014; Jin et al., 2017; Mullis et al., 2018; Sanders et al., 2012)

a) Wild Type Allele

b) Mutant Allele

Focal Allele Space
(*sd/m* Alleles)

Components of
Genotype Space

Genetic Background Space
(DGRP Backgrounds)

Intermediate Phenotype Space
(mRNA Levels)

Components of
Phenotype Space

Trait Space
(Wing Area/Shape)
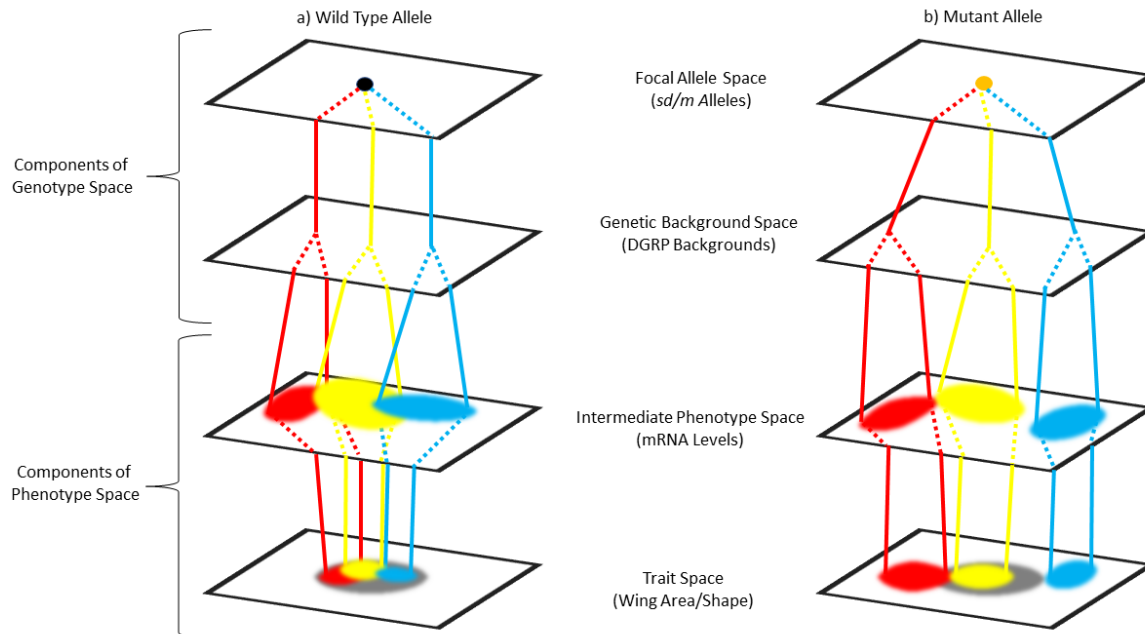
Figure 1.1: Genotype-phenotype map conceptualizing the effects of the focal allele interacting with the genetic background to influence phenotypic outcomes across multiple levels in development. Within the genetic space there is the focal allele space (*scalloped (sd)* and *miniature (m)* genes in my thesis) and the genetic background space (different wild-type DGRP strains). The focal allele space interacts with the genetic background space to affect different components of the phenotypic space. Within the phenotype space there are intermediate phenotypic spaces (mRNA levels) and the trait space (wing area and wing shape). Both the intermediate phenotypic spaces and trait space are affected by changes in the genetic background or the focal allele space. Note that there can be a multitude of intermediate phenotype spaces (not only mRNA levels) depending on the endophenotypes considered. Each colored line represents a distinct genetic background or strain. a) When there is a wild-type allele for the focal allele the result is a wild-type phenotype (gray area) within the trait space despite possible differences in the genetic background leading to variation in the intermediate phenotype spaces. b) When a mutation is introduced in the focal allele space leading to a genetic perturbation of the system, variation among genetic backgrounds is expressed in the trait space in the form of mutant phenotypes in both the intermediate phenotype space and trait space. Notably some of phenotypes in the trait space can overlap with the wild-type range of trait expression (yellow strain) and some can be completely distinct from wild-type trait expression (blue strain). It is important to remember that each space interacts with one another dictating phenotypic outcomes in the trait space. (Figure adapted from Chandler et al. 2013)

1.5 Mechanisms Underlying Robustness

While robustness is recognized and observed in a phenomenological sense, we still lack

an understanding of the mechanisms (both proximate and ultimate) modulating robustness.

Currently there are two theories regarding the mechanisms behind robustness. The first posits that robustness is due to many modifier loci acting in concert throughout the genome, to buffer against any effects of mutation, or other perturbations to a system (Green et al., 2017). This theory is akin to the omnigenic model, where each gene in the genome has an effect, albeit small, on all genes in the genome and emphasizes the existence of an organism wide buffering system. (Boyle et al., 2017; Green et al., 2017). The second posits that robustness is due to an evolved systems to buffer against perturbations (Green et al., 2017). This theory emphasizes robustness stems from the same mechanisms that generate variation in specific traits intrinsically, such as the role of heat shock protein 90 in genetic buffering (Green et al., 2017; Schell et al., 2016). Though these are two separate mechanisms affecting robustness these are not mutually exclusive, and both may be occurring simultaneously at different levels of development, to affect the genotype-phenotype relationship.

Buffering of trait robustness is thought to occur in a threshold dependent manner and is founded on the molecular basis of dominance as first proposed by Wright (1934) (Green et al., 2017; Kacser & Burns, 1981). Kacser and Burns (1981) developed a formal mathematical model, explaining the molecular basis of dominance based on gene (enzyme) activity, which acts non-linearly with phenotypic effects, whereby an organism will attempt to remain as phenotypically close to wild-type to prevent any negative effects from mutations to fitness. The non-linearity of the curve is determined by the number of enzymes between the first substrate and the final product such that when the number of enzymes increases the curve becomes more non-linear allowing for the effects of changing catalytic activity of one step to be buffered by the responses of other enzymes in the system (Kacser & Burns, 1981). Their model contains a threshold for flux (the outcome of the activities of a biochemical network, which is the phenotype) where there

will be "detectable" and "undetectable" mutant phenotypes and the level of sensitivity to variation will change depending on the position of the mutant on the non-linear curve (Kacser & Burns, 1981) (Figure 1.2). This indicates that mutant alleles with weak phenotypic effects will be less sensitive to a genetic background effect modifiers as the mutation only slightly perturbs the system (Chandler et al., 2017; Green et al., 2017; Kacser & Burns, 1981). The same is true for mutant alleles with strong phenotypic effects due to the limited capacity for genes with minimal gene activity to vary. However, alleles with moderate phenotypic effects will have increased sensitivity to genetic background modifiers to act in a compensatory manner (Chandler et al., 2017; Green et al., 2017; Kacser & Burns, 1981) (Figure 1.3).
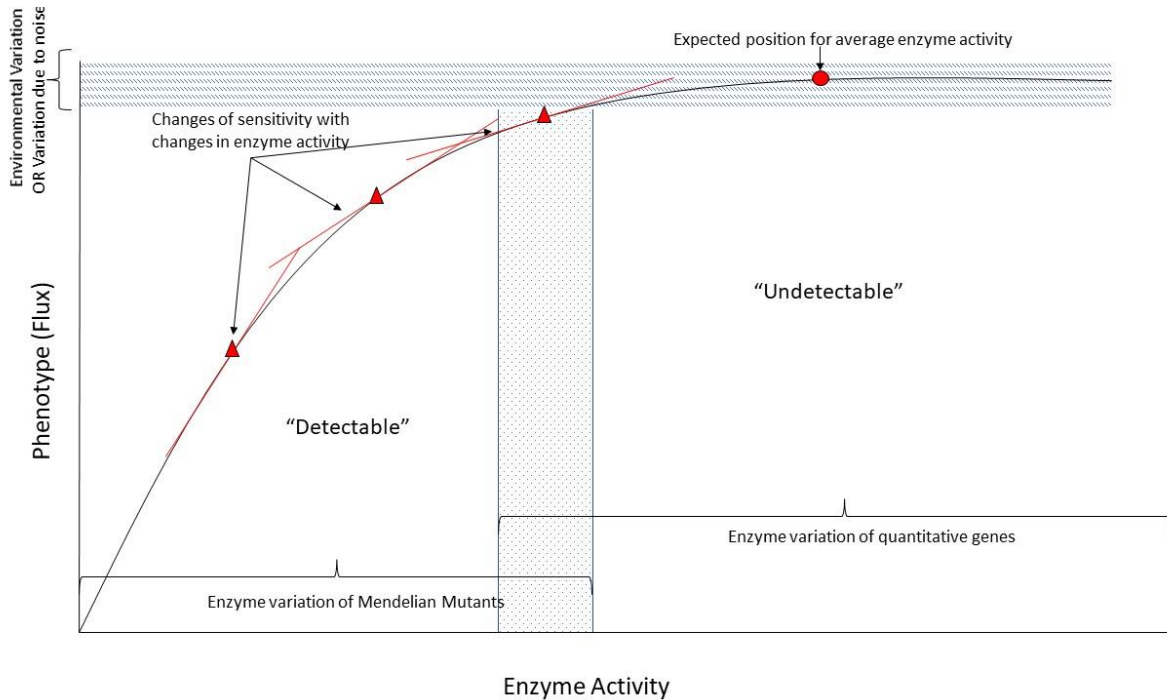
Figure 1.2: Flux enzyme curve displaying the non-linear relationship between enzyme activity and phenotype (flux) as well as the range of detectable and undetectable mutant phenotypes. On the y-axis is flux (phenotype) and on the x-axis is enzyme activity. The red circle represents the expected position for average enzyme activity (average wild-type enzyme activity). The red triangles represent various mutations resulting in decreased enzyme activity. The red lines represent the levels of sensitivity to variation. The backslash line area represents natural environmental variation or noise, it should be noted that noise and natural environmental variation is applicable to the entirety of the curve presented. The shaded doted area represents a grey area where in some instances mutants will belong to the phenotypically detectable class of mutants and some to the undetectable class of mutants depending on the classification of the focal phenotype. The phenotypically detectable class of mutants represents the enzyme flux levels that would phenotypically classify as mendelian traits and are most likely to present as the classic dominant or recessive allele relationship. The mutants that display as phenotypically undetectable (triangle in shaded dotted area) may be detected at a molecular level with quantification of enzyme or gene activity levels. As the level of enzyme activity changes the amount of flux (phenotype) becomes less buffered by the biochemical system resulting in increased sensitivity. The more enzymes involved in a biochemical system leads to more non-linearities regarding phenotype with enzyme activity. The less enzymes involved in a biochemical system results in less non-linearities regarding phenotype with enzyme activity (Figure adapted from Kacser & Burns, 1981).
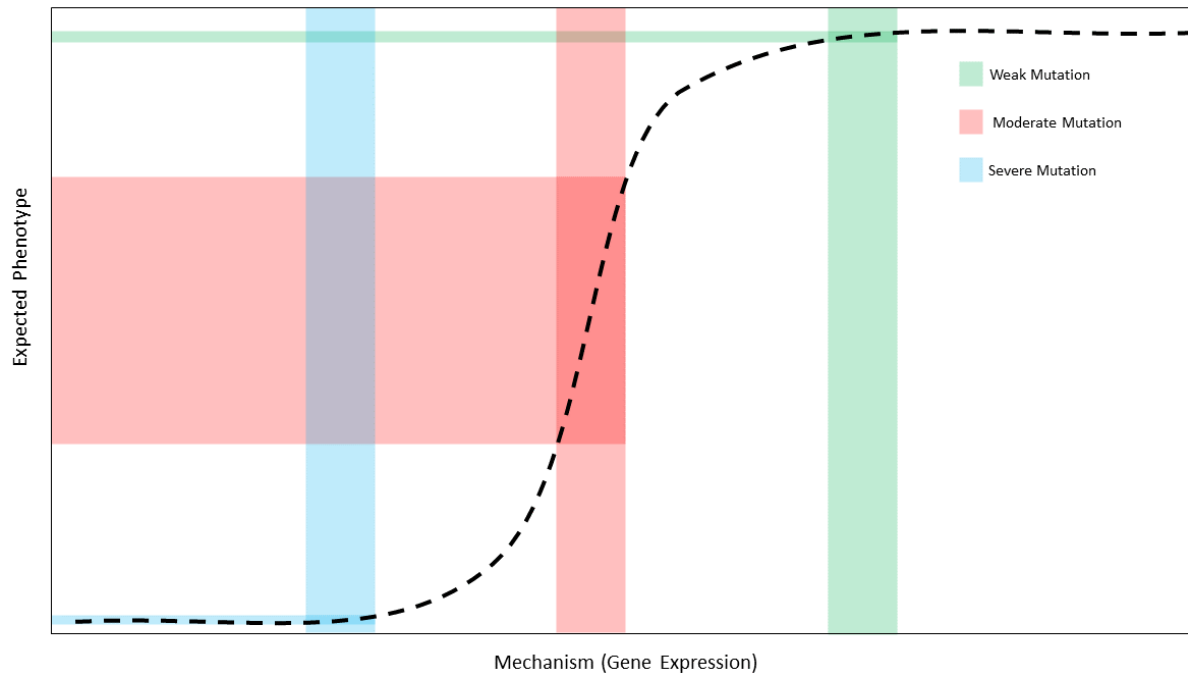
Figure 1.3: The non-linear relationship of gene expression with phenotype predicts the amount of observed phenotypic variance regarding mutational severity. This is a general model for a non-linear genotype-phenotype relationship where the amount of a developmental process (gene expression) dictates the mean expressed phenotype. The same amount of variation in the mechanism (weak mutation – green bar, moderate mutation – red bar, severe mutation – blue bar) can generate very different amounts of phenotypic variation, dependent upon the mutant's location on the curve. This model displays a canalized region where variance is buffered by the genetic background, resulting in a lack of relative variability (green horizontal bar). A region where canalization is lost and variance is not buffered by the genetic background, resulting in an increase of relative variability (red horizontal bar). A region where the mutation is so severe that robustness completely fails to buffer against the mutation resulting in a lack of variability (blue horizontal bar).

This non-linear relationship can explain many of the commonly measured genetic parameters. For dominant Mendelian mutations, homozygous wild-type individuals are located at the top of the curve (far right), above the threshold needed to cause a detectable change in phenotype (Figure 1.4; Blue Triangle). However, heterozygous individuals (assuming the dominant mutation is due to haploinsufficiency) will lead to a shift below the threshold resulting in expression of the mutation in a haplo-insufficient manner (Figure 1.4; Blue Circle & Square).

For a recessive mendelian mutation the opposite is true. In this case the homozygous and heterozygous wild-type individuals are located at the top of the curve above the threshold needed resulting in masking of the focal mutation (Figure 1.4; Red Triangle & Circle). It is not until an individual homozygous for the mutation is examined that a shift below the threshold is observed displaying the focal mutation (Figure 1.4; Red Square). This model can also be used to explain phenotypic expressivity within a population. In this example a mutation results in a noticeable change in phenotype shifting the population past the threshold onto the steep portion of the non-linear curve (Figure 1.5; Red Triangles). Where the population is shifted depends on the severity of the mutation with strong mutations shifting the population to the lower asymptote, moderate mutations shifting the population closer to the inflection point, and weak mutations shifting the population past the threshold near the upper asymptote (Figure 1.5; Blue Triangle, Red Triangle, & Green Triangle). Once shifted any changes due to modifier loci, environmental effects, or stochastic noise can result in changes in expected phenotype for individuals modifying the amount of expressivity seen from a focal mutation, with moderate phenotypic effect alleles displaying the most variable changes in phenotype (Figure 1.5). Regarding penetrance, a focal mutation may shift the population above or below the threshold (Figure 1.6; Red Triangles). From here modifier loci in the genetic background, environmental effects, or stochastic noise can shift individuals from this population above or below this threshold (Figure 1.6; Green Triangles & Blue Triangles). The result from these shifts in individuals is a variance in the number of individuals within a population displaying the focal allele of interest (Figure 1.6). Thus, understanding how the genetic background affects robustness can be key in understanding how genetic variation relates to phenotypic variation for complex multigenic traits and testing the

casual relationships between genes involved in monogenic disorders, particularly for illness

causing disorders.
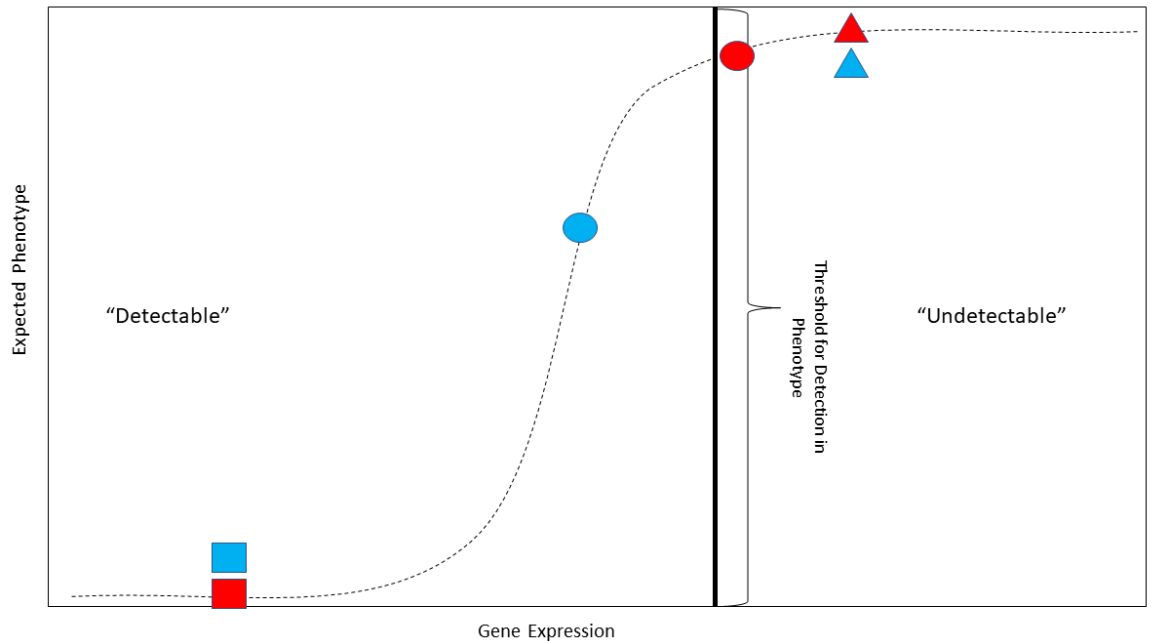
Figure 1.4: The non-linear threshold dependent relationship between gene expression and phenotype explains Mendelian dominance and recessive mutations. Red corresponds to a theoretical Mendelian recessive mutation where one copy of the allele does not mask the effect of a different variant on the same gene. Blue corresponds to a theoretical Mendelian dominance mutation where one copy of the allele does mask the effect of a different variant on the same gene. Shapes correspond to zygosity; triangles correspond to wild-type homozygotes, circles heterozygotes, and squares mutant homozygotes. Shifts above or below a threshold (bold black line) signify a detectable change in phenotype. For a Mendelian dominant mutation, homozygous wild-type individuals (blue triangle) will remain above the threshold for detectable phenotypic change while heterozygotes (blue circle) , and homozygous mutant individuals (blue square) will fall below the threshold for detectable phenotypic change. For a Mendelian recessive mutation homozygous wild-type (red triangle) and heterozygotes (red circle) will remain above the threshold for detectable phenotypic change while homozygous mutant (red square) individuals will fall below the threshold for detectable phenotypic change.
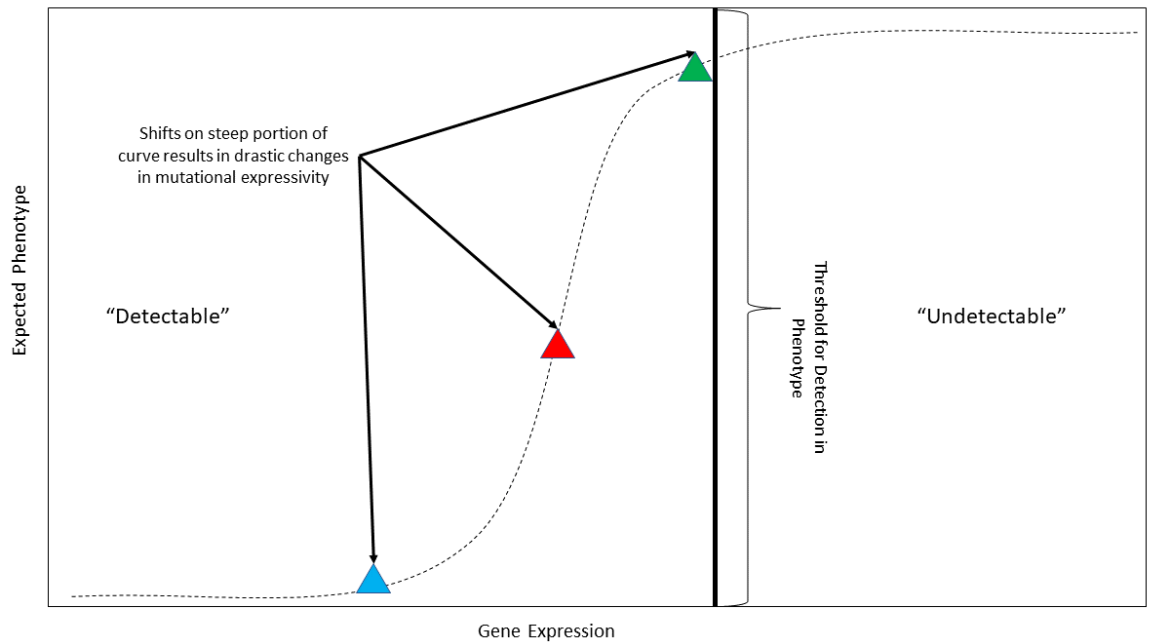
Figure 1.5: The non-linear threshold dependent relationship between gene expression and phenotype explains variation in mutational expressivity. Shifts from a theoretical wild-type allele correspond to color with green corresponding to a weak mutation, red a moderate mutation and blue a strong mutation. Shifts above or below a threshold (bold black line) signify a detectable change in phenotype. Where the population is shifted depends on the severity of the mutation with strong mutations shifting the population to the lower asymptote, moderate mutations shifting the population closer to the inflection point, and weak mutations shifting the population past the threshold near the upper asymptote. Once shifted any changes due to modifier loci, environmental effects, or stochastic noise can result in changes in expected phenotype for individuals modifying the amount of expressivity seen from a focal mutation. Moderate phenotypic effect alleles will display the most variable changes in phenotype due to the population shift to the steep portion of the curve. Both weak and severe phenotypic effect alleles will display the least variable changes in phenotype due to the population shift to the flat portions of the curve.
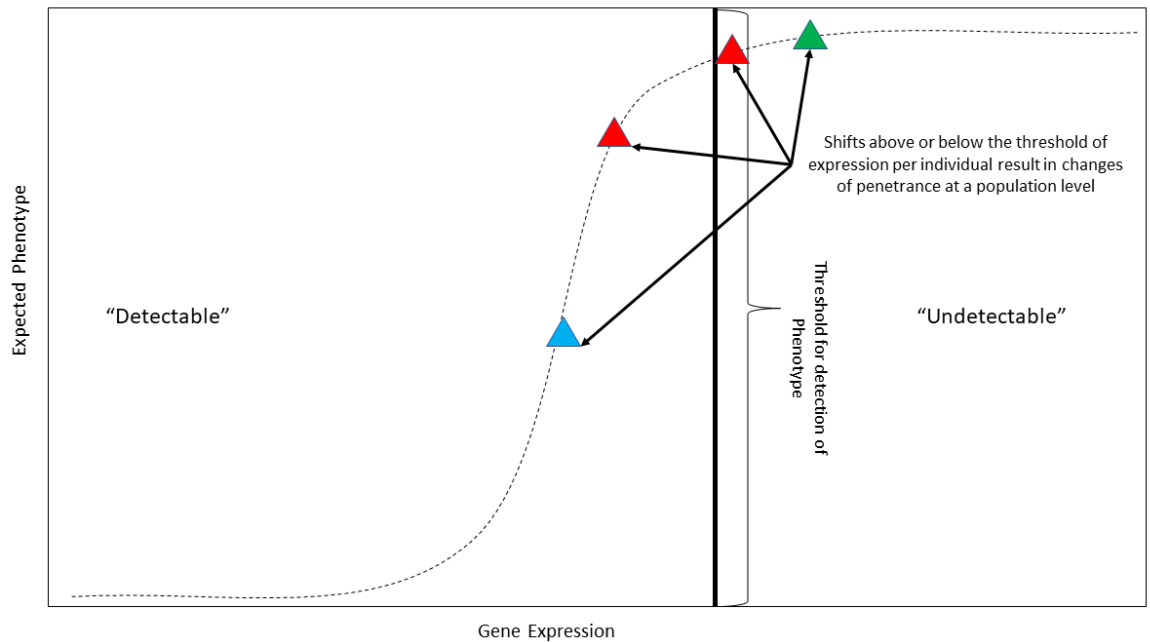
Figure 1.6: The non-linear threshold dependent relationship between gene expression and phenotype explains penetrance. Initial shift of phenotypic trait means due to a mutation corresponds to red triangles resulting in a population slightly above or slightly below the threshold (bold black line) for a detectable change in phenotype. From these means individuals from the population can be shifted above the threshold as visualized by a green triangle or below the threshold as visualized from a blue triangle. This shift can be attributed to modifier loci in the genetic background, environmental effects, or stochastic shifts from noise. This results in various levels of penetrance of a mutation within a population as some individuals will phenotypically express the mutation while others will not.

1.6 A Mechanistic Model for Background Dependence

In a paper by Chandler et al. (2017) the authors investigated genetic background effects on the ordering of allelic series and patterns of complementation exploiting the *D. melanogaster* wing as a model system. The authors sought to answer the question of how the genetic background and environment influence penetrance and expressivity by investigating two non-mutually exclusive explanations (Chandler et al., 2017). The first is genetic background effects might be unpredictable and heterogenous in cause and outcome dependent upon each allele being examined. The second is genetic background effects are determined through the developmental or physiological constraints of a genetic trait or network, not due to unique properties of specific

alleles, as outlined in the figures above (Chandler et al., 2017). The authors used allelic series in

the *scalloped (sd)* and *vestigial (vg)* genes in Samarkand and Oregon-R genetic backgrounds and

examined how the patterns of complementation and ordering of allelic effects are influenced by

the genetic background and environment (Chandler et al., 2017). The authors discovered that the

rank ordering of allelic effects generally remained consistent but observed alleles of moderate

phenotypic effect having the strongest degree of background dependence as homozygotes,

hemizygotes, and in hetero-allelic combinations (Chandler et al., 2017). This observation

resulted in a reverse hourglass pattern where alleles of severe and weak phenotypic effects

displayed modest background dependence relative to moderate phenotypic effect alleles which

showed increased background dependence (Figure 1.7).
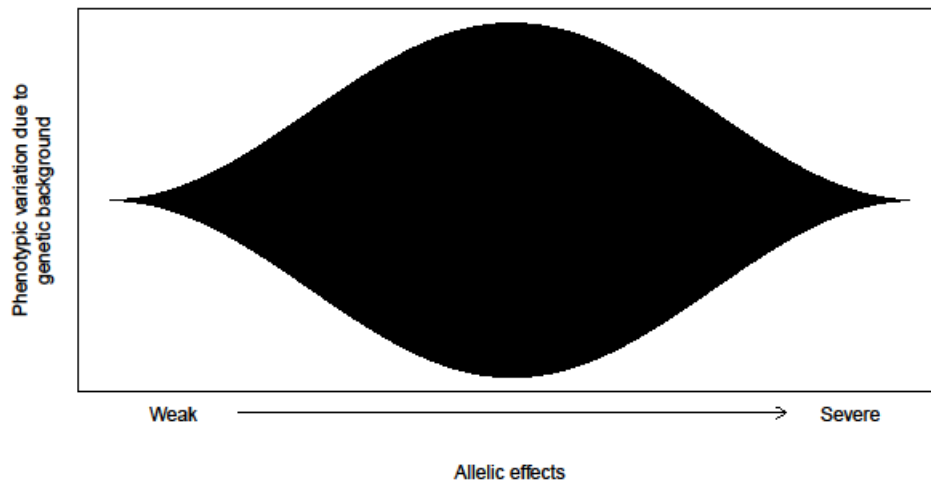
Figure 1.7: Conceptualization of the reversed hourglass figure exhibiting the amount of observed phenotypic variation from the genetic background increases with moderate phenotypic effect alleles relative to weak and severe phenotypic effect alleles. Mutant alleles of moderate phenotypic effects display increased between genotype phenotypic variation and genetic background dependence compared to alleles of severe and weak phenotypic effects (Figure recreated from Chandler et al., 2017).

The observed reverse hourglass pattern across trans-heterozygotes, hemizygotes, and

homozygotes for both *vg* and *sd* alleles suggests that genetic background effects may be

predicable, following the severity of overall genotypic effect rather than specific allelic effects.

As depicted in the models above for expressivity, the moderate phenotypic effect alleles would lead to a shift onto the steep portion of the curve, weak phenotypic effect alleles would remain on the upper asymptote and strong phenotypic effect alleles would shift to the lower asymptote (Figure 1.3, Figure 1.5). Chandler et al. (2017) confirmed this generalizability through crossing of the *sd* alleles to an additional 16 randomly selected wild-type strains from the *Drosophila* Genetics Reference Panel (DGRP) and examining F1 hemizygous male progeny. The results displayed a similar pattern of increased background dependence of moderate effect alleles and a lack of reordering of the allelic series (Chandler et al., 2017). There was one surprising finding that was inconsistent with the model discussed above. While moderate phenotypic effect alleles display increased variability between wild-type backgrounds compared to severe and weak phenotypic effect alleles, the same pattern is not observed for among individual, within-genotype variability. Within-genotype variability (variability due to micro-environmental or developmental noise) was found to be highest in alleles of severe phenotypic effect (Chandler et al., 2017). This suggests a level of independence between genetic background effects and sensitivity to micro-environmental or stochastic variation within genotypes, not predicted by the model, and also inconsistent with previous research (Marie Anne Félix & Barkoulas, 2015; Green et al., 2017). However, it should be noted that the experimental design of Chandler et al. (2017) was not optimally suited to assess among individual within genotypic effects. In a further study, Caitlyn Daley (2019) examined this question in depth and observed that among individual, within genotypic variation was high for both moderate and severe mutations in *scalloped*, but was significantly higher for mutations of moderate effect (Figure 3.34, Figure 3.36). Furthermore, she demonstrated a relationship between how far a mutant allele (in a given wild-type background) reduced wing size relative to its corresponding wild-type background and the

amount of variation among individuals within that genotype (Figure 3.27, Daley, 2019). While more complex than initially expected, they are generally consistent with the predictions of the overall model.

Though these findings display some of the effects the genetic background has on allelic ordering and complementation, it is still unclear if these findings are characteristic of *sd* and *vg* alone, a function of genes with similar developmental mechanisms, a function of genes with similar phenotypic effects, or generalizable to other genes involved in the *Drosophila* wing network. To address these questions Caitlyn Daley (2019) expanded on this work implementing crosses of allelic series in the *sd, beadex(bx), cut (ct),* and *optomotor blind (omb)* genes with 73 DGRP lines, and later with a larger s*d* allelic series and the same *bx* series with a 20 DGRP subset. The hemizygous wings of these adult flies were dissected, and sizes quantified and analyzed. The results obtained from these experiments confirm and extend results from Chandler et al. (2017) of alleles with moderate phenotypic effects displaying increased background dependence relative to alleles with weak or severe phenotypic effects (Daley, 2019). Results also suggest that background dependence is highly positively correlated between alleles of the same gene and genes in the same network. The highest positive correlation of background dependence was observed with alleles from different genes but of the same levels of phenotypic effect. Further, among individual, within genotypic variation was high for both moderate and severe mutations (in *scalloped*) but was significantly higher for mutations of moderate effect (Daley, 2019; Figure 3.34, Figure 3.36). Furthermore, Daley (2019) demonstrated a relationship between how far a mutant allele (in a given wild-type background) reduced wing size relative to its corresponding wild-type background and the amount of variation among individuals within that genotype (Figure 3.27). While more complex than initially expected, these results are generally

consistent with the predictions of the overall model. Interestingly no correlation in the magnitude of within-genotype variability in the wild-type line and how severe the mutation effects will be in that strain was observed (Daley, 2019). Nonetheless, consistent with both the mechanistic predictions, and the findings in other developmental systems in the *C. elegans* vulva and cranio-facial development in mice this suggested that the background dependence may be, in part explained by this same model for wing development (Barkoulas et al., 2013; Green et al., 2017). More specifically, the model can explain wing development regarding the impact of *scalloped* and *vestigial* and other genes influencing growth and patterning during larval wing imaginal disc development.

1.7 *D. melanogaster* Early Wing Imaginal Disc Development

The adult *D. melanogaster* wing first begins as a group of about 50 cells that invaginate from the embryonic ectoderm forming the future wing imaginal disc, a single cell layered sac of epithelial cells that undergoes patterning and growth during later larval stages (Bate & Martinez Arias, 1991; Matamoro-Vidal et al., 2015; J. A. Williams et al., 1993). During the first larval instar the wing imaginal disc grows moderately with moderate cell division which later becomes exponential during the second and final instars (Mandaravally Madhavan & Schneiderman, 1977; Matamoro-Vidal et al., 2015). During the second larval instar, the developing wing is subdivided into compartments creating a dorsal-ventral (D/V) boundary while maintaining anterior-posterior (A/P) boundaries (De Celis, Garcia-Bellido, et al., 1996; García-Bellido et al., 1973; J. A. Williams et al., 1993). These boundaries are determined through gene products Apterous which is expressed throughout the dorsal compartment in the D/V axis and Engrailed which is expressed throughout the posterior compartment in the A/P axis (De Celis, Garcia-Bellido, et al., 1996; J. A. Williams et al., 1993). The boundaries of these axes secrete organizational signals Wingless (Wg) from the *wnt* signalling pathway for dorsal-ventral

patterning and Decapentaplegic (Dpp) a member of the TGF-β/BMP family for anterior posterior-patterning (Halder et al., 1998; Kim et al., 1996). Both Wg and Dpp induce expression of various target genes through both Distal-less (Dll) and Vestigial (Vg). Dll is expressed in a graded fashion centered on the wing margin and is required for wing margin differentiation (Houlston & Tomlinson, 1998; Neumann & Cohen, 1997; Zecca et al., 1996). Vg expression is mediated through both a *vg* quadrant enhancer (*vgQE*) and *vg* boundary enhancer (*vgBE*) (Kim et al., 1996; Klein & Arias, 1999; Parker & Struhl, 2020; Jim A. Williams et al., 1994). The *vgBE* is initially activated during early 2nd instar and appears along the D/V axis and later the A/P axis while the *vgQE* is activated later and regulates expression away from the D/V and A/P axes in the developing wing blade (Klein & Arias, 1999). To function, Vg heterodimerizes with Scalloped which is a member of the TEA/ATTS class of transcription factors (Bray, 1999; Neto-Silva et al., 2009; Simmonds et al., 1998; Srivastava et al., 2004). This complex binds to cis-regulatory elements for wing specific genes regulating wing cell identity including *spalt* which affects central wing pattern formation, *blistered* which affects intervein cell differentiation, and *cut* which specifies wing external sensory organs and non-innervated bristles (De Celis, 1999; De Celis, Barrio, et al., 1996; Halder et al., 1998; Jack et al., 1991; Montagne et al., 1996; Zecca et al., 1996).

Along with affecting wing cell identity, the Sd-Vg complex has also been implicated in cell proliferation and death (Baena-Lopez & García-Bellido, 2006; Delanoue et al., 2004; Paumard-Rigal et al., 1998; Simmonds et al., 1998). Cell proliferation is affected through antagonization of *dacapo,* a cyclin-dependent kinase inhibitor, inducing *drosophila E2F1* and it's targets *string* and *drosophila ribonucleotide reductase* both of which affect cell cycle progression. (Delanoue et al., 2004; Duronio et al., 1995; Neufeld et al., 1998) Cell death is

affected through the induced expression of *dihydrofolate reductase* shifting dorsal-ventral

boundary cells to a cell death sensitive state correlated with *reaper* induction and *diap1*

downregulation. (Delanoue et al., 2004) Scalloped also affects wing development through

dimerizing with Yorkie to affect cell proliferation, cell growth, and apoptosis (Huang et al.,

2005; Zecca & Struhl, 2010; Zhang et al., 2008). Yorkie *(*Yki*)* is a member of the *hippo (hpo)*

signalling pathway, and a lack of Hpo signalling results in Yki translocating to the nucleus and

binding to Sd to promote cell proliferation and inhibit apoptosis through target genes cell death

inhibitor *diap1,* cell cycle regulator *cyclin E*, and cell proliferation microRNA *bantam.* (Huang et

al., 2005; Thompson & Cohen, 2006; Zhang et al., 2008) Yki activity has also been implicated in

the feedforward wave, employing Wg and Dpp which is needed to initially activate the *vgQE* in

pre-wing cells in the developing wing (Parker & Struhl, 2020; Zecca & Struhl, 2010). This

activity leads to the expression of Vg which later substitutes for Yki to autoregulate its own

expression (Parker & Struhl, 2020).

1.8 The *miniature* gene

Unlike s*calloped, miniature (m)* contributes structurally in development, and is required

for proper denticle formation and late stage pupal wing formation (Chanut-Delalande et al.,

2006; Roch et al., 2003). *m* first appears in early embryo development under the transcriptional

control of *shavenbaby (svb)* affecting trichome cell apical membrane–cuticle interactions in the

developing embryo (Chanut-Delalande et al., 2006). *svb* regulates the transcription of several

transmembrane proteins containing zona pellucida domains affecting denticle differentiation and

pigmentation in developing wing tissue and is under the control of *Drosophila epidermal growth*

factor receptor (*DER)* and *wg* pathways (Chanut-Delalande et al., 2006; Fernandes et al., 2010;

Payre et al., 1999). Zona pellucida domains (ZPD) are highly conserved domains, that serve a

variety of functions within multiple organisms (Jovine et al., 2005). While responsible for a
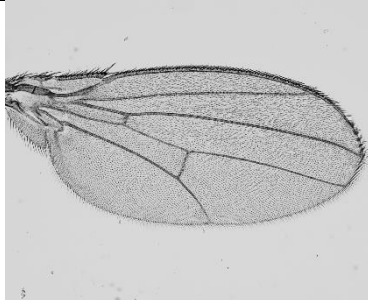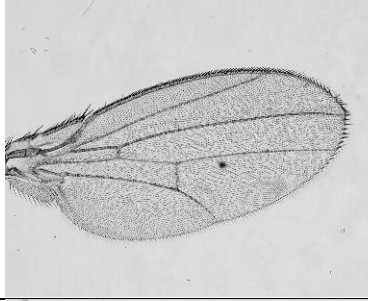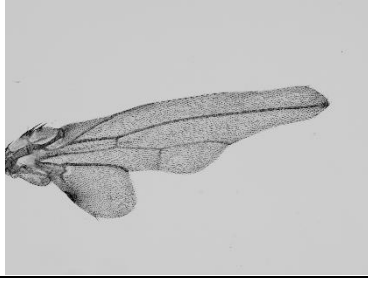
multitude of biological functions, ZPDs primarily act as polymerization molecules causing these domains to frequently be found in extracellular proteins that polymerize into higher-order structures such as extracellular filaments or extracellular matrices (Fernandes et al., 2010; Jovine et al., 2005). Miniature also appears during late-stage wing development and is a 682 amino acid single pass transmembrane protein containing a short cytoplasmic tail and large ZPD resembling Cuticlin-1 in *C. elegans* (Fernandes et al., 2010; Jovine et al., 2005; Roch et al., 2003; Sebastiano et al., 1991).
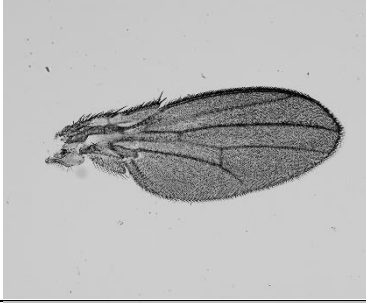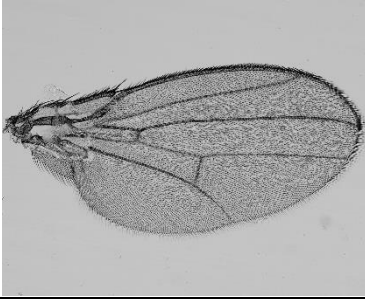
Morphology of wing cuticle during pupal development can be distinguished into four stages, envelope development from 36-48 hrs after white pupal development (awp), epicuticle deposition (52 hrs awp), procuticle thickening (62-88 hrs awp) and period of cuticle maturation and thickening of the adhesion layer and pigmentation of basal procuticle (88-96 hrs awp) (Sobala & Adler, 2016). It is the stage of envelope development at 42 hours during pupal development that *miniature* along with *dusky* and *dusky-like* act allowing for proper wing development (Roch et al., 2003; Sobala & Adler, 2016). *miniature* mutants result in incomplete adherence of wing epithelial sheets, wing hair orientation defects and loss of flattening of the initially columnar wing epithelial sheets with no changes to cell numbers or qualitative change in wing shape in comparison to wild-type wings, though wing shape changes have never been quantified (Dobzhansky, 1929; Newby et al., 1991; Roch et al., 2003). Miniature affects wing development by polymerizing to the apical extracellular matrix to hold the flattened wings in their star shaped pattern, without which results in smaller, thicker, and less translucent wings with increased cell density (Dobzhansky, 1929; Fristrom, 1988; Newby et al., 1991; Roch et al., 2003). Further work by Bilousov et al. (2012) also implicated *m* in the regulation of diffusion and stability of the hormone bursicon in pharate wing tissue. Whereby *m* acts upstream of

bursicon and removal of *m s*lows apoptosis and potentially the epithelial-mesenchymal transition (EMT) (Bilousov et al., 2012). Bursicon is required for proper wing formation and is responsible for initiation of the epithelial-mesenchymal transition and programmed cell death needed for proper wing formation post-eclosion (Bilousov et al., 2012; Kiger et al., 2007; Kimura et al., 2004).

1.9 Phenotypic effects of *scalloped* and *miniature* alleles
Table 1.1: Descriptions and images of *scalloped a*nd *miniature* mutant alleles utilized in this study. Both genes are located on the X-chromosome.

Allele	Description	Lesion	Image
ORE	Oregon-R laboratory strain.		
$sd^{29.1}$	Hemizygotes present minor loss of posterior wing margin especially near wing hinge. Homozygotes show weak scalloping at tip of wing, heterozygotes have variable notched wing phenotype.	P{GawB} insertion on first large intron after the translational start site, close to the 5' splice site.	
sd^1	Hypomorphic allele. Presents as scalloped wing margins, thickened veins, and ectopic bristles on wing blade. Phenotype does not overlap with wild-type.	X-ray hypomorphic mutation, cytogenically normal (no rearagement in sd region)	
sd^{ETX4}	Hypomorphic allele. Homozygous female and hemizygous males display nicking of the anterior and lateral margins of the wing blade, males have a more severe phenotype.	P{lacZ} insertion in the first intron, approximately 400 bp upsteam of traslational start site.	
sd^{E3}	Homozygotes and hemizygotes present with scalloped wings. Heterozygotes have effect on anterior wing shape but no effect on posterior region.	P{wE} insertion in an intron 5kb downstream of translation start site.	

sd^{58d}	Hypomorphic allele. Present as strong wing reduction.	Gamma ray induced chromosomal aberration, caused by chromosomal inversion; In(1)sd^{58d}.	
m^{D}	Homozygote and hemizygous wings present smaller than wild-type. Viable in 20-50% in hemizygous males and 5% in homozygous females, majority die in embryo, reduced fertility in homozygous females.	X-ray hypomorphic dominant mutation	
m^{1}	Loss of function allele. Presents as strong reduction in size of wings, slightly longer than abdomen with normal proportions. Have dark grey and less transparent appearance with wing cells smaller and thicker than normal.	Deletion of downstream of start of translation. Causes frameshift mutation and premature stop codon within coding region.	
m^{74F}	Presents as small reduction in wing size, slightly longer than abdomen but normal proportions. Less pronounced than m^{1} and m^{D}.	EMS hypomorphic mutation	

2. *miniature* Project Overview

For my first project I aimed to expand on the findings of Chandler et al. (2017) and recent work done in the Dworkin lab to address if genetic background effects (GBEs) are a property of individual alleles, genes, developmental mechanisms or the "trait" itself, using *Drosophila melanogaster* wing size and shape as the phenotype of interest through the genetic perturbation of mutant alleles (Daley, 2019). This is an ideal model system as we have available allelic series

in *Drosophila* and the ability to quantify wing size and shape in a relatively high throughput

manner. Wings are easily phenotyped and are relatively easy to generate large enough sample

sizes to examine small changes in size. I took advantage of a small *miniature* allelic series,

(Figure 2.1, Table 1.1) that has been previously introgressed into the Oregon-R (ORE) laboratory

strain. I crossed these alleles to 19 DGRP strains, to generate hemizygous males (Daley, 2019).

Given the fact that *miniature* and s*calloped* are both involved in wing development, and produce

"reduced" adult wings as mutants, but affect different mechanisms of development at different

timepoints (Table 2.1), this assisted with determining if the Chandler et al. (2017) model is

generalizable or specific to the *vestigial* and *scalloped* developmental mechanisms and

phenotype. Furthermore, to allow for comparability with previously conducted experiments

using *scalloped* and *beadex* I included both the sd^1 and sd^{ETX4} alleles that had been previously

examined. Crosses were conducted with 19 of the 20 DGRP lines used in a previous subset

experiment with crosses to the ORE^{w^-} genetic background with the DGRP lines to act as

controls (Daley, 2019).
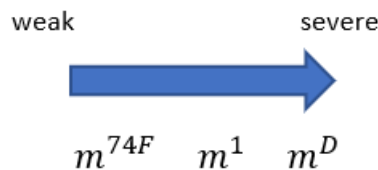
Figure 2.1: Graphical representation of the *miniature* allelic series from weak to severe.

Table 2.1: Summary of developmental differences between *scalloped* **and** *miniature* **during wing development.**

Role in development	*scalloped*	*miniature*
Timing of active role	Earlier, 3rd larval instar stage	Later, late pupal stage
Mechanisms affecting wing size	Patterning and determination, cell proliferation, growth and apoptosis	Cell shape
Pleiotropy	Highly pleiotropic	Minimally known pleiotropy
Protein type	TEA/ATTS class transcription factor	Trans-membrane protein with zona-pellucida domain

2.1 Hypothesis

As proposed by the Chandler et al. (2017) model, I hypothesized that the degree of background dependence would be predicted based on the degree of phenotypic perturbation from the mutant allele. Alleles with strong and weak phenotypic effects would display limited background dependence, indicated through decreased variation between phenotypes. Alleles with moderate phenotypic effects would display increased background dependence relative to weak and severe alleles indicated by relatively increased variation between phenotypes. Furthermore, the allelic order would remain consistent across genetic backgrounds.

2.2 Objectives

1. Confirm the utility of the Chandler et al. (2017) model, predicting background dependence at the allelic level.

2. Confirm if genetic background effects are specific for alleles, developmental mechanisms, and/or phenotypic effects of the wing.

3. Determine if allelic order remains consistent across genetic backgrounds and correlations between s*calloped* and *miniature* remain consistent.

3. scalloped **Project Overview**

For the second half of my project, I aimed to understand some of the mechanistic causes of genetic background effects to understand how genotype affects phenotype in the developmental network. I have exploited *Drosophila* wing imaginal discs as they are relatively easy to generate, to dissect, and the wing developmental network has largely been mapped. I have crossed a (co-isogenic) *scalloped* allelic series to 6 DGRP wild-type backgrounds that have been previously identified to range from weak to severe with regards to genetic background effects. (Daley, 2019; Figure 4.1 & Supplimental Table 8.2). I then examined gene expression levels of various genes involved in wing development in the *Drosophila* wing development network utilizing qPCR in late third instar discs.

3.1 Hypothesis

There are four hypothesized outcomes explaining the relationship between gene activity and phenotype and how they can explain genetic background effects and their predictions (Figures 9-12).
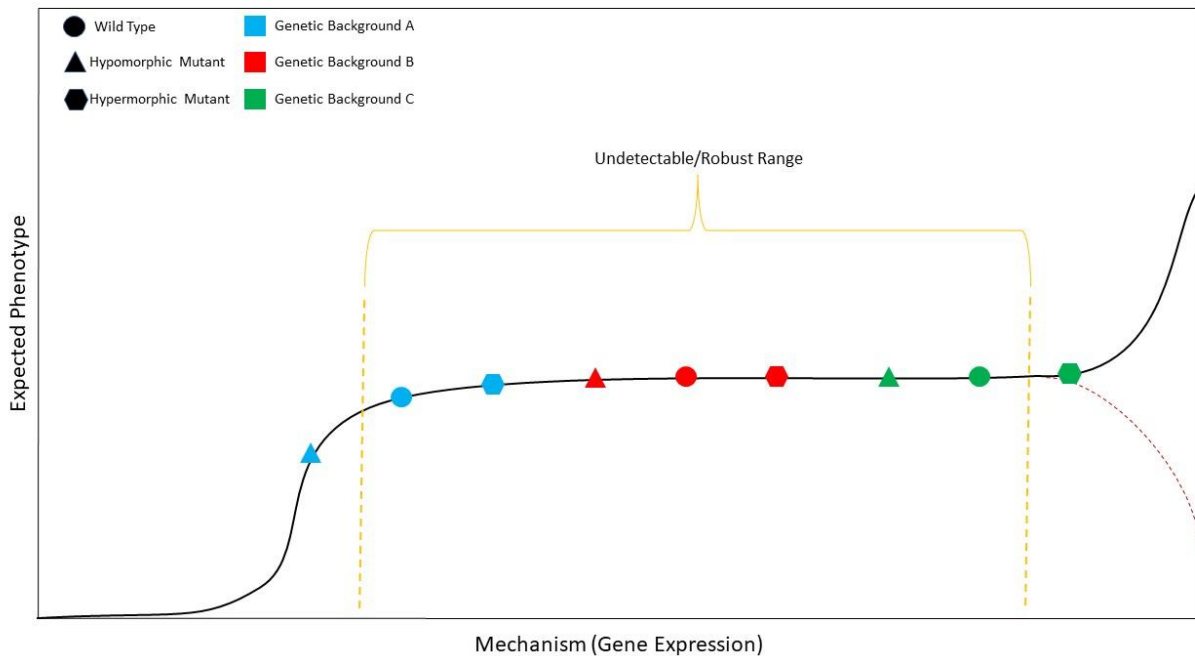
Figure 3.1: Genetic background effects model 1 – each wild-type background differs with respect to starting gene activity levels. Each wild-type genetic background has a set level of gene activity (measured as gene expression levels) that presents phenotypically wild-type (robust range). In this model, a particular hypomorphic or hypermorphic mutant allele behaves the same in each genetic background, resulting in the same decrease or increase in gene expression levels in all backgrounds. This results in backgrounds that have less wild-type gene expression being more sensitive to hypomorphic alleles while backgrounds with higher wild-type gene expression levels being robust to hypomorphic alleles. Conversely, wild-type backgrounds that have higher wild-type gene expression levels are more sensitive to hypermorphic alleles while backgrounds with less wild-type gene expression are more robust to hypermorphic alleles (Figure adapted from Daley, 2019).
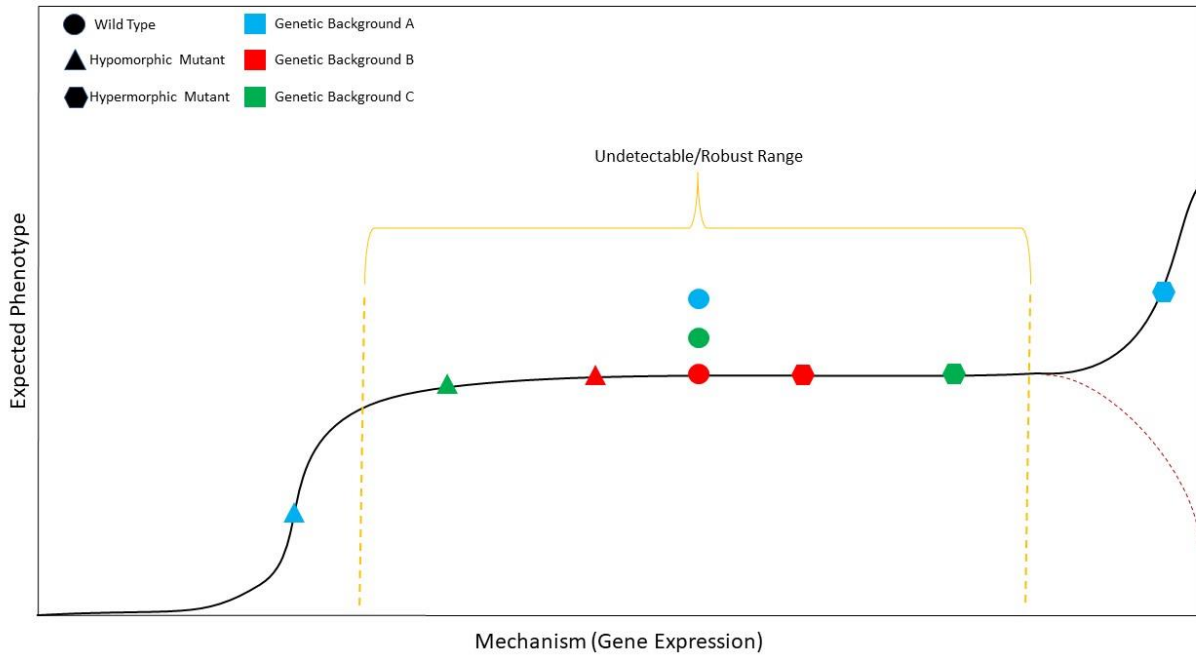
Figure 3.2: Genetic background effects model 2 – each wild-type background differs with respect to mutational robustness. Each wild-type genetic background has the same level of gene activity (measured as gene expression levels) that presents phenotypically wild-type (robust range). Within each background the hypomorphic or hypermorphic allele displays different sensitivities resulting in different amounts of gene expression reduction or increase in each background. This might suggest the mutant allele is sensitive to genetic background effects (showing different degrees of robustness between strains) (Figure adapted from Daley, 2019).
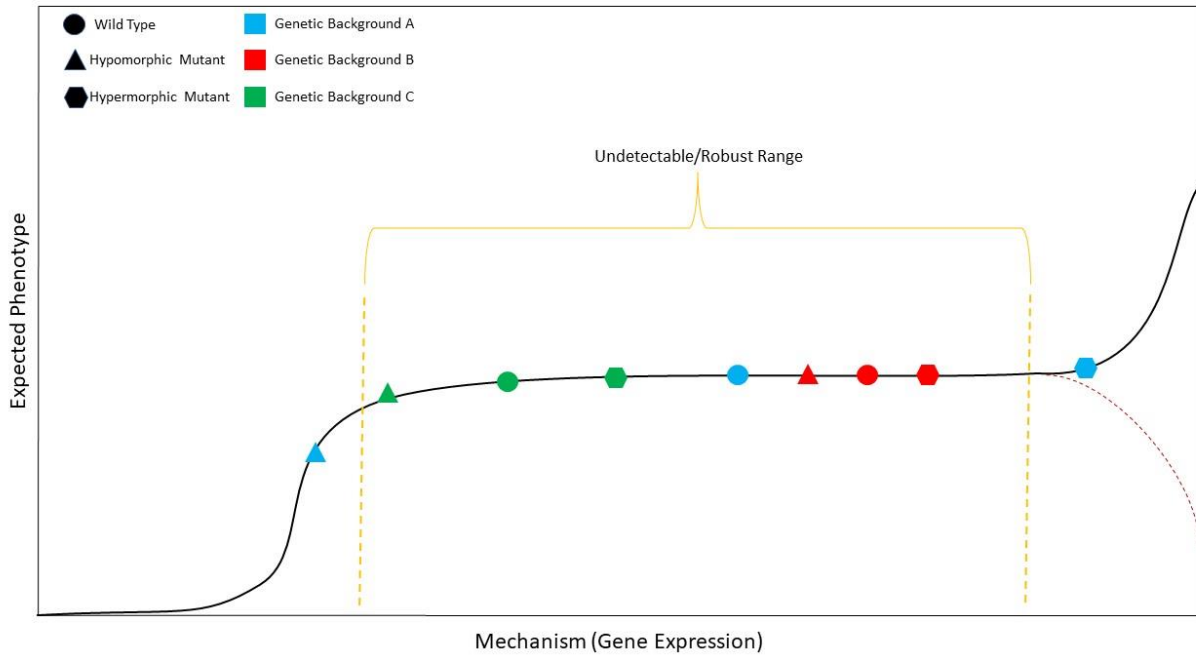
Figure 3.3: Genetic background effects model 3 – each wild-type background differs with respect to mutational robustness and gene activity. Each wild-type genetic background has different levels of gene activity (measured as gene expression levels) in the phenotypically wild-type (robust range). Additionally, within each background the hypomorphic or hypermorphic allele displays different sensitivities to mutational perturbation resulting in different amounts of gene expression reduction or increase in each background. These effects make the activity of the mutant allele less predicable and could be representative of sensitivity elsewhere in the network (Figure adapted from Daley, 2019).
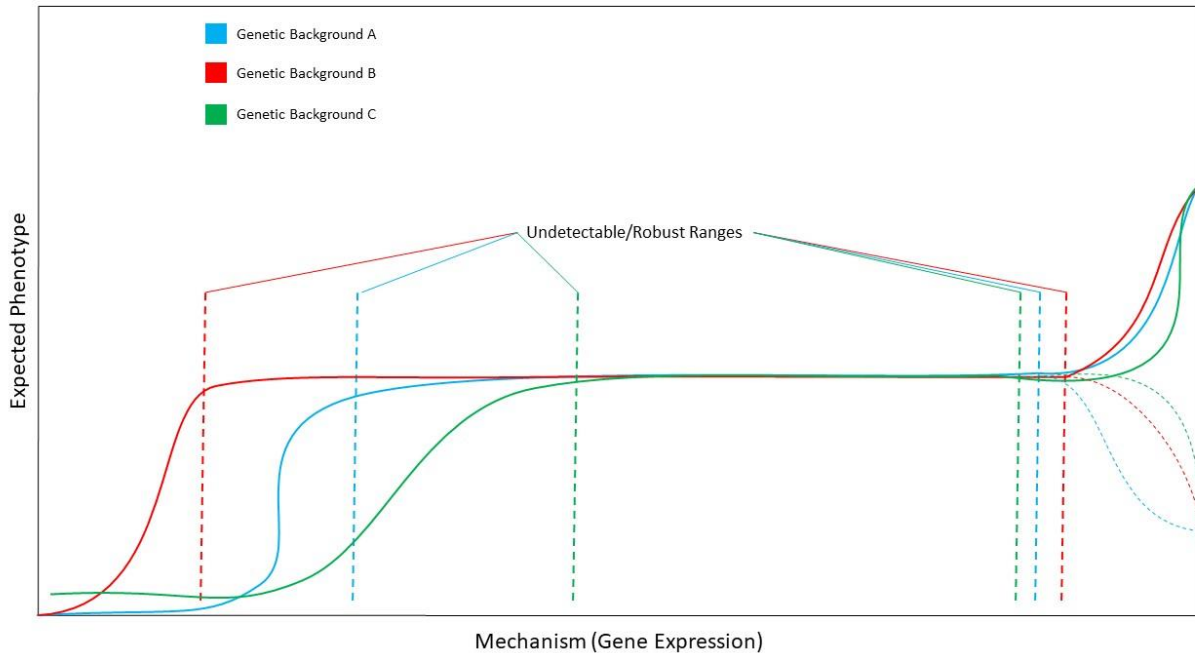
Figure 3.4: Genetic background effects model 4 - each wild-type background differs in the shape of the genotype-phenotype relationship. Each genetic background has its own unique genotype-phenotype relationship that exhibits a unique robust range (Figure adapted from Daley, 2019).

3.2 Objectives

1. Determine the relationship between gene activity and phenotype within each genetic

    background and if this relationship is consistent for each *scalloped* allele within each

    background.

2. Determine the relationship between gene activity and phenotype between genetic

    backgrounds and if this relationship is consistent for each *scalloped* allele across each

    background.

4. Methods

4.1 *miniature* Crossing Scheme

   I used 19 DGRP lines (Supplemental Table 1.1) for crossing to mutant alleles

$sd^1, sd^{ETX4}, m^{74F}, m^1$ and m^D as well as to the ORE^{w-} laboratory strain background. Each

mutant allele had been previously introgressed into the same ORE^{w-} genetic background by Caitlyn Daley (2019). Each cross was conducted using 5 virgin mutant females and 5 DGRP males (for each DGRP) then allowed to lay at 24°C for 5 days after which the crosses were flipped out of the initial vial into a second vial and left for 5 days before being cleared and disposed of. This ensured that there were two vials producing offspring (on the same food) per replicate cross conducted. The food that the flies were flipped onto for the two vials were taken from the same cook to minimize environmental effects. The original intent was to cross each allele into each background twice allowing for two unique biological replicates of each cross. However, due to contamination, lack of female virgins, failed crosses, and lack of progeny, replicate blocks 3, 4, and 5 were created to ensure 2 unique biological replicates for each cross. When biological replicates 3, 4, and 5 were created I made sure to include crosses that were also done previously and overlapped with previous blocks, to enable proper estimation of block effects without confounding effects.

4.2 *miniature* Phenotyping & Fly Collection

Within 48 hours post eclosion, full scleritized heterozygous females and hemizygous males were sexed, phenotyped, and stored in Eppendorf tubes with 70% ethanol for wing dissection. Collections continued for a maximum of 12 days after first eclosion to prevent collection of F2 progeny. Collections ranged from very little (~3-5 individuals) to very large sample sizes ~90 from a given cross. Collections between the two vials within a replicate block were stored in the same Eppendorf tube if the two vials were of the same cook. In one instance of collections the 2nd vial contained food from a different cook and these samples were stored independently and treated as an independent replicate cross for statistical analysis.

4.3 *miniature* **Wing dissection, Imaging, Measuring Wing Area, and landmarking.**

Wings of male hemizygous (for *m* and *sd* alleles) flies were dissected and mounted in a

glycerol based mounting solution. On average there were 15 wings dissected per genotype per

replicate cross. Wing imaging was conducted employing brightfield microscopy, on an Olympus

BX43 microscope with a 4X objective lens (40X magnification total). Images were collected

with an Olympus DP80 camera and cellSens Standard (V1.14) software, at an image resolution

of 4080 x 3072 pixels. Images of wings were edited to exclude any body segments. In the case of

any wing damage, a wing damage score was assigned to each wing and recorded in a spreadsheet

for future analysis. The damage scores ranged from zero to three, with zero being very little to no

damage from dissections and folding due to mounting to three being very damaged and or wing

folding rending the image likely not usable for image analysis. The images were then measured

by means of a custom ImageJ macro and wing sizes in pixels were converted into mm. 15 point,

2D landmarking was conducted by an undergraduate volunteer (Francesco Ruso) implementing a

15-point landmarking macro courtesy of Dr. Chris Klingenberg. The 15 point landmarking

allowed me to quantify changes in wing shape (Adams & Otárola-Castillo, 2013; Baken et al.,

2021). Exploiting the 15-point landmarking system also allowed me to quantify wing centroid

size as an independent measure for wing size, and I found no discernable difference in results

between wing areas from our ImageJ macro and wing centroid size (Adams & Otárola-Castillo,

2013; Baken et al., 2021).

4.4 *miniature* **Statistical modeling**

4.4a Generalized Linear Mixed Modeling Approach

The resulting data set was first log transformed then modeled with the R programming

language and the lme4 package with linear mixed models fit via maximum likelihood estimation

(Bates et al., 2015). The response variable was set for the $\log_2$ wing area with the predictor

variable as the mutant allele with the random effect of replicate vials and the random intercept

and slope of the mutant alleles within the DGRP groups (1). For each individual measure of

(log2 scaled) wing size, y_i, for the ith individual, we fit the following linear mixed model:

$$y_i = \hat{\beta}_0 + \sum_{j=1}^{6} \hat{\beta}_j x_{i,j} + \epsilon_i$$

(1)

Where replicate (block) effects are accounted for by:

$$\beta_0 \sim N(0, \hat{\sigma}_b^2)$$

(2)

And random effects among wild-type DGRP strains:

$$\begin{matrix} \beta_1 \\ \vdots \\ \beta_6 \end{matrix} \sim MVN(\mathbf{0}_6, \Sigma_{G\ 6x6})$$

(3)

With model intercept, $\hat{\beta}_0$, coefficients estimating allelic treatment contrasts ($\hat{\beta}_j$)

associated with appropriate dummy coding for the jth , allele the for each sample ($x_{i,j}$), with

ϵ_i represents unmodeled variation for size (1) $\hat{\sigma}_b^2$ represents variance associated with

experimental blocking with β_0 normally distributed with a mean of zero (2). The $\Sigma_{G\ 6x6}$, is the 6-

by-6 genetic variance-covariance matrix associated with the genetic effects of the DGRP (genetic

backgrounds) for each of the 6 alleles, which is of major interest for this study (represented as

genetic correlations). $\begin{matrix} \beta_1 \\ \vdots \\ \beta_6 \end{matrix}$ is the vector from β_1 to β_6 which are multivariate normal with a mean

of zero. Using the coding conventions of lmer and glmmTMB, this model is fit as:

log₂(WingSize) ~ allele + (1| replicate_vial) + (0 + allele | DGRP)

We confirmed our estimation by excluding severely damaged wings of a damage score of two or more. We did not observe any substantial differences in the estimates and opted to include all wings within the analysis to allow for a larger dataset and increased power. We further checked our estimates from the lmer model in lme4 exploiting the glmmTMB package which differs in how it estimates the model likelihoods (Brooks et al., 2017). From these models we discerned no substantial differences in model fit and so employed the glmmTMB model for downstream analysis and data visualization. The inclusion of dispformula = ~0 + allele in glmmTMB allows us to estimate allele specific residual variation, after accounting for the effects of variation in wing size due to allele, random effects of replicate vial and genetic variation for the influence of allele by DGRP background.

4.4b Broad Sense Heritability and Coefficient of Genetic Variation
Employing the estimates provided we calculated broad sense heritability (H^2) and coefficient of genetic variation (CV_G). Broad sense heritability was calculated as the proportion of total genetic variance (V_G) to total phenotypic variance (V_P) such that an H^2 value of 1 indicates that all phenotypic variance is due to genetic effects, while an H^2 value of 0 indicates that all phenotypic variance is due to environmental variance (4). CV_G provides a related measure scaled by group means (5) (Dworkin, 2005a).

$$H^2 = \frac{V_G}{V_P}$$

(4)

$$CV_G = \sqrt{\frac{V_G}{\mu}}$$

<div align="right">(5)</div>

To better evaluate the uncertainty for the within line (DGRP) variation, we implemented a Bayesian approach (using Markov Chain Monte Carlo to sample from the posterior distribution) for generalized linear mixed models, via MCMCglmm (Hadfield, 2010). This approach differs from the lme4 models in that it permits the use of double hierarchical modeling, allowing mutant alleles within the model to vary for residual variance (Hadfield, 2010). Unlike glmmTMB this more easily enables us to estimate sampling uncertainty to generate confidence intervals. Through this method we can differentiate between and biologically capture the combined effects of environmental and stochastic variability. While using this approach we also accounted for the effects of replicate vials and mutant alleles within DGRP groups. It should be noted that this approach achieved very similar results as the lme4 and glmmTMB model with respect to fixed and random effects and among line variation genetic variances and covariances.

4.4c Levene's Statistic
To further understand the relative contributions of allelic effects, DGRP effects and their interactions on among-individual, within-line variation, we calculated Levene's statistic in its median form for within line variation. This is a useful statistic as it does not rely on normally distributed data like standard deviation and variance, and large datasets are not needed like for the coefficient of variation (Dworkin, 2005b; Marie Anne Félix & Barkoulas, 2015; Schultz, 1985). To calculate Levene's statistic in is median form the absolute deviation of each individual (*i*) is taken from the median of each group (6) (Dworkin, 2005b; Marie Anne Félix & Barkoulas, 2015; Schultz, 1985).

$$LS_{ijk} = |x_{ijk} - md(x_{jk})|$$

(6)

Where LS_{ijk}, is the levene's deviate for individual i, with wing size x_{ijk}, and $md(x_{jk})$, is

the median value for the jth allele and k^{th} DGRP.

4.4d Levene's Statistic Generalized Linear Mixed Modeling
   Once we calculated the Levene's statistic we modeled the relationship of the statistic with

mutant allele with the random effect of replicate vials and the random intercept and slope of the

mutant alleles within the DGRP groups as above. However, as the distribution is folded (because

of the absolute values on the deviates) we used a gamma distribution (continuous positive

valued) with a log link function utilizing glmmTMB. Using the coding conventions of lmer and

glmmTMB, this model is fit as:

   glmmTMB(LS ~ allele + (1| replicate_vial) + (0 + allele | DGRP),
      family = Gamma(link = "log"))

   The implementation of a gamma distribution was necessary because all our values were

continuous with none of the values below zero. However, gamma distribution cannot handle

zeros in the dataset. To deal with this, we added a small constant to all response values. We

found the approximately lowest value of Levene's deviates and added 10% of this value to all

observations (5.75×10^{-7}). A large difference between this model and the previously fitted models

is that we no longer allow the residual variation in dispersion as this is what we are estimating

through modeling the Levene's statistic.

   Initially we had trouble fitting the model due to convergence errors. Convergence errors

are a result of the model not stably converging on a single estimate. As such, we fit the same

model using multiple optimizers in glmmTMB and lme4 and observed similar results among

them. Notably the variance-covariance matrices and fixed effects were similar, showing that the

average per individual variation within alleles was similar as well as the correlations of among

individual within line variances displayed similar results across models.

4.4e Procrustes Superimposition & Geomorph Modeling
   Next, we wanted to understand how shape is affected by the mutant alleles and if there

are any observable pattern. To understand the effect size has on shape we calculated centroid size

ensuring that we conducted Procrustes superimposition on the landmarked wings (Adams &

Otárola-Castillo, 2013; Baken et al., 2021). Procrustes superimposition optimally translates,

rotates, and uniformly scales the objects of interest so that their placement and size in space is

accounted for. Once calculated centroid size was extracted, we transformed the centroid size to a

logarithmic scale then modeled the relationship of wing shape with log centroid size while

accounting for the effects of the genetic background and the mutant allele employing the

Geomorph R package (Adams & Otárola-Castillo, 2013; Baken et al., 2021). We conducted this

analysis of variance using residual randomization for type 1 and type 2 sum of squares for 1000

permutations within each analysis and found similar results with both. We report type 1 results as

this iteration considers portions of the model that occur in sequential order to allow for

observation of allometric effects first (in other words, account for the effects of size on shape

prior to considering effects of allele or DGRP). Type 2 analysis differs as it considers all main

effects and adjusts the main effects of the model's results based on all other effects. Both type 1

and type 2 give similar results (not shown). Type 1 was chosen as we recognized that size effects

are closely tied to allelic effects, so we wanted to account for the size effects first then look at the

allelic and genetic background effects and how they affect wing shape.

$$procD.lm(shape \sim logCS * strain * allele,$$
$$data = wings, SS.type = "I", iter = 999)$$

4.4d Principal Component Analysis, Phenotypic Integration, and Total Variance

To examine patterns of variation for shape I utilized principal component (PC) analysis to perform dimensional reduction based on major axes of variation in the data, and then plotted the data for the first few principal components (ordination plots). Principal component analysis (PCA) is a multivariate dimension reduction technique that analyzes data described by several dependent variables which are typically inter-correlated (Abdi & Williams, 2010). The goal of a PCA is to extract important information from the data and display it in orthogonal variables called principal components (PCs). Doing this allows for the display of the patterns of similarities of the dataset and the variables as points on ordination plots allowing for the observation of variation within the dataset. These PCs are linear combinations of the original variables in the dataset and is accomplished through single value decomposition to create the eigenvalue of that PC (Abdi & Williams, 2010). Next, we sought to understand patterns of within-line variance and covariances. To assess the variance in shape within each combination of *miniature* allele and DGRP strain the total variance was estimated. The total variance is the sum of Procrustes residual landmark variances, computed as the sum of the trace of the relevant variance-covariance matrix (Pesevski & Dworkin, 2020). Total variance does not account for covariation, and as such we used "Phenotypic Integration" to capture aspects of variation in different directions of shape space (Haber, 2011). Phenotypic integration for each variance-covariance matrix was estimated using the evolQG library (v0.2-9) in R (Melo et al., 2016). This approach essentially computes the principal components for shape for each combination of allele and DGRP and examined the evenness of magnitudes of the variances in each of these directions (the eigenvalues). Specifically, phenotypic integration estimates the standard deviation among eigenvalues. If the PCs examined are similar in magnitude, each direction of variation is about the same, and the trait is not highly integrated as the variation in shape is spread (approximately

equally) in all possible directions. In such a case, there would be a small standard deviation observed between PCs. However, when one PC accounts for a large amount of variation (in other words, the first eigenvalue is much larger than all the rest) you will have a large standard deviation. In other words, the lower the integration the more the object appears as a "soccer ball" in multivariate space. The higher the integration the more the object appears as an "American football" in multivariate space. While the higher to total variance the large the "ball" in multivariate space. The higher the integration value the more directionality there is to the variation in wing shape observed.

4.5 *scalloped* Manipulating gene expression levels

To perturb the system a *scalloped* mutant allelic series was employed that ranges from very weak to very severe phenotypic effects (Figure 13, Table 1.1). Notably, this is the same allelic series that has been used previously in experiments involving wing size (Daley, 2019). A key caveat to this experimental design is the use of only hypomorphic alleles, giving us no indication of how the system will react to an overexpression of Scalloped. As mentioned previously with the sd^{ETX4} and sd^1 allele each proposed allele has been introgressed into the Oregon-R laboratory strain (Daley, 2019). Previous experiments attempted to titrate Sd expression through the application of a *nubbin*-Gal4 driver. Results from this experiment displayed differences in lethality among different temperature regimes and different strains for Sd overexpression (Daley, 2019). For *sd* knockout the results showed differing responses to the different temperature regimes between the two backgrounds examined. Whereby, between the tested genetic backgrounds Samarkand and Oregon-R the Oregon-R background displayed higher sensitivity to perturbation (Daley, 2019). However, these results were not obtained without difficulty as two *vestigial*-Gal4 drivers were tested and found to have an incomplete

expression pattern in the wing pouch displaying the acknowledged mosaic expression from the

UAS Gal4 system (Halpern et al., 2008).
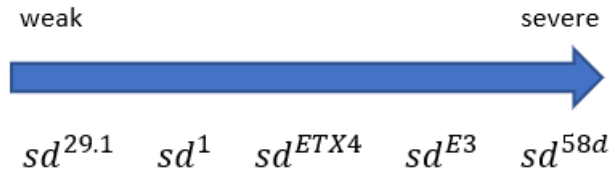
Figure 4.1: Graphical representation of the *scalloped* allelic series from weak to severe.

4.6 *scalloped* Crossing Scheme

The s*calloped* mutant allelic series was crossed to a subset of 9 DGRP lines from

previous experiments that range from having severe to weak genetic background effects on wing

size (Supplemental Figure 1.1, Supplemental Table 8.2). 15-50 virgin mutant females and 15-30

DGRP males were crossed in a cage at $24 \circ$C and allowed to lay onto apple juice agar plates with

an orange juice yeast paste smear. When conducting the crosses, we ran into issues with sexing

certain DGRP lines (likely due to hybrid dysgenesis) leading to the narrowing of the subset lines

from 9 DGRP backgrounds to 6 and resulting in the replacement of one of the originally chosen

9 with a different DGRP background (Figure 4.2, Table 4.1). Over the course of 6 crossing

blocks each mutant allele has been crossed to each DGRP line twice.

Table 4.1: List of Drosophila Genetic Reference Panel (DGRP) genotype numbers and their respective Bloomington stock numbers utilized in experiment 2. The replaced DGRP line that was substituted into the experiment due to hybrid dysgenesis has been coloured red.

DGRP Genotype	DGRP Bloomington stock number
DGRP038	28125
DGRP391	25191
DGRP301	25175
DGRP385	28191
DGRP229	29653
DGRP048	55016
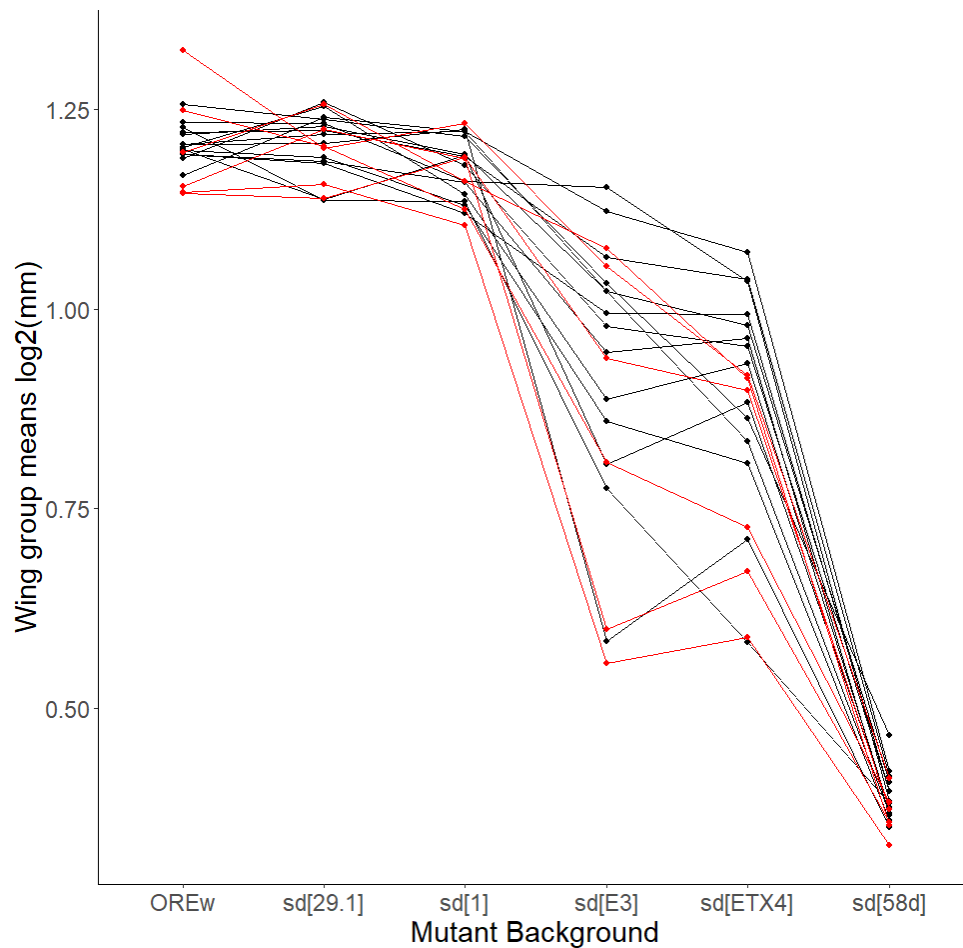
Figure 4.2: A reaction norm of the mean plot displaying wing group means for the scalloped allelic series with the DGRP lines utilized for gene expression analysis highlighted in red. Each line represents a distinct DGRP strain with each dot representing group averages in wing size. The goal was to employ DGRP lines that captured the range of among line variation for wing size (red lines).

4.7 *scalloped* **Larval staging, Larval sexing, Wing Imaginal Disc Dissection and Wing Imaginal disc Collection**

Larva were staged to allow for dissection in late third instar before the ecdysone pulse induces molting +/- 1 hour of the 80-hour mark. Once staged the larva were sorted by sex through examination of the larva for the appearance of testes which presents as a large clear oval on the posterior half of the larva. When sexing in four of the nine original lines the male gonads appeared smaller or not present, we have attributed this to hybrid dysgenesis (Crews & Gore,

2014). It was due to this that we reduced the number of lines to be examined to 6 and replaced

one of the four lines. Once sexed, male larvae were everted in PBS and stored in RNA later in

Eppendorf tubes. The everted larvae were then dissected in a 1:1 mixture of RNA later and PBS

to remove the wing imaginal discs. The discs were stored in RNA later in Eppendorf tubes of 30

discs per tube and stored at $-80°C$ until qPCR analysis.

4.8 *scalloped* **qPCR**

The collected discs underwent RNA extraction following standardized laboratory

protocols applying the MagMax -96 Total RNA Isolation Kit. Once RNA was extracted from the

imaginal discs, cDNA synthesis and qPCR employing TaqMan assays was completed. This was

done to examine changes in mRNA levels for a list of target genes involved in wing development

whose roles in development have been previously outlined above (Table 4.2). We aimed to

include both *ribosomal protein L32* (*RPL32)* and *TATA-box binding protein (TBP)* as the

normalization genes as both genes have been shown to be stably expressed in third instar wing

imaginal discs despite various forms of morphological variation and implementing two genes

reduces error (Kozera & Rapacz, 2013; Matta et al., 2011). Unfortunately, due to difficulties

with shipping TaqMan assay probes we were unable to conduct qPCR on proposed genes

involved in wing development in the timeline originally set forth. As such we have completed

qPCR on *sd, vg,* and *cycE* and measured mRNA expression levels exploiting the ΔC_t method to

discern mRNA levels. In qPCR result are expressed as a cycle threshold (C_t) which is the

amplification cycle number where the fluorescence of the reaction well crosses the threshold

value (Livak & Schmittgen, 2001). The ΔC_t is the difference in C_t values for the gene of interest

and the endogenous control gene. The mean ΔC_t values are means of the ΔC_t values for multiple

technical replicates of the same gene of interest (Livak & Schmittgen, 2001). A caveat to this

approach is the assumption that gene expression (mRNA levels) is a representative readout of

47

protein expression, mRNA half-lives, protein activity, protein half-life, transcription rates and

protein interactions (Buccitelli & Selbach, 2020). Furthermore, this is a temporally specific

timepoint of late 3rd instar larva gene expression levels. To attempt to mitigate these limitations

we aimed to target genes up and downstream of Sd activity as an increase or decrease in these

mRNA levels may better reflect the change in expression we aim to induce. Further, the addition

of these genes involved in the wing developmental network gives greater insight into the effects

of the genetic background on the developmental network itself. The ΔC_t values for target genes

sd, vg, and *cycE* were collected from 36 distinct crosses with two replicates per crosses and

minimum two technical replicates. To account for block effects, I made sure to include

genotypes that were also done previously and overlapped with previous plates, to enable proper

estimation of plate effects without confounding effects.

Table 4.2: List of target genes targets for use qPCR to investigate the relationship of genetic background effects on gene expression and phenotypic expression. Direct targets of Sd are bolded, normalizer genes are underlined.

wingless	*decapentaplegic*	*yorkie*	***spalt***	*distal-less*	<u>*TATA-box binding protein*</u>
cut	***blistered***	***death-associated inhibitor of apoptosis 1***	***cyclin-E***	*vestigial*	<u>*ribosomal protein L32*</u>

4.9 *scalloped* Statistical Modeling

Statistical analysis began with the fitting of a linear model with the glmTMB R package

to correct for PCR plate effects (block effects) by setting the response variable as the mean ΔC_t

values, the predictor as the targeted gene, and including a variable for random plate effect (Bates

et al., 2015) Using the coding conventions of lmer and glmmTMB, this model for *sd* is fit as:

glmmTMB(delta_ct_mean ~ allele + (1|Plate_ID) + (0 + allele|DGRP),
    data = wing_expression_sd

Once the mean ΔC_t values were model corrected we began by examining the overall expression differences between the *scalloped* alleles. Next, we began model fitting examining various process models, including a Michaelis Menten curve, followed by a Gompertz curve, then a Monod curve, next an additive logistic curve, subsequently a three-parameter logistic curve, and finally a four-parameter logistic curve. With initial data, the fit of the four-parameter logistic was found to be the best fit through the Akaike information criterion (AIC) and allowed us to extract information of the minimum and maximum points of responses, the inflection point, and the hill coefficient. Model fits were performed in R using custom scripts written by Dr. Ian Dworkin. Estimation was performed using maximum likelihood estimation, using the mle2 wrapper in bbmle (v1.0.24) for the optim function.

5. Results

5.1 *miniature* Size Results
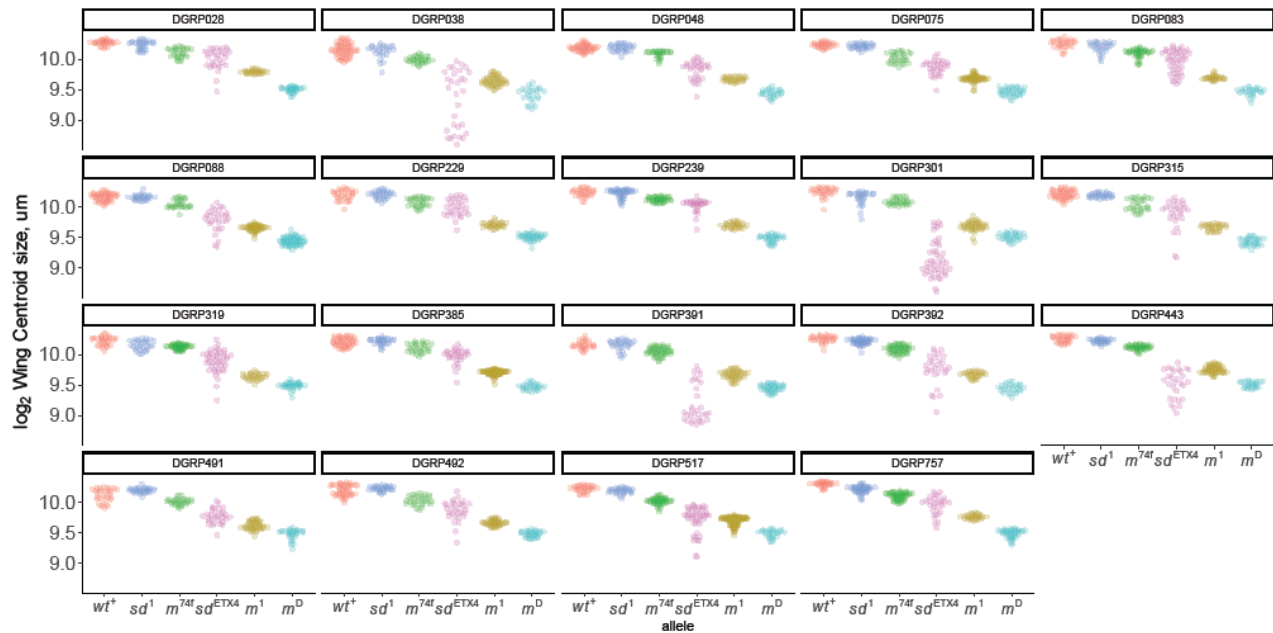
Figure 5.1: Relationship of Log2 Wing Size (μm) with *miniature* and *scalloped* mutant alleles by DGRP background with background dependence observed for among and within-line variance for scalloped alleles but not miniature alleles. Each point represents a distinct wing measurement. There is no change in allelic order by background but there is an observed increase in among and within line variation for moderate phenotypic effect sd^{ETX4} but not for the moderate phenotypic effect allele m^1. This is indicative of the *miniature* allelic series differing from the predicted mechanistic model of background dependence.

To begin our size analysis, we first visualized the effects of the mutant alleles by plotting the raw data of individual flies (log$_2$ wing size in μm) with the alleles used in the *miniature* allelic series, sd^{ETX4} and sd^1 by DGRP background. (Figure 5.1). There is an observable pattern of decreased mean wing size for the *miniature* allelic series from wild-type to m^D that remains consistent across DGRP backgrounds (Figure 5.1). Furthermore, we see a lack of variability within *m* alleles for the severe (m^D), moderate (m^1), and weak (m^{74f}) phenotypic effect alleles on wing size (Figure 5.1). Regarding the s*calloped* alleles there is also a relatively low amount of variability in the sd^1 weak phenotypic effect allele. In contrasts, there is a large amount of variability in the sd^{ETX4} phenotypic effect allele (Figure 5.1). Further, DGRP genetic background

effects can be seen between DGRP lines regarding sd^{ETX4} expression with some lines displaying large within line variation, such as DGRP038, DGRP391, and DGRP301 and some lines displaying relatively low within line variation, such as DGRP048, DGRP075, and DGRP385 (Figure 5.1). This change in variation is not observed for the m^1, m^{74f}, m^D, and sd^1 alleles (Figure 5.1). Overall, by examining the raw data there is observable variation in $\log_2$ wing size (μm) among and within DGRP genetic backgrounds for sd^{ETX4} but not for the miniature allelic series and sd^1.

5.2 Quantitative estimates for wing size, variance, H^2, and CV$_G$ for *miniature* and *scalloped*

To quantify the affects of *miniature* and *scalloped* mutations on wing size mean wing size for each allele among all DGRP strains was estimated (Table 5.1) in a linear mixed model. For the *miniature* allelic series, the phenotypic range is characterized with m^D having a larger affect on wing size than m^1 which has a larger affect on wing size than m^{74f} (Table 5.1). Regarding the s*calloped* alleles sd^1 shows the weakest affect on wing size in the study and sd^{ETX4} displays a moderate affect on wing size in the study (Table 5.1). Each allele was found to be significantly different from one another with a P-value of 0.01 or less with most having a P-value of $< 2^{-16}$ (Table 5.1).

Phenotypic variance among DGRP lines for all alleles was measured utilizing model adjusted estimates of variance (Table 5.1). These estimates indicate the genetic variance among DGRP for the sd^{ETX4} allele was much higher than wild-type, all *miniature* alleles, and sd^1. This increase in variation can be further observed in the drastic increase in the spacing between DGRP lines for moderate phenotypic sd alleles in Figure 5.2A in comparison to all m alleles in 5.2B. This drastic change in variation for sd can be further visualized by each of the m alleles showing a relatively smaller amount of genetic variance among DGRP lines, and largely similar

magnitudes of genetic variance for the weak, moderate, and severe mutant alleles compared to the moderate phenotypic effect allele sd^{ETX4} (Figure 5.2B, Figure 5.3, Table 5.1). When comparing among line variation between different DGRP backgrounds *miniature* appears to be characterized by a largely linear relationship (Figure 5.2B, Figure 5.3, Table 5.1). This differs from previously generated data on a *scalloped* allelic series where there is an observed increase in among line variation for moderate phenotypic effect *sd* alleles on wing size relative to weak and severe phenotypic effect *sd* alleles (Daley, 2019, Figure 5.2A, Figure 5.3).

When examining H^2 and CV_G it becomes apparent that both are much higher for sd^{ETX4} than the *miniature* allelic series, wildtype, and sd^1. Indeed, as highlighted in blue text for sd^{ETX4}, the genetic variance (and CV_G) is approximately eight to ten times higher for sd^{ETX4} than all other alleles (Table 5.1). Notably the broad sense heritability is higher, but only about 2X higher. This is both due to the limits on H^2 (bounded at 1), and due to the increased environmental variance observed for this allele described below.

Table 5.1: Model effects from size glmmTMB model where miniature displays a lack of among line variance. The statistical model estimates for the miniature and scalloped alleles. N=4096. ANOVA analysis: Mutant. In this table the variance represents the among line (DGRP) variance for wing size (total genetic variance). Standard Deviation is the square root of this estimate. sd^{ETX4} has been highlighted blue to better exemplify the differences between other alleles.

Allele	Mean Estimate (log_2 wing size)	Standard Error of the mean	P-Value	Genetic Variance (DGRP)	Standard Deviation (DGRP)	Broad Sense Heritability (H^2)	Coefficient of Genetic Variation (CV_G)
Wildtype (ORE)	10.21	0.011	$< 2^{-16}$	0.0019	0.044	0.445	0.85
sd^1	10.19	0.009	0.01	0.0007	0.026	0.239	0.50
m^{74f}	10.07	0.009	$< 2^{-16}$	0.0016	0.040	0.469	0.78
sd^{ETX4}	9.76	0.058	$< 2.9^{-15}$	0.0669	0.259	0.736	5.30
m^1	9.69	0.006	$< 2^{-16}$	0.0017	0.041	0.528	0.84
m^D	9.47	0.009	$< 2^{-16}$	0.0006	0.025	0.231	0.53
Replicate Vial				0.0002	0.013		
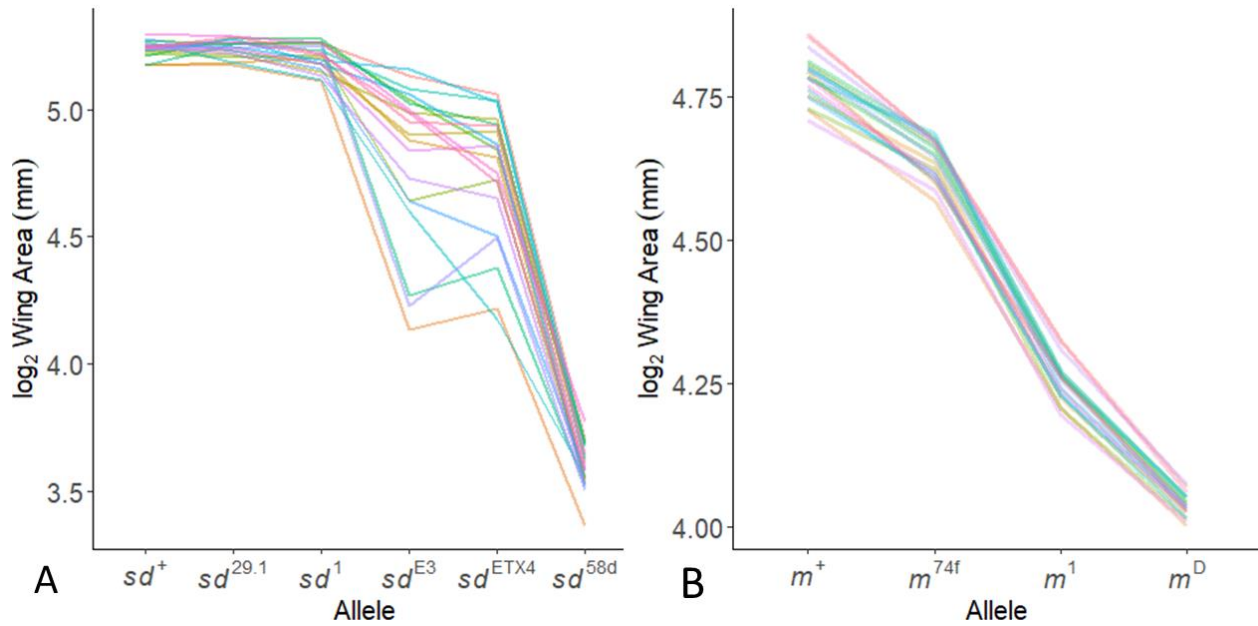
Figure 5.2: Reaction norm plots displaying differences in the background dependence for wing group means between the *scalloped (sd)* (A) and *miniature (m)* (B) allelic series. Each coloured line on the graphs represents a distinct genetic background (*sd*: 20, *m*:19 DGRP backgrounds, data for *sd* alleles was generated using data from Caityln Daley, 2019). There is an observed non-linear relationship for the *scalloped* allelic series and a much more linear relationship for the *miniature* allelic series.
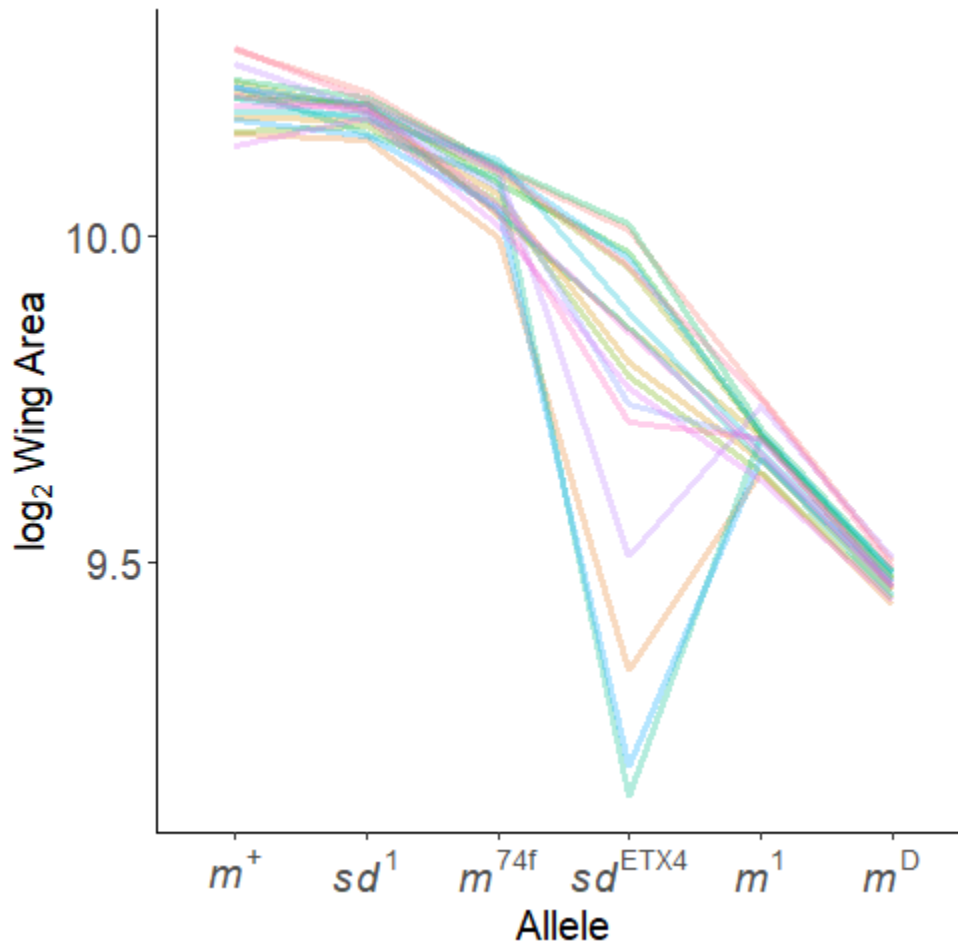
Figure 5.3: Reaction norm plots displaying wing group means of the *scalloped (sd)* and *miniature (m)* alleles exemplifying a linear relationship for *m* and non-linear relationship for *sd* for genetic background effects. Each coloured line on the graphs represents a distinct genetic background (19 DGRP backgrounds). There is an observable increase in variance and genetic background effects for the moderate sd^{ETX4} allele relative to the weak phenotypic effect sd^1 allele and all *miniature* alleles.

5.3 Relationship of Mutational Severity with *miniature* and *scalloped* Allelic Expression

To assess if genetic background effects are specific to individual alleles, similar across

alleles of the same gene, or genes with similar mutational severity, genetic correlation

coefficients were calculated among *miniature* and *scalloped* alleles across DGRP backgrounds.

When examining the correlation of mutational severity across backgrounds, *miniature* is strongly

positively correlated with mutational severity (Figure 5.4B, Figure 5.5). The strongest correlation

is between wild-type and m^1 at 0.95 with the weakest being between m^{74f} and m^1 at 0.62 (Figure

5.4B, Figure 5.5). Perhaps most surprisingly, considering the results previously observed by Daley (2019) for *sd*, is the magnitude of the genetic correlations of the *m* mutant alleles with the wild-type alleles across the DGRP. Furthermore, even among most strongly correlated mutant alleles of *sd*, the genetic correlations were generally weaker. Both sd^{ETX4} and sd^1 show variable and weak correlations with mutational severity (Figure 5.5). When compared to previously investigated patterns of background dependence *sd* alleles show largely weak and variable correlations with mutational severity (Daley, 2019, Figure 5.4, Figure 5.5). The strongest positive correlation is between sd^{E3} and sd^{ETX4} at 0.74, the strongest negative correlation is between sd^1 and sd^{E3} at -0.31, while the weakest correlation is between sd^1 and sd^{ETX4}.
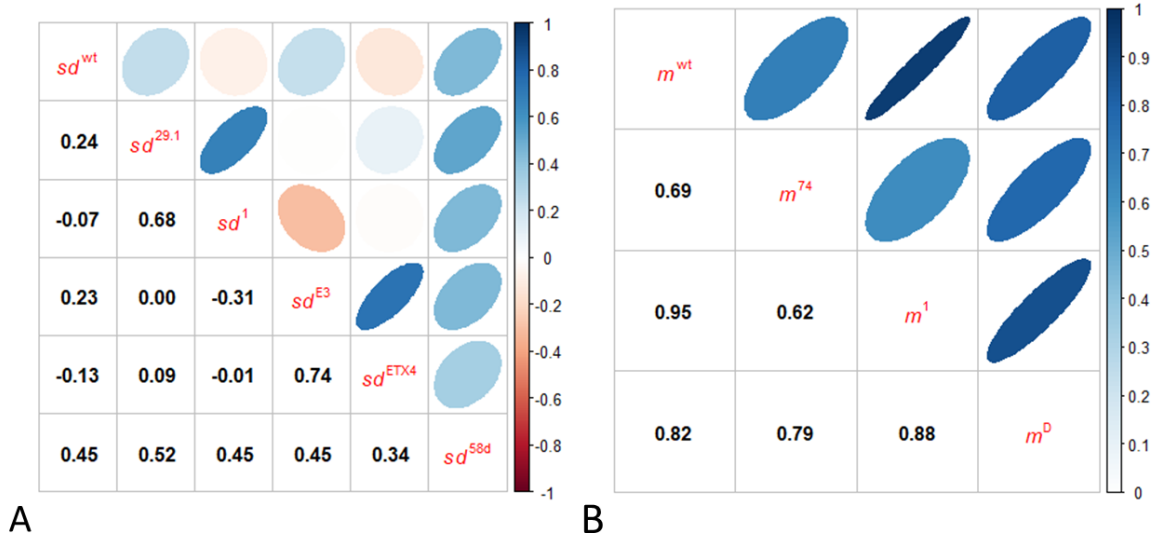
Figure 5.4: Differences in genetic correlations of *scalloped (sd)* (A) and *miniature (m)* (B) mutant alleles with mutational severity. The correlations display log2 wing area among wild-type genetic backgrounds (*sd*: 20, *m*:19 DGRP backgrounds, data for *sd* alleles was generated using data from Caityln Daley, 2019). A) The *sd* allelic series is characterized by a variable and moderate correlations with mutational severity while B) the *m* allelic series is characterized by a strong positive correlation with mutational severity.
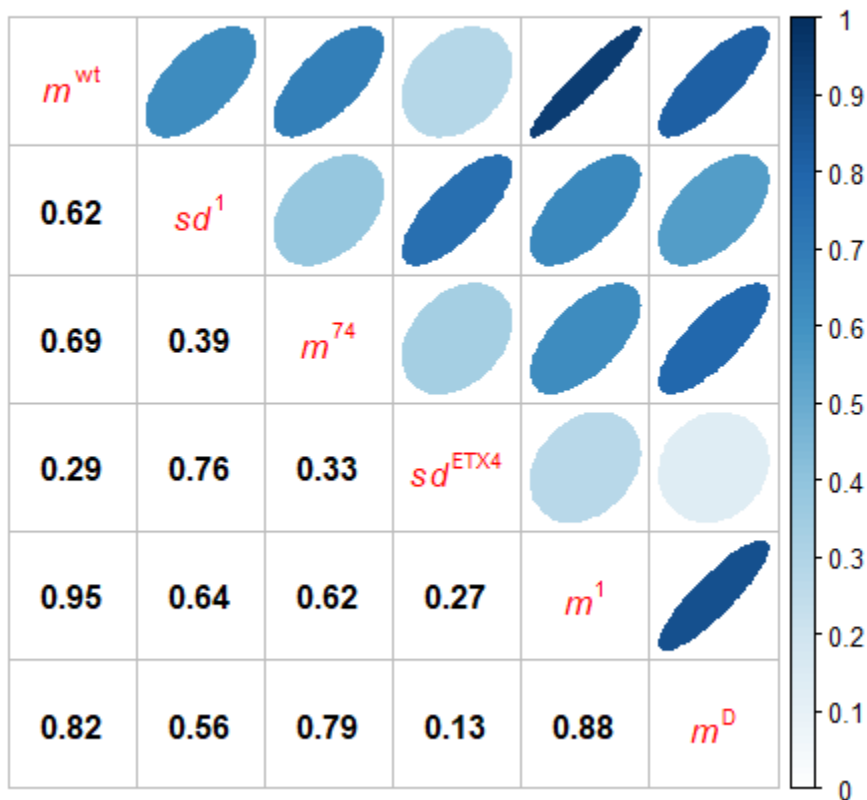
Figure 5.5: Genetic correlations of *scalloped (sd)* **and** *miniature (m)* **alleles with mutational severity.** The correlations display log2 wing area among wild-type genetic backgrounds (19 DGRP backgrounds). The *m* alleles display strong positive correlations with mutational severity while showing weak correlation with *sd* alleles while the *sd* alleles show weak positive correlations with mutational severity.

5.4 Relationship of Intra-Line Variability (Environmental and Stochastic Effects) with Mutational Effects for *miniature* and *scalloped*

To investigate the relationship of mutant alleles on environmental variances (in other words, within-genotype, among-individual variation) a Bayesian approach using Markov Chain Monte Carlo model was used to simultaneously estimate genetic and environmental variances for each allele (Figure 5.6). Another unique feature of *miniature* is the lack of increased variation observed regarding stochastic and environmental effects (Figure 5.6). This is a drastic shift from

sd^{ETX4} which displayed about a ten-fold increase in residual variation for moderate phenotypic

effect alleles relative to wild-type, *miniature* alleles, and sd^1 (Figure 5.6).

posterior distribution
log2 wing area
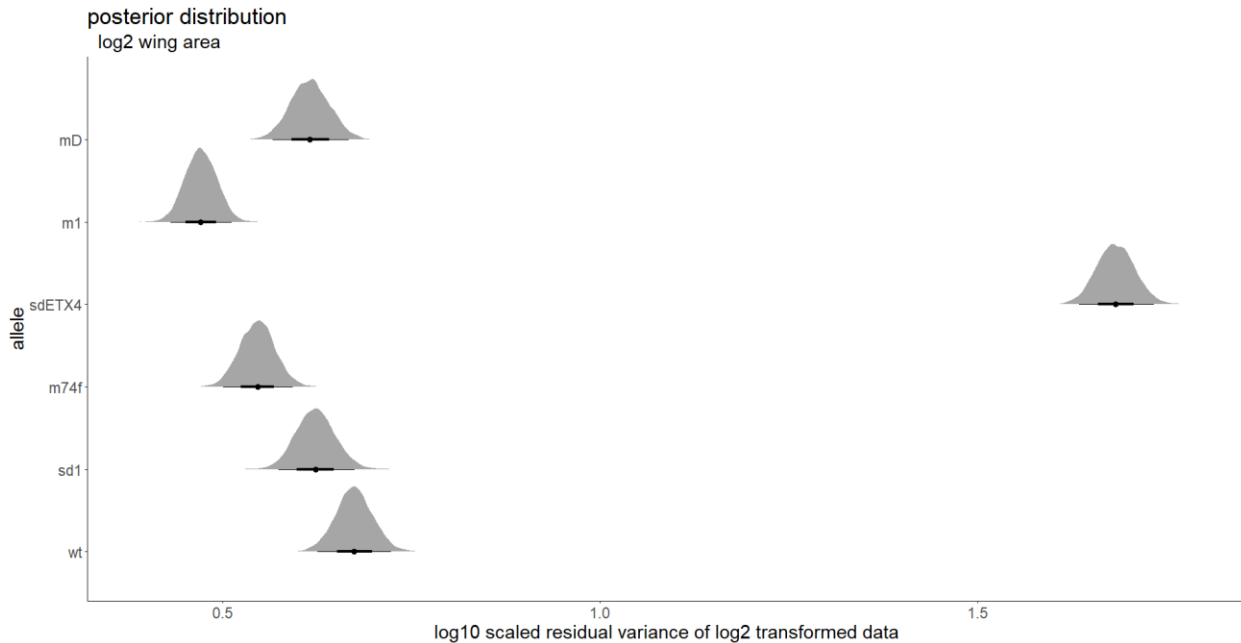
Figure 5.6: Posterior distributions for allele specific residual variation displaying a lack of variation for *miniature (m)* alleles relative to the moderate phenotypic effect *scalloped (sd)* allele. This is a measurement of within allele environmental variation from wild-type (wt) to m^D with higher residual variance indicative of increased variability due to stochasticity and environmental effects. There is an observed drastic increase of environmental sensitivity for the moderate phenotypic effect sd^{ETX4} allele relative to the weak phenotypic effect sd^1 allele and all *m* alleles. Black bars represent 95% credible intervals while grey shaded regions represent the full posterior distribution. Note the x-axis is on a $\log_{10}$ scale.

To better understand the relationship between these effects and environmental sensitivity

we computed Levene's deviates for the 19 DGRP lines by 6 alleles, to measure within-line

(intra-line) variation as a measure of environmental variability. Average estimates of intra-line

variability indicate that sd^{ETX4} displays about double the amount of within line variation among

DGRP lines than wildtype, *m* alleles, and sd^1 (Table 5.2, Figure 5.7, Supplemental Figure 8.3). It

is also clear that the variation among DGRP for within-line variance differs substantially among

lines. This is particularly clear for the sd^{ETX4} allele. Furthermore, both m and sd alleles display

variable genetic correlations among individuals for within-line variance as previously seen in

between line mutational severity (Figure 5.8). The strongest positive correlation occurred

between m^D and sd^{ETX4} at 0.87, the strongest negative correlation occurred between m^1 and m^{74f} at

-0.40, and the weakest correlation occurred between wild-type and sd^1 at 0.04 (Figure 5.8).

Table 5.2: Model estimates from the Levene's statistic glmmTMB model displaying low variation for *miniature* alleles and much higher variation for the *scalloped*^{ETX4} allele. The statistical model estimates for the miniature and scalloped alleles. N=4096. ANOVA analysis: Mutant. Model estimates are from a gamma distribution on a log link scale.

Allele	Mean Levene's Statistic Estimate (log)	Standard Error	Genetic Variance	Standard Deviation
Wildtype (ORE)	-2.63	0.091	0.0136	0.116
sd^1	-0.153	0.104	0.0736	0.271
m^{74f}	-0.0635	0.109	0.0647	0.254
sd^{ETX4}	0.999	0.107	0.1400	0.374
m^1	-0.272	0.0771	0.0645	0.254
m^D	-0.0635	0.0798	0.0228	0.151
Replicate Vial			0.0136	0.116
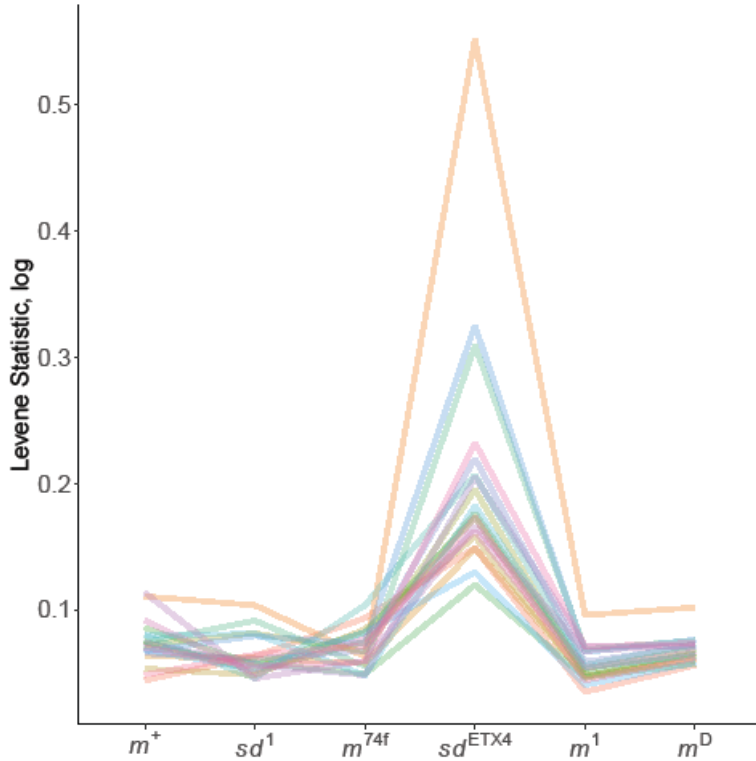
Figure 5.7: Reaction norm displaying Levene's statistic on a natural logarithmic scale with a lack of within-line variation for *miniature* and *scalloped¹* alleles and large within-line variation for the *scalloped^{ETX4}* allele. Each coloured line on the graphs represents a distinct genetic background (19 DGRP backgrounds). There is a lack of within-line variation due to environment and stochastic noise observed for all *miniature* alleles but not for all *scalloped* alleles.
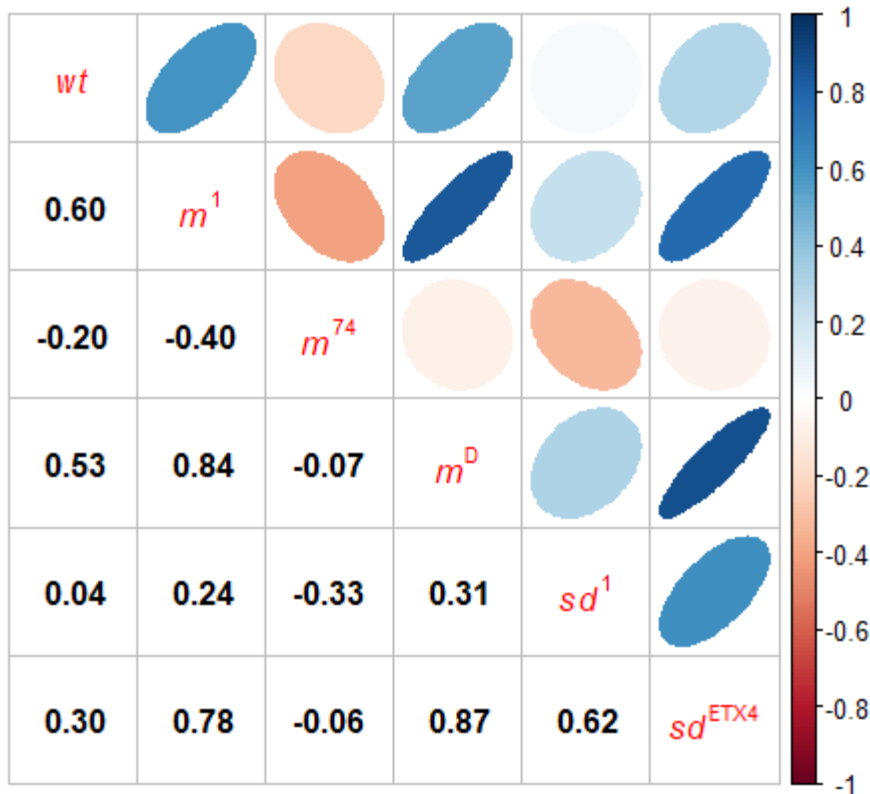
Figure 5.8: Genetic correlations for intra-line variance of *scalloped* and *miniature* mutant alleles across DGRP lines with mutational severity. The correlations display $\log_2$ Levene's statistic among 19 DGRP genetic backgrounds. There is an observed variability in correlations of intra-line variance with mutational severity for both *miniature* and *scalloped* alleles.

5.5 Procrustes Superimposition and Allometric Effect on *miniature* Wing Shape

To begin our shape analysis on the effects of the *miniature* alleles (m^+, m^{74f}, m^1, m^D), we first conducted Procrustes superimposition to optimally translate, rotate, and uniformly scale the wings to allow for comparability of the 15 landmarked points (Figure 5.9). Next, we investigated the effect wing centroid size (CS) (wing size) has on overall wing shape. Using model adjusted estimates, each term within the model was found to be highly significant but the variance in *miniature* wing shape is not simply due to allometric effects with centroid size (Table 5.3, Figure 5.10) which accounts for 60.7% of the variation in shape. This large contribution of allometry is

unusual for *Drosophila* wings, but not surprising for this data set given the profound impact that the miniature alleles have on wing size. Interestingly, even after accounting for all isometric and allometric effects of size on shape, the miniature mutant alleles still account for 24% of all variation in shape, while the wild-type background accounts for 5.5% of shape variation (Table 5.3). It should be noted that analyzing mean wing centroid size across DGRPs follows the same pattern observed by the wing size measurements.
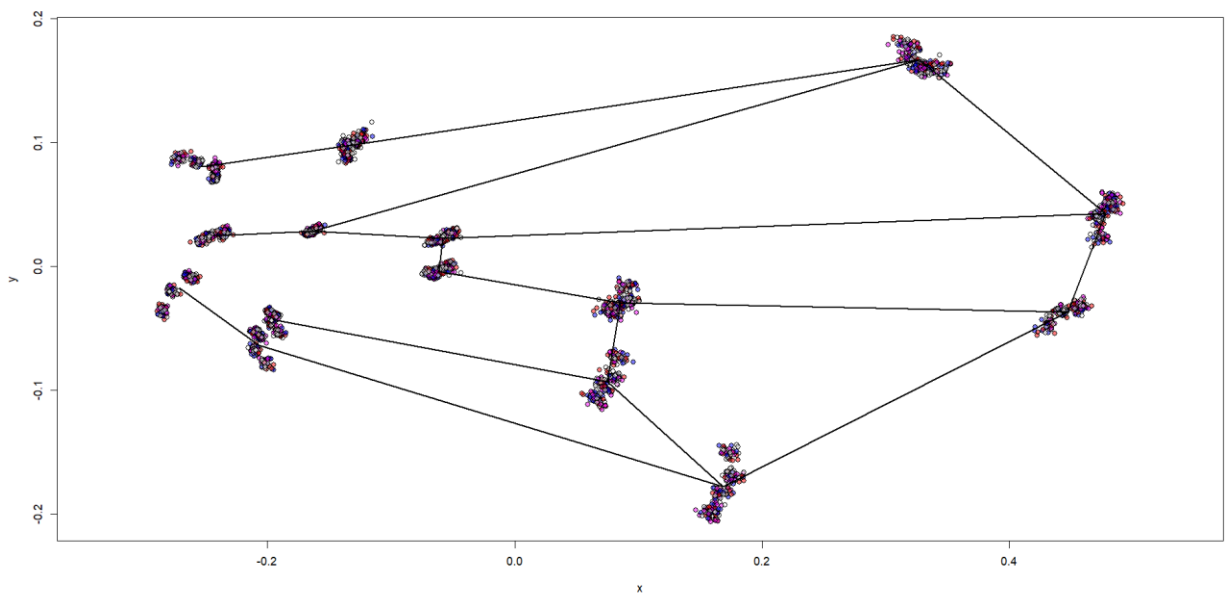
Figure 5.9: Skeleton diagram of a combination of 200 random miniature alleles (m^+, m^{74f}, m^1, and m^D) 15-point landmarked wings exemplifying both the possible locations of the 15 landmarks and the variation in positions of the 15 landmarks. Each point represents a landmark for a particular wing. There is observed clustering of some of the landmarks based on the genotype the sample was taken from.

Table 5.3: Type 1 (sequential) Analysis of Variance using residual randomization exhibiting the large effect wing size has on wing shape. Permutations = 1000. Ordinary least squares method. Model adjusted estimates from Geomorph shape analysis. Size (logCS) has the largest effect on wing shape followed by allelic effects (allele) with genetic background effects (strain) having a modest effect on wing shape (R^2). Note that interaction effects, while significant have relatively modest contributions on shape after having accounted for main effects (R^2).

Model Term	Degrees of freedom	Sum of Squares	Mean Squares	R^2	P-Value
logCS	1	3.35	3.35	0.607	0.001
strain	18	0.31	0.02	0.055	0.001
allele	3	1.33	0.44	0.24	0.001
logCS:strain	18	0.02	0	0.004	0.001
logCS:allele	3	0	0	0.001	0.001
strain:allele	54	0.05	0	0.008	0.001
logCS:strain:allele	54	0.02	0	0.003	0.001
Residuals	2699	0.45	0	0.082	
Total	2850	5.52			

When we conduct a principal component analysis on the observed landmark residual data (in other words, prior to model fitting), we observe strong clustering based on mutant alleles across PC1 and PC2 (Figure 5.10). This clustering of data by alleles is also observed in PC3 and it isn't until examination of PC4 and PC5 that clustering on allelic effects become imperceptible (Figure 5.10, Figure 5.11, Figure 5.12). Furthermore, 78.51% of the shape variation occurs on PC1 due to shape and allometric size variation (Figure 5.10). When examining a scree plot of the proportion of variance accounting for each principal component, PC1 accounts for 78.5% of the shape variation while PC2 accounts for 7.1%, and PC3 accounts for 5.2% (Figure 5.13). This is indicative that before model fitting and estimation allometric size and allelic variation account for large proportions of variation in shape for *miniature* mutation wings, with the majority the

variation in wing shape separating over PC1, 2, and 3.
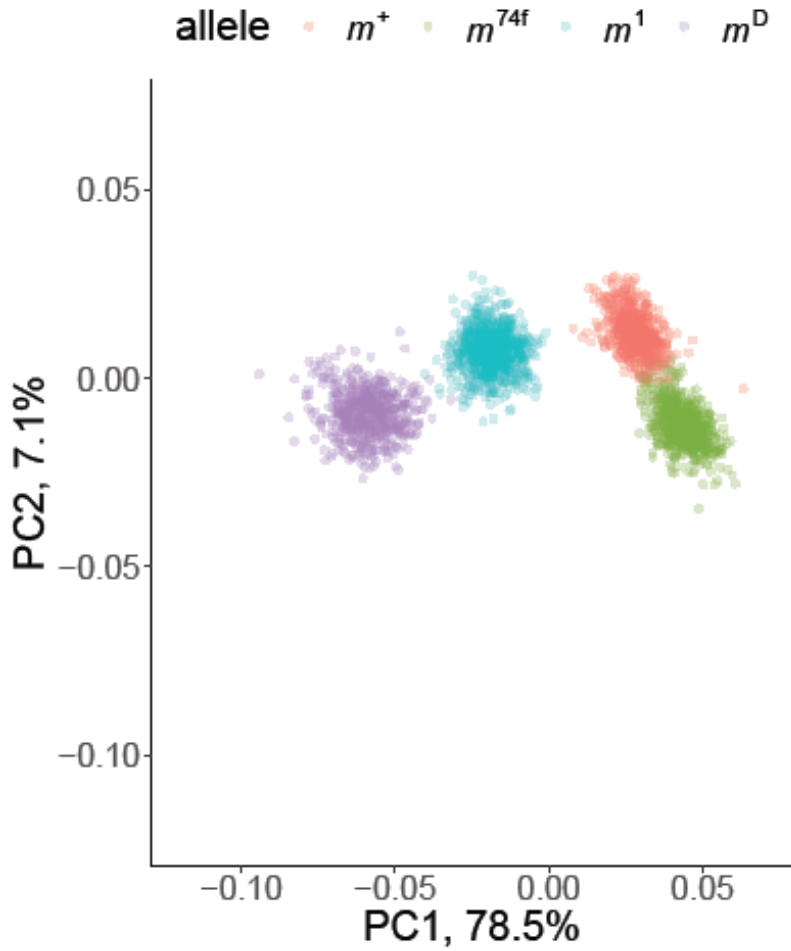
Figure 5.10: Ordination plot of shape variation for the *miniature* alleles (PC1/2) where most variation in wing shape occurs across PC1 related to wing size and clustering based on allelic effects is exemplified. Each dot represents a distinct wing.
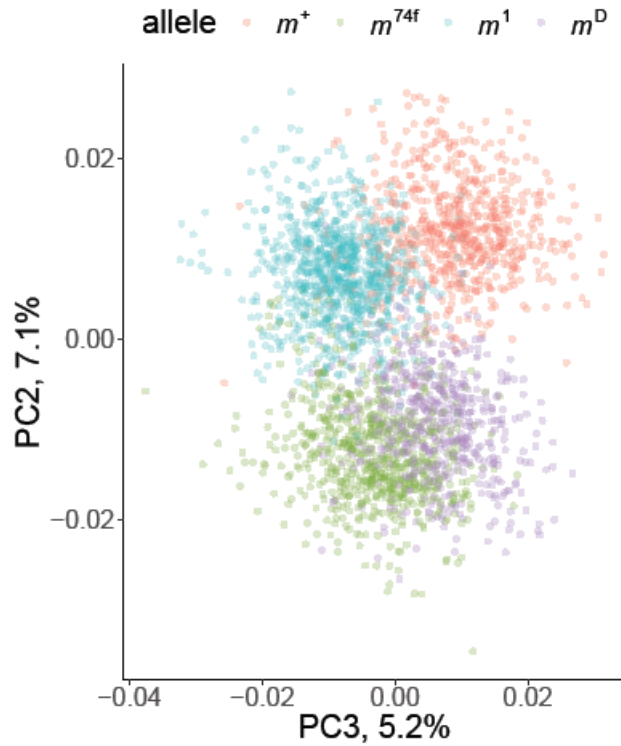
Figure 5.11: Ordination plot of shape variation for the *miniature* alleles (PC2/3) displaying separation of mutate alleles occurring with PC2 and PC3. Each dot represents a distinct wing. Though most variation in shape is captured by PC1, in PC 2 and 3 there is still clear separation of mutant alleles.
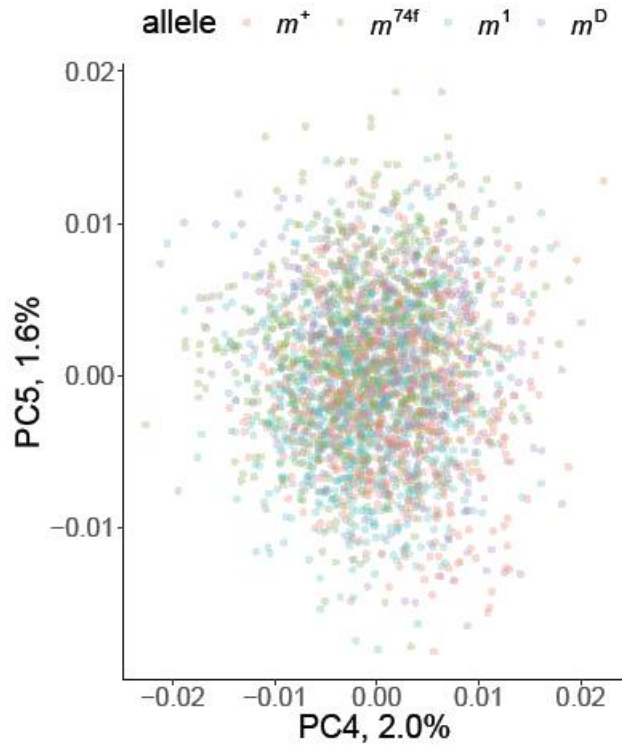
Figure 5.12: Ordination plot of shape variation for the *miniature* alleles (PC4/5) where there is a lack of observable clustering based on allelic effects. Where each dot represents a distinct wing. Separation of mutant alleles can be observed in PC 1, 2, and 3, once you examine PC 4 with PC 5 this separation is not observable.
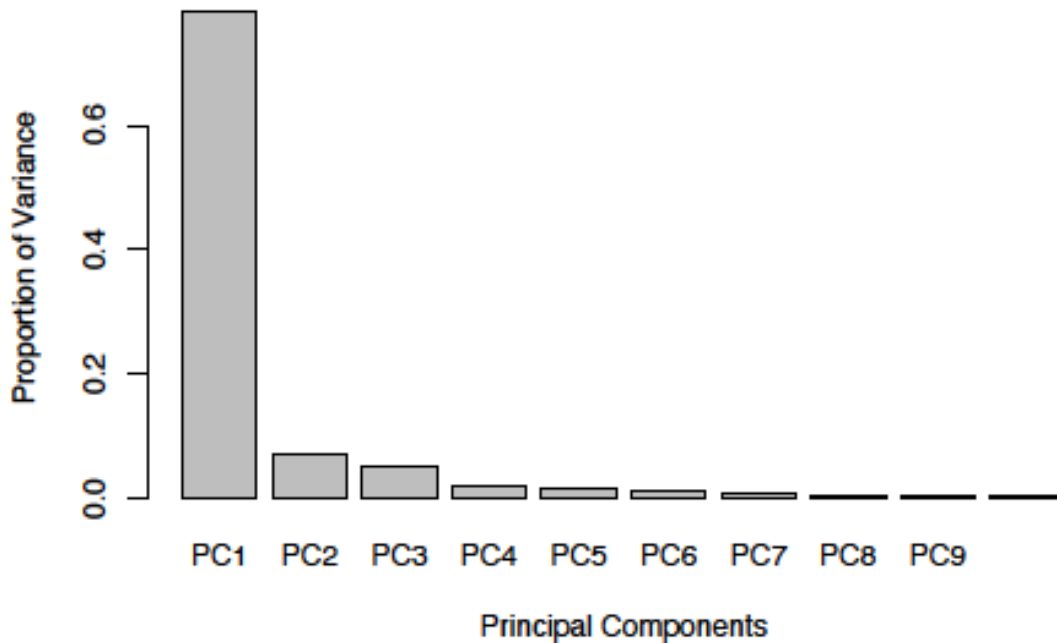
Figure 5.13: Scree plot of *miniature* alleles principal component analysis exemplifying most variation in wing shape occurs in PC1. Each bar represents a PC from PC1 on the left to PC 10 on the far right.

5.6 Relationship of *miniature* Wing Size with Wing Shape

Allometric effects typically contribute a great deal to shape variation, and this is particularly likely for this dataset given the profound effects of *miniature* on wing size. As such, we accounted for common allometric effects across all strains and alleles, and we conducted a principal component analysis for the residual shape variation (Figure 5.14, Figure 5.15). Once common allometric effects are accounted for PC1 accounts for 55.3% of the remaining shape variation, while PC2 and 3 represent 14.6%, and 8.6% of the variation respectively. While there is still clustering of datapoints by allelic mutations (Figure 5.14), it becomes imperceptible when examining PC3 and PC4. With majority the variation in wing shape separating over PC1, 2, and 3. Visualizations of the effects of PC1, 2, and 3 on wing shape change after accounting for allometric size effects can be seen in Figures 5.17, 5.18, and 5.19, where grey points and lines

represents wild-type wings while black points and lines represents changes along the principal component axis.

With the modeled residual variances and standard deviations we computed the total amount of variation remaining after accounting for allometric size effects and found that 39.3% of variation exists in wing shape once accounting for allometric size, which is a close approximation with results from the type 1 ANOVA analysis (Table 5.2). We then sought to understand the relationship between allometry, and wing size and plotted model fitted PC 1 values against wing size as the predictor variable in the model (Figure 5.20). From this we can observe changes in the allometric relationship and observe a large effect due to mutant alleles with wing projections separating based on mutant allelic effects (Figure 5.20). Furthermore, from this fit strain level effects can be observed where some effects are slightly different (as observed by the changing dotted line orientations) most however are not (Figure 5.20). When examining patterns of variation within allele the there are similar patterns among DGRP lines regarding variation in shape due to size and a large allelic effect resulting in clustering and separation of datapoints based on mutational strain (Figure 5.21). These results demonstrate that while there is a substantial impact of allometry, the mutant allelic series of *miniature* also has a strong impact on shape.
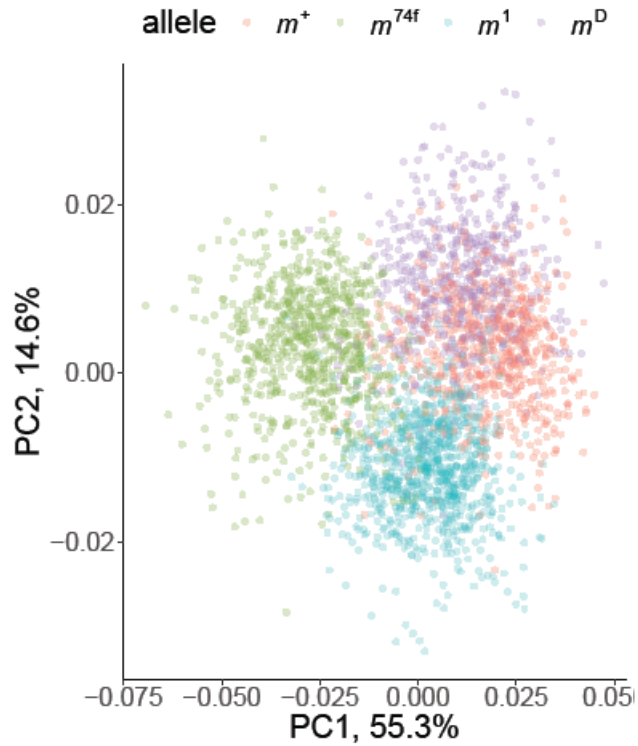
Figure 5.14: Ordination plot of shape variation for the *miniature* alleles (PC1/PC2) after accounting for common allometric effects where there is separation based on allelic effects. Where each dot represents a projected fitted wing onto the ordination plot. Once accounting for shape effects due to size there is observed clustering based on mutant alleles with majority of the variation in shape captured in PC1.
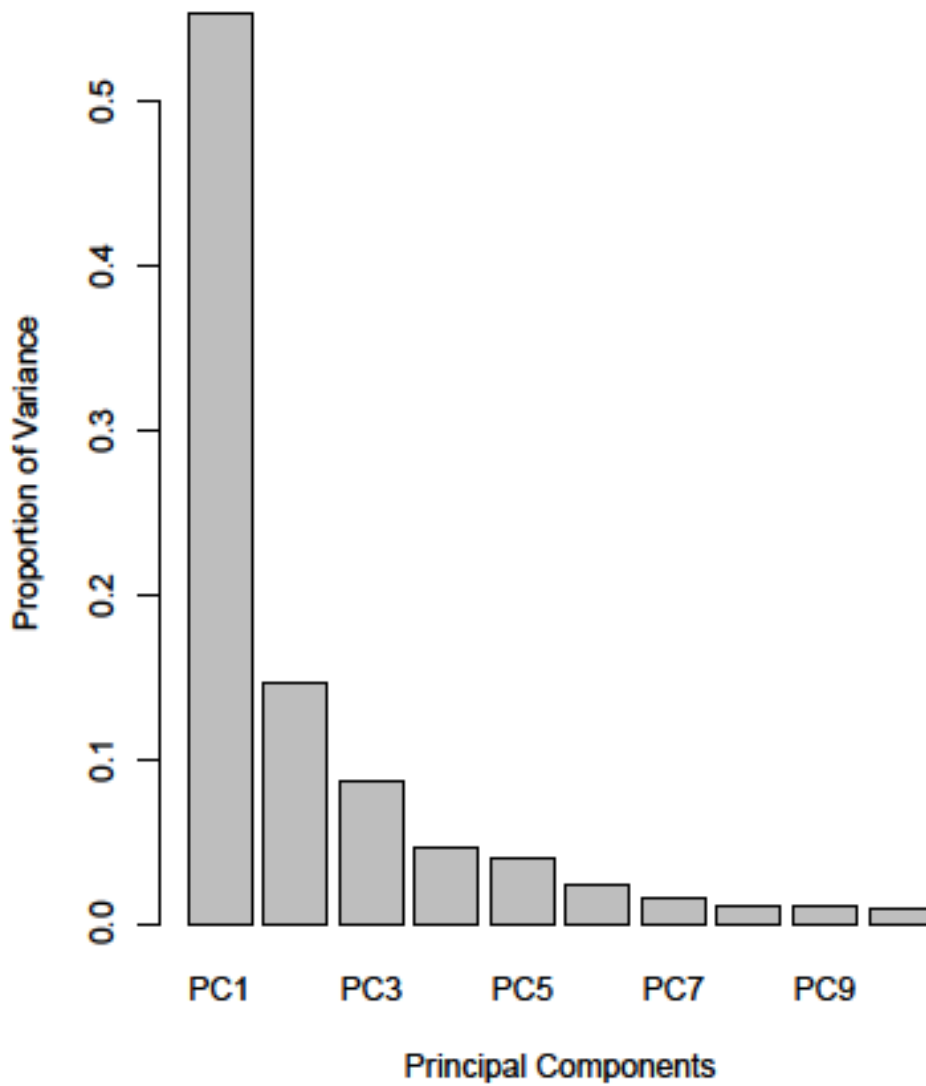
Figure 5.15: Scree plot of *miniature* principal components after accounting for common allometric effects where PC1 accounts for most variation in wing shape. Each bar represents a PC from PC1 on the left to PC 10 on the far right.
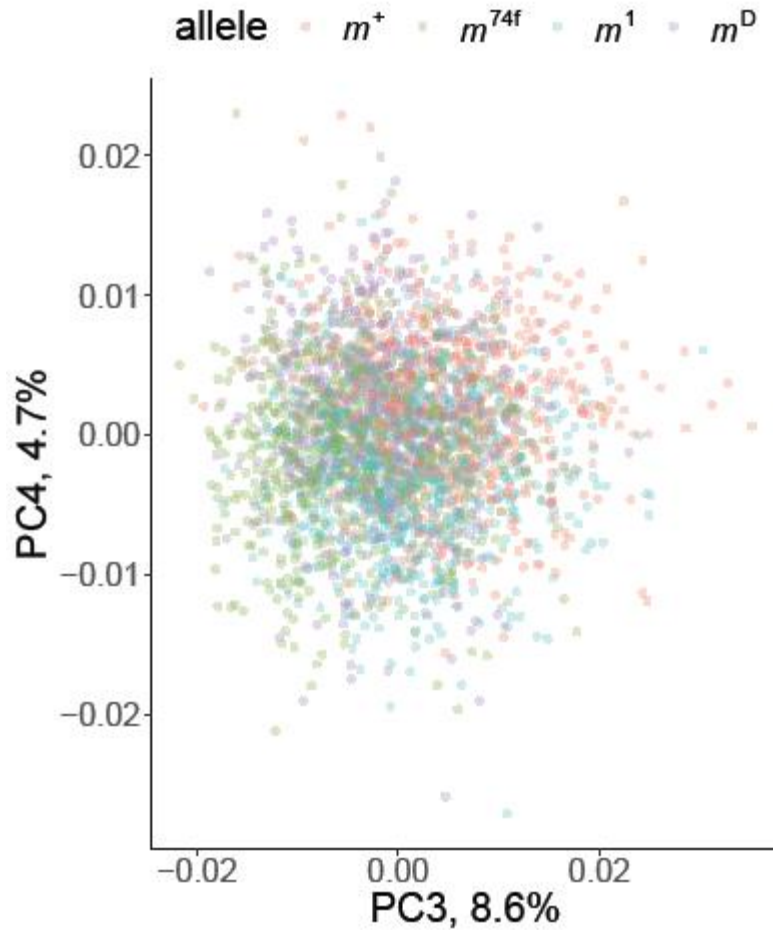
Figure 5.16: Ordination plot of shape variation for the *miniature* alleles (PC3/PC4) after accounting for common allometric effects where there is a lack of observable clustering based on allelic effects. Where each dot represents a projected fitted wing onto the principal component plot. Separation of mutant alleles can be observed in PC 1, and 2. Once you examine PC 3 with PC 4 this separation is not observable.
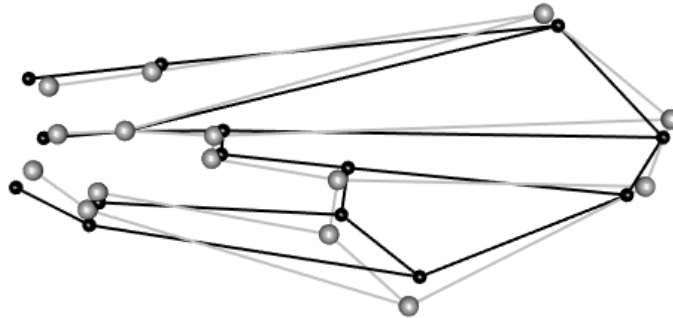
Figure 5.17: Skeleton diagram showing *miniature* perturbation shape changes associated with PC1. Grey represents the mean, black represents a change in direction along PC 1. This diagram is an approximation the shape changes for a given m^D allele for PC1.
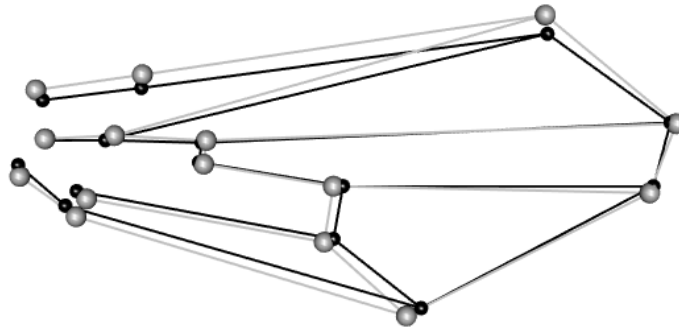
Figure 5.18: Skeleton diagram showing *miniature* perturbation shape changes associated with PC2. Note this is at 2X magnification to better see the effects. Grey represents the mean, black represents changes along PC 2. This diagram is an approximation the shape changes for a given m^D allele for PC2.
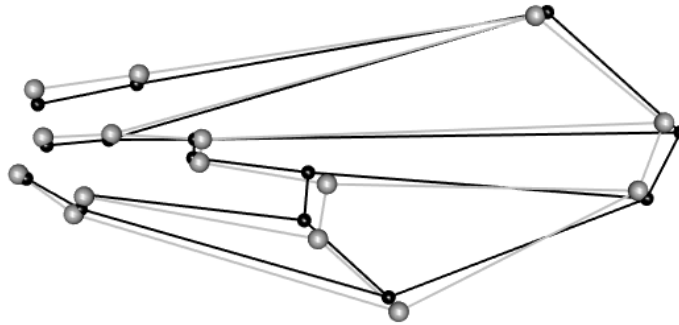
Figure 5.19: Skeleton diagram showing *miniature* perturbation shape changes associated with PC3. Note this is at 2X magnification to better see the effects. Grey represents the mean, black represents changes along PC 3. This diagram is an approximation the shape changes for a given m^D allele for PC3.
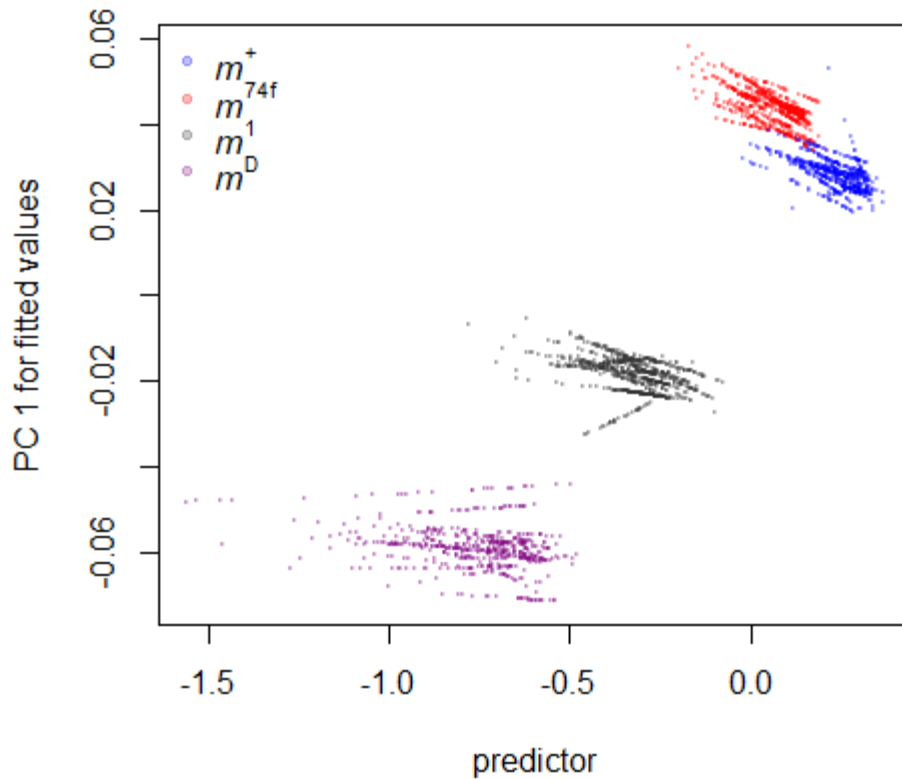
Figure 5.20: Allometric effects of size on shape, broken down by *miniature* allele where clustering based on allelic effects is observed, and modest strain effects. Each dot represents a distinct wing (predicted shape based on multivariate linear model) on the Y axis with the predictor ($\log_2$ centroid size) on the X axis. Observable clustering based on allelic effects can be discerned with strain (DGRP background) level effects observed based changing of orientation of dots, though most are not.
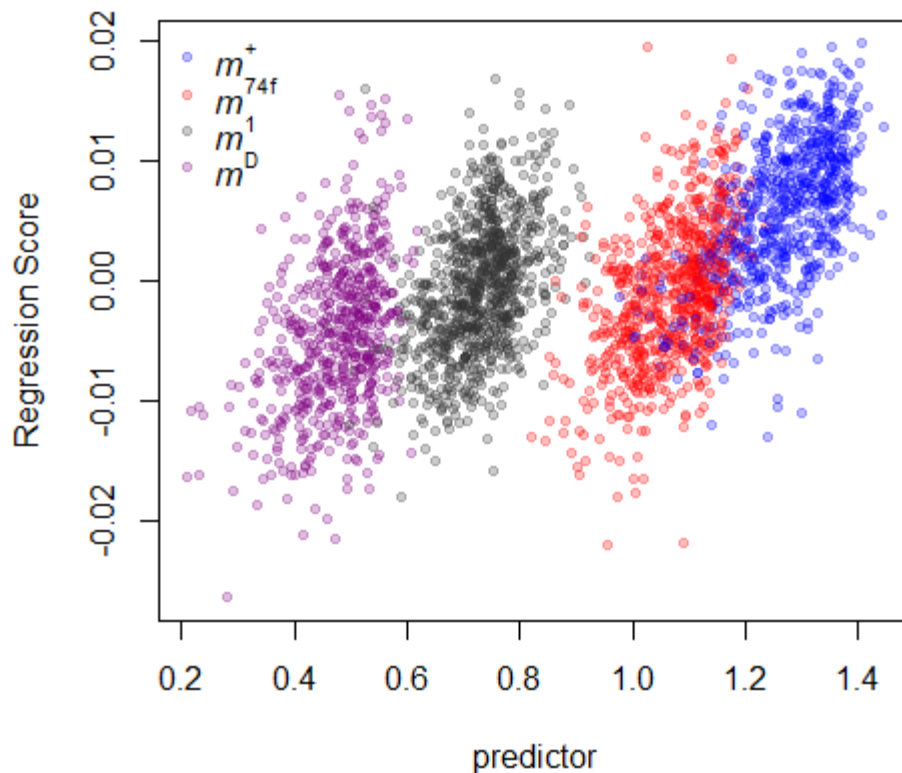
Figure 5.21: The relationship between *miniature* shape and size where there is observed clustering based on allelic effects. The regression score of shape is a readout for shape (projection of individual shape data onto the vector of allometric effects) against the size predictor. There is observed clustering based on allelic level effects and most DGRP backgrounds appear to show a lack of within line variation.

5.7 Relationship of *miniature* Intra-line Variation with Wing Shape

While we observed modest impacts of the miniature alleles on within-line variance for

size, shape is often a more sensitive read-out (Haber & Dworkin, 2017). As such we conducted

analogous approaches to assess patterns of variation and covariation among individuals within

genotypes (within combinations of DGRP and *miniature* mutant alleles) Specifically, we sought

to further characterize this relationship through examining the relationship of phenotypic

integration and total variance by allele (Figure 5.22, Figure 5.23). Phenotypic integration

provides a metric that measures the correlation of multiple functionally related traits to eachother

(Pigliucci, 2003). It provides an explanation for how phenotypes are maintained by relationships between traits (Pigliucci, 2003). For phenotypic integration and total variance there is an observed directionality of variance for *miniature* alleles (Figure 5.22, Figure 5.23). Furthermore, for m^D displays higher levels of phenotypic integration and total variance than the remainder of the *miniature* allelic series (Figure 5.22, Figure 5.23).
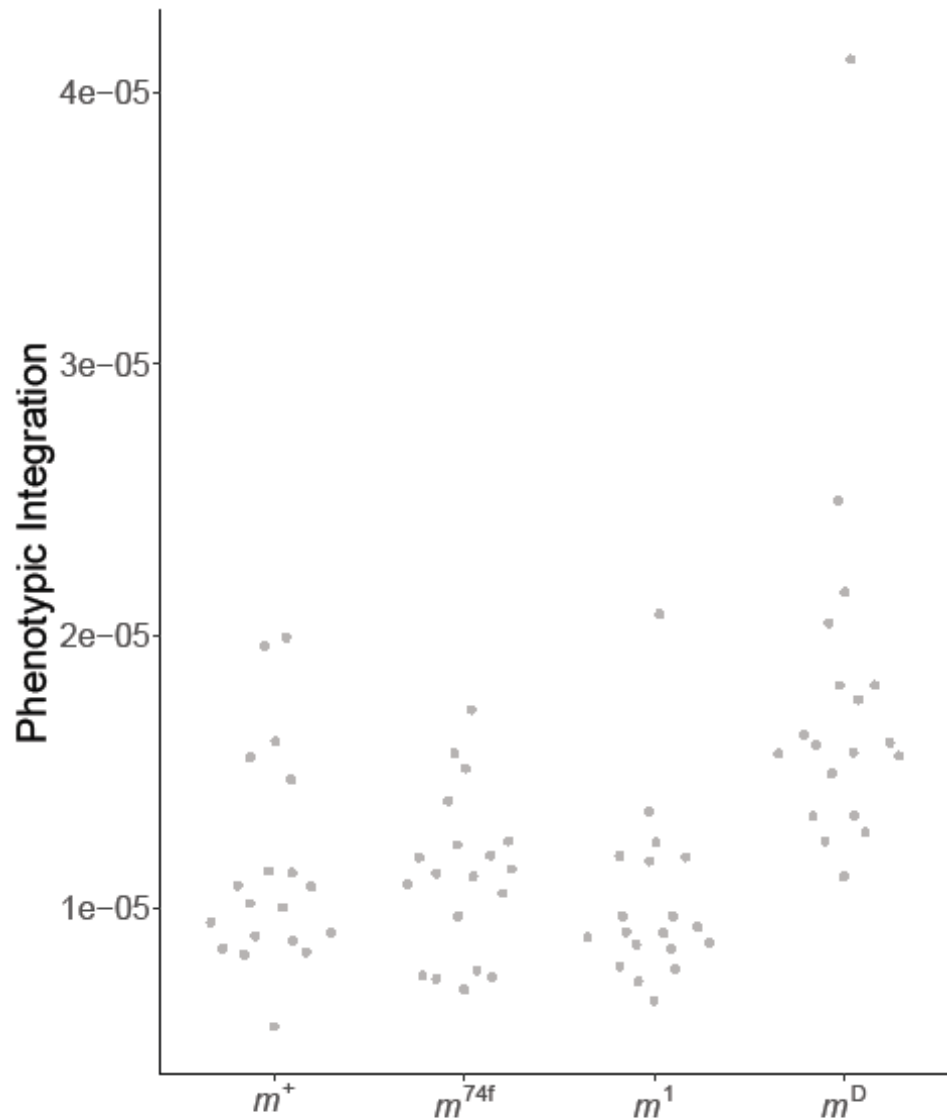
Figure 5.22: Phenotypic integration among *miniature (m)* mutant alleles for wing shape with each *m* allele showing similar levels of phenotypic integration. Each point represents the among individual within line phenotypic integration for a given DGRP line. Each point is the mean of 30-90 individuals. There is slightly higher phenotypic integration for m^D however, phenotypic integration across *m* alleles remains relatively consistent indicating each *m* allele has similar affects on wing shape.
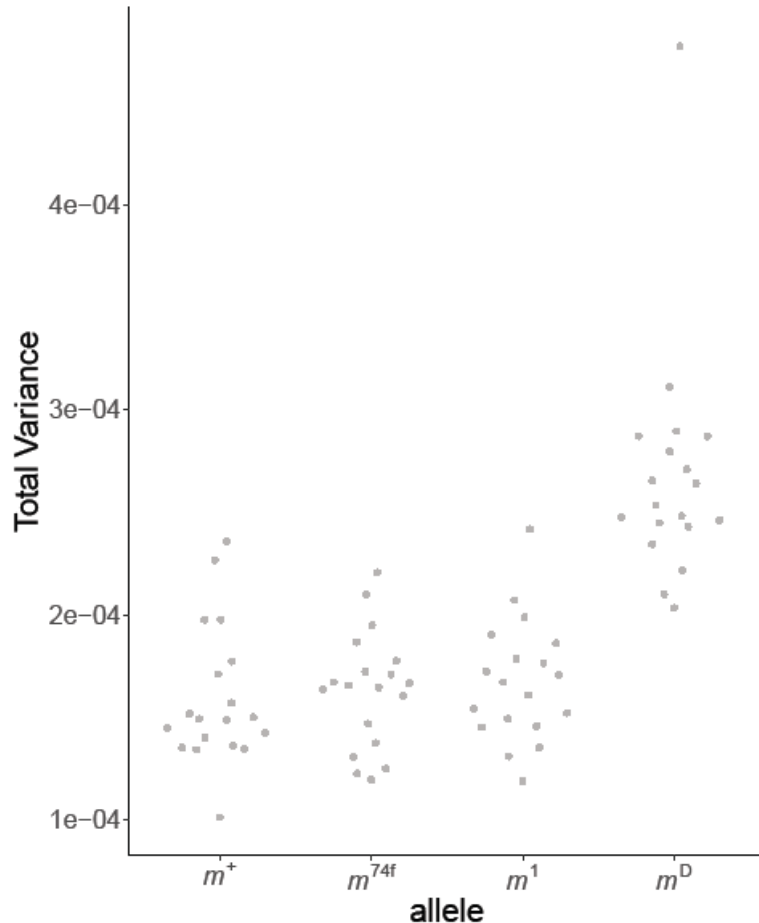
Figure 5.23: Total variance among *miniature (m)* mutant alleles for wing shape with each *m* allele displaying similar levels of total variance. Each point represents the among individual within line total variance for a DGRP line. Each point is the mean of 30-90 individuals. There is slightly higher total variance for m^D however, total variance across *m* alleles remains relatively consistent indicating each *miniature* allele has similar amounts of variation in wing shape.

5.8 Scalloped **Gene Expression Levels**

To examine the effect of *scalloped (sd)* and *vestigial (vg)* on wing expression we began

by plotting mean ΔC_t values with the wing phenotype (Figure 5.24). The mean ΔC_t values

provide a mean value for normalized gene expression levels on a per gene basis. The From this

plot we can observe that as mutations in the *sd* gene perturb the system there is a decrease in

both *sd* and *vg* gene expression levels as well as a simultaneous decrease in wing phenotype

(Figure 5.24). We then normalized gene expression levels and compensated for any plate level

effects. Exploiting the model adjusted estimates, we fit estimated marginal means which shows

the average expression differences relative to wild type (Figure 5.25). Next, we fit 4-paramater logistic region models to both *sd* and *vg* gene expression data with the semiquantitative wing size data generated by Caityln Daley (2019) (Figure 5.26, Figure 5.27). The result of this fit is a non-linear relationship between gene expression and wing size that resembles theoretical predictions (Figure 1.3). Next employing model adjusted estimates mean ΔC_t values for *sd* expression were plotted against the *sd* allelic series considering DGRP backgrounds (Figure 5.28). There is a perceptible difference in the DGRP background wild type *sd* gene expression levels as seen by the different ΔC_t levels for sd^+ gene expression (Figure 5.28). Furthermore, there is an observable background dependence of among line variation regarding robustness to perturbations as different DGRP lines show a drastic increase in among line variance and line crossing occurring for the moderate phenotypic effect sd^{ETX4} allele and a slight increase in among line variance for the moderate phenotypic effect sd^{E3} allele (Figure 5.28). We further quantified this relationship measuring the relative change in gene expression levels against each DGRP wild-type gene expression levels and largely recapitulated previous results, accentuating the variance among lines for sd^{ETX4} (Figure 5.29). Unfortunately, due to time constraints we were only able to analyze the results for *sd* and model for *sd* and *vg* and not for *cyclinE*.
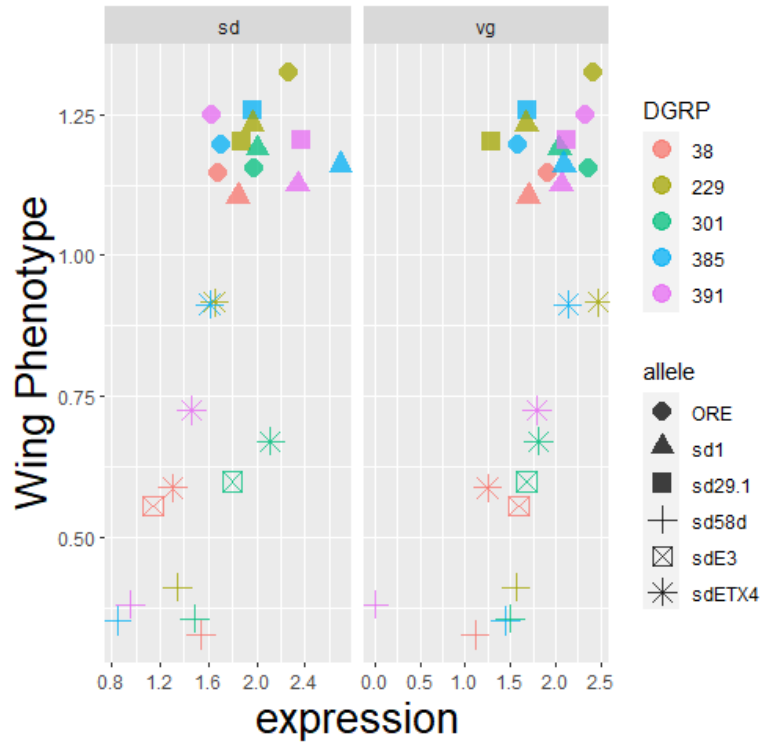
Figure 5.24: Mean gene expression values of *sd* and *vg* with wing phenotype showing an expected decrease in gene expression levels resulting in an increase in mutational severity. Each colour represents a DGRP genetic background while each shape represents the wild-type or mutant *sd* allele crossed to the DGRP genetic background. Higher wing phenotypes represent more wild-type wings while lower wing phenotypes represent more severely mutated wings. There is a corresponding decrease in wing phenotype with a decrease in gene expression levels.
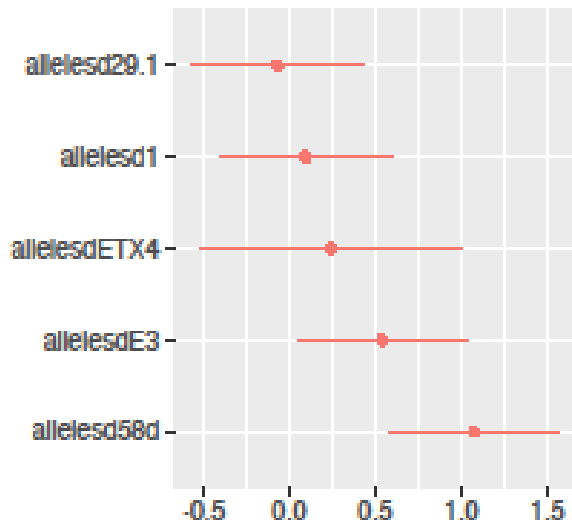
Figure 5.25: Average gene expression differences of *scalloped* alleles relative to wild-type (Oregon-R genetic background). Note that these are expressed as differences from wild-type with gene expression levels. As the severity of the mutation increases there is a corresponding increase in differences of gene expression from wild-type expression across the *scalloped* allelic series.
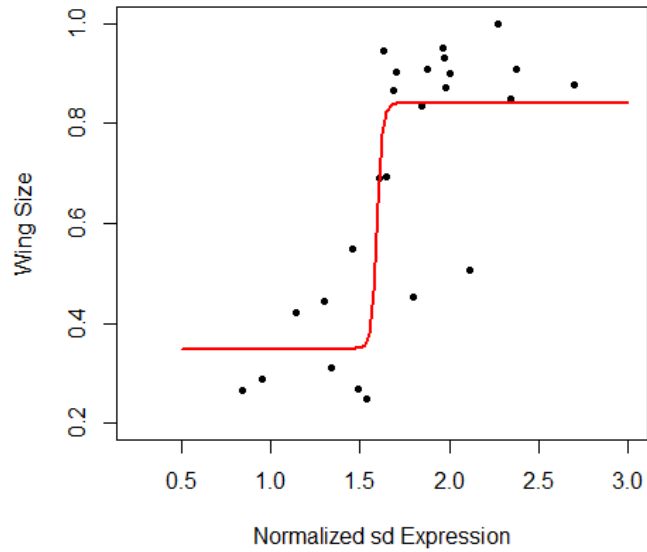
Figure 5.26: Four parameter logistic regression curve of normalized *scalloped* expression with wing size exemplifying the theoretical non-linear relationship between gene expression levels (normalized) and phenotypic effect (wing size). Each dot represents the normalized gene expression levels of ~30 *Drosophila melanogaster* wing discs.
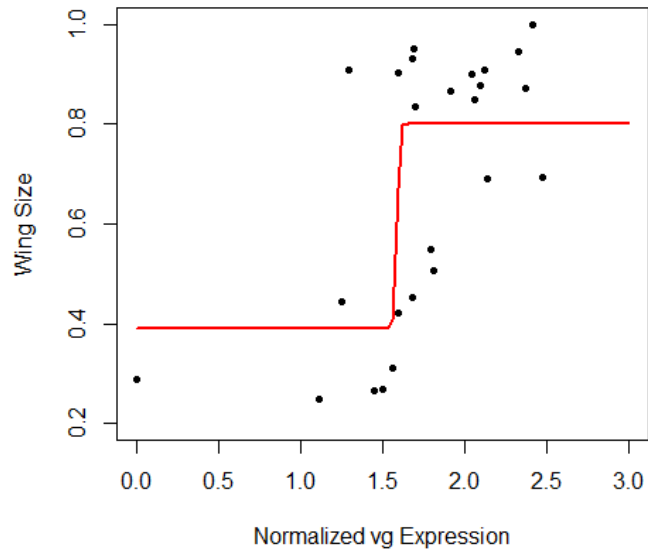
Figure 5.27: Four parameter logistic regression curve of normalized *vestigal* expression with wing size exhibiting the theoretical non-linear relationship between gene expression levels (normalized) and phenotypic effect (wing size). Each dot represents the normalized gene expression levels of ~30 *Drosophila melanogaster* wing discs.
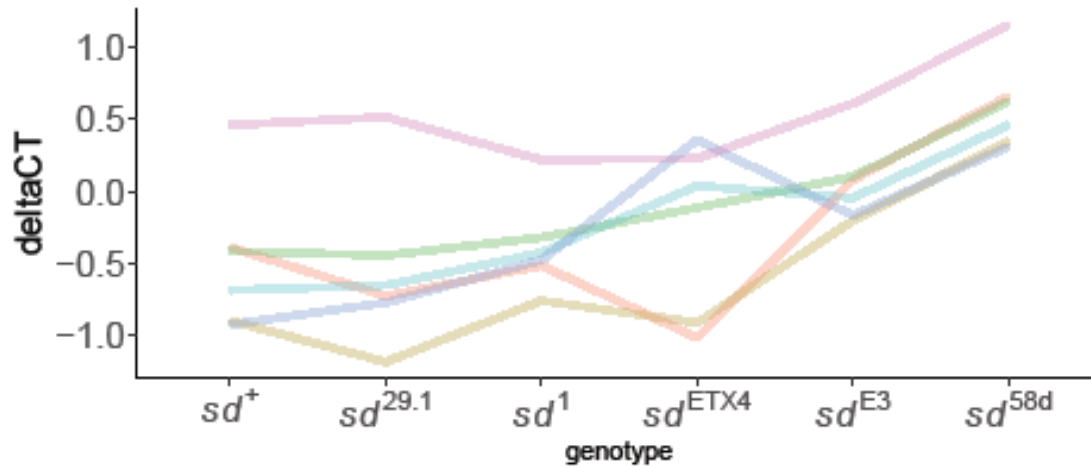
Figure 5.28: Reaction norm plots displaying wing ΔC$_t$ means of *scalloped (sd)* expression for the *sd* allelic series indicating differences in robustness and starting gene expression levels on a genetic background basis. Each coloured line on the graphs represents a distinct genetic background (6 DGRP backgrounds). Each mean is the average of two biological replicates of the mean of multiple technical replicates with each biological replicate containing ~30 *Drosophila melanogaster* wing discs. There is a perceived difference between the starting levels of gene expression for *sd* based on the genetic background and there is background dependent robustness as seen by the increase in variance for *sd^{ETX4}* and slightly for *sd^{E3}*.
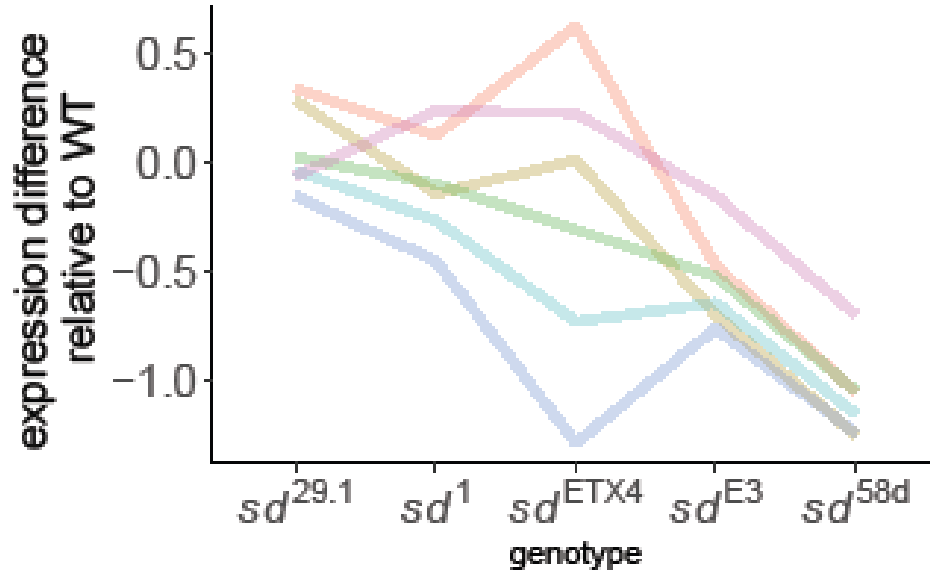
Figure 5.29: Reaction norm plots displaying expression differences of *scalloped* gene expression levels relative to wild-type for the *sd* allelic series exemplifying differences in robustness and starting gene expression levels on a genetic background basis. Each coloured line on the graphs represents a distinct genetic background (6 DGRP backgrounds). Each mean is the average of two biological replicates of the mean of multiple technical replicates with each biological replicate containing ~30 *Drosophila melanogaster* wing discs. This accentuates the noticeable the background dependent robustness as seen by the increase in variance for *sd*^{ETX4} and *sd*^{E3}.

6. Discussion

6.1 Among-Line Variation in Wing Size

   Previous work has outlined a mechanistic model whereby moderate phenotypic effect

alleles display increased background dependence and phenotypic variance relative to weak and

severe phenotypic effect alleles (Chandler et al., 2017). This pattern has been observed in a

variety of model organisms including recently within adult *Drosophila melanogaster* wing tissue

with *scalloped, vestigial, optomotor-blind/bifid, cut,* and *beadex* allelic series (Barkoulas et al.,

2013; Daley, 2019; Green et al., 2017). This model suggests a predictive effect of mutational

severity with background dependence and one aim of this study was to confirm this model for

the same trait by examining a very different developmental mechanism. To do this F1

hemizygous males for X-chromosome mutations *miniature* and *scalloped* among 19 previously

investigated DGRP backgrounds were analyzed focusing on wing size and shape morphology

(Daley, 2019). Every individual analyzed was genetically identical other than the focal mutation

of interest in the Oregon-R background and their respective DGRP autosomal chromosomes.

Phenotypic mutational severity was determined through changes from wild-type wing size or

shape. Wing size changes were characterized using a custom ImageJ macro while changes in

wing shape were characterized using geometrics morphometrics.

Despite profound effects on both wing size and shape, we did not observe evidence of

strong background dependence for the *miniature (m)* moderate effect allele (m^1) relative to the

others, and the effects across DGRP backgrounds were strongly genetically correlated across *m*

alleles. Furthermore, we did not observe increased variance and background dependence with

moderate phenotypic effect alleles in the *m* allelic series across 9 genetic backgrounds (Figure

5.1, Figure 5.2B). This is an unexpected shift, and inconsistent with the model outlined in the

introduction and experimentally observed in previous studies as discussed in the previous

paragraph. This result is unlikely an experimental artefact. We conducted the experiment with *m*

alleles along with two previously examined *scalloped (sd)* alleles, sd^1 and sd^{ETX4}. Both alleles

showed results consistent with the overall model, and previous results. Specifically, there was an

observed increased in variance (both genetic and environmental) of the moderate effect

hypomorphic allele, sd^{ETX4}, and the relative modest impact of in the weak effect hypomorphic

sd^1 allele, within the current analysis (Daley, 2019; Figure 5.1, Figure 5.2, Figure 5.3). When

examining correlations of mutational severity across DGRP strains *miniature* does not follow

previously observed relationships of *sd* across the identical DGRP strains (Daley, 2019).

Previous correlations of *sd* mutational severity across DGRP strains are variable, however

miniature alleles display strong positive correlations across DGRP strains (Figure 5.4, Figure

5.5). This implies that large wings in a select DGRP background crossed to the wild-type strain

remained large in the same background when crossed to the *m* mutants. The same cannot be

reliably said for s*d* alleles within the same DGRP backgrounds (Figure 5.4, Figure 5.5, Daley,

2019), which is a fairly typical observation for other studies of genetic background effects

(Dworkin, 2005a; Gibson & Van Helden, 1997; Milloz et al., 2008; Polaczyk et al., 1998)

One concern for this study may be that the allelic series implemented may have not

landed on the steep portion of the non-linear curve to result in increased changes in variation

(Figure 1.3). However, we do not believe this is the case as the sd^{ETX4} allele appears to be less

expressive than *m74f* and slightly more expressive than m^1 with some DGRP lines expressing

higer phenotypic severity for sd^{ETX4} than any background in with m^1 and m^D mutations (Figure

5.1, Figure 5.2, Figure 5.3, Table 5.1). Another concern is that the m^1 and m^D mutations may be

too severe to present as moderate phenotypic effect alleles and thus be constrained to the lower

asymptote (Figure 1.3). We again do not believe this to be the case, as if this was, we would

expect m^1 means to be much closer to sd^{58d} and m^D line means. A final concern for the study was

damaged and partially folded wings were used in the analysis. To account for this we assigned

wing damage values from zero to three and conducted analyses including and excluding the

damaged wings. There was no noticeable difference between the results of including and

excluding the damaged wings on the model estimates and as such we opted to include these

wings to increase the power of the dataset. Overall, these results do not follow the previously

described model whereby mutations of moderate phenotypic effect display increased variance

and background dependence relative to weak and severe phenotypic effect alleles (Figure 1.3).

These results also show that correlations among DGRP lines with regard to mutational severity

do not follow the same results generated previously, but allelic order does remain consistent across DGRP backgrounds (Daley, 2019).

6.2 Within-Line Variation in Wing Size

The results from our intra-specific analysis showcase another unique feature of *miniature* alleles. Our results show a lack of sensitivity to environmental and stochastic noise in the *miniature* allelic series (Figure 5.6, Figure 5.7, Table 5.2). This is different than previously reported relationships involving *sd* and *beadex (bx)* allelic series whereby moderate phenotypic effect alleles displayed increased environmental sensitivity (Daley, 2019). Along with observing this with posterior distributions of our MCMCglmm results we analyzed this utilizing the median form of the Levene's statistic which showcases a drastic increase in variation for the moderate phenotypic effect sd^{ETX4} allele but not for the *m* alleles or the weak phenotypic effect sd^{1} allele (Figure 5.7, Table 5.2). When we investigated correlations across DGRP strains for intra-line variation with *m* and *sd* alleles we observed a variable relationship between intra-line variation and mutational severity for all alleles involved in the study (Figure 5.8). These results are congruent with previous studies for *sd* and *vg* allelic series done by Chandler et al. (2017) but in disagreement with previous studies for *sd* and *bx* (Daley, 2019). Interestingly, sd^{ETX4} and sd^{1} appear strongly positively correlated for intra-line variation among DGRP strains, more so than previously reported (Daley, 2019). This may indicate that the *sd* allelic series does comform to the previously mentioned non-linear relationship for environmental sensitivity, but the *miniature* allelic series does not (Figure 1.3).

The application of mixed model approaches allowed us to distinguish between fixed and random estimates providing us with readouts of relative contributions of genetic and environmental effects on phenotypic outcomes for each mutant allele. Broad sense heritability

(H^2) and coefficient of genetic variation (CV_G) give us statistics of the relative proportions of genetic and environment effects on phenotypic outcome for each allele investigated. H^2 estimates indicate ($H^2 > 0.5$) that both moderate phenotypic effect alleles m^1 and sd^{ETX4} genetic contributions are quite high (Table 5.1). However, once taking trait means into account by examining the CV_G we can observe an 8 to 10 times higher genetic variation in sd^{ETX4} than all other alleles involved in this study. This increase is expected for a non-linear GP map (and why both genetic and environmental variances are so much greater for sd^{ETX4} than other alleles), but it makes the results observed for the *miniature* alleles even more intriguing.

From these results it is evident that environmental effects play a large role in phenotypic variation and trait expression for majority of the alleles included in this study. This is important as these environmental effects can modulate the correlation of mutant alleles among and between genes and affect estimates of variability. To account for this, the replicate vial random effect was accounted for in all models and variation due to replicate vials was found three times less than the smallest variance recorded (0.0002) for among line variation and equal to the variation observed in wild-type strains (0.0136) for within line variation (Table 5.1, Table 5.2). Overall, these results do not follow the previously identified mechanistic model whereby mutations of moderate phenotypic effect display increased variance and background dependence relative to weak and severe phenotypic effect alleles (Figure 1.3). These results also show that correlations within DGRP lines with regard to mutational severity do not follow the same results generated previously (Daley, 2019).

6.3 Mutations in *miniature* Influence Wing Shape Beyond the Effects of Allometry
Previous studies had concluded that there is no observable change in wing shape due to *miniature* mutational effects (Dobzhansky, 1929; Newby et al., 1991; Roch et al., 2003).

However, in each case, these inferences were made entirely based on a qualitative assessment of wing shape, without explicitly measuring it. To our knowledge this is the first study that has characterized quantifiable changes in wing shape due to *miniature* mutations. As described further below, we demonstrate that the effects that the *miniature* mutations have on shape are substantial, even after accounting for the influence of the size effects on shape. Using geometrics morphometrics, we used 15, 2D landmarks to characterize changes in wing shape (Figure 5.9). It should be noted that geometrics morphometrics was suitable for use in only the *miniature* allelic series as *scalloped* mutations result in loss of wing tissue (and consequently landmarks) hampering the use of this approach for those alleles. From this we initially calculated centroid size of the wings involved which recapitulated previous results obtained from the wing size measurements with the ImageJ macro directly estimating wing area (data not shown). Given the profound effect of the *miniature* alleles on wing size, and the potential contribution of shape by size allometry to confound our analyses, we examined the effects of allometry on wing shape. We observed that a large proportion of the variation in wing shape observed was, as expected, due to allometry. Specifically, when analyzing unfitted data, we observe that most variation in wing shape occurs along the first principal component with the first three principal components accounting for 90% of the observed shape variation. This is indicative of allometry, alleles and the genetic backgrounds accounting for a large proportion of the unfitted phenotypic variation observed in wing shape among lines. Further, by observing clustering of datapoints by allele it is evident that *miniature* allelic effects play a large role in shape variation (Figure 5.10, Figure 5.13)

However, while informative we wanted to investigate the role of size on shape while accounting for common allometric effects observed across mutant alleles. As such we applied

model fitted values that were projected back onto the multivariate regression model to give an idea of the shape-size relationship (Figure 5.14). The result of this largely recapitulates results obtained from the unfitted data whereby we can see most of the variation occurs with the first three fitted principal components. Once common allometry is accounted for, these three PCs account for about 78% of the observed variance in shape due to wing size, mutant allele, and genetic background (Figure 5.14, Figure 5.15). Furthermore, clustering of individuals by m alleles is still observed, indicating that even once allometric effects on shape are accounted for allelic effects are a large component of the observed variation in wing shape. One important caveat of this approach is that it does assume a "common" allometric relationship. That is the major direction of allometric effects on shape is largely similar within and between alleles. Previous work into this question does suggest that many (but not all) mutant alleles do tend to share similar directions of allometric effects, albeit this previous study only examined weak mutational effects for genes involved with TGF-Beta and Hedgehog signaling (Testa & Dworkin, 2016). In this study, while there was a significant interaction between allelic effects and size, this contributed only about 1% of variation to shape for this data set, after having accounted for main effects of size (~60%), m alleles (~24%) and variation among the DGRP strains (~5%). As such, this assumption is unlikely to be strongly violated.

Utilizing the modeled residual variances, we calculated the amount of variation in wing shape remaining after accounting for common allometric effects and found that 39.3% of variation exists in wing shape. This is a close approximation with results from the type 1 ANOVA analysis with the differences in estimates attributed to rounding errors (Table 5.1). This indicates that before accounting for allele and strain effects, allometry accounts for about 60% of the variation in shape, leaving 40% of the remaining variation in shape to be investigated

exploiting fitted values. From these fitted values approximately 78% of the variation can be explained by PC1, PC2, and PC3 indicative of size, allelic effects, and strain effects comprising a large majority of the observed variation in shape.

Next, we sought to investigate the effects of shape change related to size with size changes taking account DGRP backgrounds (Figure 5.20, Figure 5.21). Importantly, what this is elucidating is the relationship of allometry and wing size across DGRP backgrounds. The result of this is a noticeable clustering and separation based on mutant alleles indicating that mutational severity has a large effect on shape variation among DGRP lines. Furthermore, some strain (DGRP background) effects can be observed but appear relatively modest when compared to size and mutant level effects which is in concordance with the type 1 ANOVA analysis (Figure 5.20, Table 5.1) We then employed the regression score as a readout for shape change and examined the relationship of shape with size (Figure 5.21). From this, the between line variation appears to be similar with mutant alleles showing a large effect on shape based on clustering of datapoints. Furthermore, within mutant allele effects seem to be similar among DGRP lines examined (Figure 5.21). Overall, these results conform with previous *miniature* wing size results displaying no substantial increased inter-line variation and background dependence for moderate phenotypic effect allele m^1 relative to m^{74f} and m^D, and consistent allelic order across DGRP backgrounds.

6.4 Within-Line Variation in Wing Shape

Within-line variation effect on size were surprisingly similar. However, the use of shape (and in general multivariate approaches) allows us to investigate patterns of shape variation and covariation in an analogous way to what we did with size. Examining phenotypic integration and total variance for each genotype (i.e. each combination of DGRP and _m_ allele) variance-

covariance matrix show a largely consistent picture to what was observed for wing size. While there are subtle increases for the m^D allele, the estimates for total variance (think of the volume of the hyper-sphere or "ball") and phenotypic integration (shape of the "ball") are similar across alleles. Overall, these results largely recapitulate previous *miniature* wing size results of within-line variation where there is a lack of increased intra-line variation and background dependence in wing shape for the moderate phenotypic effect m^1 allele relative to the m^{74f} and m^D alleles.

6.5 Why is *miniature* Different*?*

The results observed in this study for *miniature* are simultaneously very interesting, but quiet confounding. What is clear, is that unlike other studies investigating similar questions in different model systems and organisms, the results of *miniature* stand out. Currently we are unsure of what might be causing the differences between *miniature* and all previously tested allelic series. We have multiple (yet untested) hypotheses for why *miniature* is different. These hypotheses involve the decreased pleiotropy of *miniature,* the time at which *miniature* plays an active role in development, or the mechanical effect Miniature has during development anchoring cells to the matrix. Miniature acts much further downstream with regard to gene regulatory networks, compared to *sd* (Bray, 1999; Neto-Silva et al., 2009; Roch et al., 2003; Simmonds et al., 1998; Srivastava et al., 2004). Miniature is apical extracellular membrane (aECM) protein that is responsible for denticle formation, plays a role in *bursicon* signalling, and proper cell shape changes during wing formation in developing flies (Bilousov et al., 2012; Chanut-Delalande et al., 2006; Dobzhansky, 1929; Newby et al., 1991; Roch et al., 2003). *miniature* does not encode a transcription factor, nor a component of a signaling pathway like many of the previously tested genes (for similar studies) including *sd, vg, bx, fibroblast growth factor, and epidermal growth factor* (Barkoulas et al., 2013; Chandler et al., 2013; Daley, 2019; Green et al., 2017). As such, it might be the nature of the gene itself and its restricted and

"mechanical" role it plays on development which is why we observe these drastic changes from the expected non-linear relationship between genotype and phenotype. Another reason for this change could be the time at which *miniature* plays an active role in wing development. Miniature primarily acts to affect wing morphology late in pupal development whereas most previously examined genes involved in *Drosophila* wing development act much earlier, during larval development (Chandler et al., 2013; Daley, 2019; Roch et al., 2003; Sobala & Adler, 2016). We hypothesize that due to the late acting timing of *miniature* there may not be enough time for the system responsible for buffering perturbations to respond to mitigate the effects of *miniature* perturbations, limiting opportunities for genetic background effects. A final reason we have hypothesized for the difference in our results from *miniature* from previously tested systems is the role *miniature* plays in wing development. We hypothesize that due to the role Miniature plays on development as an aECM protein the system may not be able to buffer perturbation to replace or mitigate the effect of the *miniature* perturbation on protein binding to the ECM. However, it should be noted that previous studies on the *sevenless* and *ellipse* genes, which code for transmembrane receptor tyrosine kinase proteins, showed sensitivity to genetic background effects (Polaczyk et al., 1998). While these genes do not encode transcription factors and are responsible for encoding transmembrane proteins like Miniature*,* the proteins encoded are receptors and intimately involved in signalling cascades integrated into gene regulatory networks while Miniature affects mechanical forces involved in development (Dobzhansky, 1929; Newby et al., 1991; Roch et al., 2003). We hypothesize it is the inability to compensate for the lack of mechanical force caused be the *miniature* perturbation that affects the capacity of the genetic background to buffer the effect of *miniature* mutant alleles. Clearly these multiple hypotheses suggest multiple potential avenues for further research.

6.6 Miniature Concluding Remarks

In conclusion, here we have demonstrated *miniature* alleles show an unexpected lack of background dependence for alleles of weak, moderate, and severe phenotypic effect across a range of DGRP wild-type genetic backgrounds derived from natural populations. Previous work has implicated a mechanistic model where alleles of moderate phenotypic effect show increased background dependence and variance between and among genetic backgrounds relative to weak and severe phenotypic effect alleles (Daley, 2019). Here, exploiting an allelic series in the *miniature* gene which affects *Drosophila melanogaster* wing development we have shown that adult wing shape and size does not follow the expected model previously observed in a variety of model organisms (Figure 1.3, Barkoulas et al., 2013; Chandler et al., 2013; Daley, 2019; Green et al., 2017). Further, we have measured inter-line and intra-line correlations for mutational severity assessing both wing size and shape and have found that *miniature* mutational severity across DGRP backgrounds displays a strong positive correlation while *miniature* mutational severity within DGRP backgrounds reveals a variable correlation with mutational severity. These results are tangential to previously generated results with *sd* and *bx* allelic series (Daley, 2019 but are congruent with expectations for *sd* and *vg* allelic series investigated previously (Chandler et al., 2017).

Regarding stated objectives of this study, we cannot confirm the Chandler et al. (2017) mechanistic model for predicting background dependence at the allelic level. We present possible evidence that genetic background effects may be specific for genes, or developmental mechanisms and not for overall phenotypic effect on the wing. We have also confirmed that allelic order does remain consistent across genetic backgrounds, but we are unable to confirm correlations between *sd* and *m* remain consistent across genetic backgrounds. To our knowledge this is the first study to display this degree of linear relationship between genetic perturbation

and phenotype. Recent work on genetic background effects on transvection using Malic enzyme in 149 DGRP wild-type flies has shown a slightly linear relationship in among and within line variation and background dependence (Rzezniczak et al., 2022). Though the degree of linearity is not nearly as evident as the one reported here. Further, this study is the first to report subtle but quantifiable differences in wing shape due to mutation within the *miniature* gene through the application of geometrics morphometrics. This is dissimilar to previous studies that have noted changes in wing size with no qualitative changes to wing shape (Dobzhansky, 1929; Newby et al., 1991; Roch et al., 2003).

Future work should aim to elucidate the differences between *miniature* and previously studied genes. A method of accomplishing this could be to investigate allelic series with functionally related mechanism such as *dumpy*, *narrow*, *dusky*, *dusky-like*, *tapered,* and *lanceolate* to help discern if lack of genetic background dependence is due to gene or developmental specific mechanisms and if these differences in mechanistic action are why there is an observable difference in *miniature* over *scalloped* phenotypic expression (Ray et al., 2015; Roch et al., 2003). For example, an experiment like the one performed using *miniature* could be conducted on other ZPD proteins. *Dusky* and *dusky-like* are both paralogous ZPD proteins next to *miniature* on the genome and represent good candidates for this study to see these proteins are as desensitized to genetic background effects as *miniature* (Adler et al., 2013; Roch et al., 2003) A further experiment could be designed to examine different correlates of trait expression such as examining interactions between cells and extracellular matrix binding to find genes involved in transcription factor signalling, with the goal of comparing these genes to genes that serve a more mechanistic role in extracellular matrix binding (Dobzhansky, 1929; Fristrom, 1988; Newby et al., 1991; Roch et al., 2003). This will aid in determining if the mechanistic model that

has been proposed by Chandler et al. (2017) is a model that is limited to genes involved in regulation or signalling pathways. The precedent for this has already been set by Kacser & Burns (1981) where the more enzymes involved in a pathway the more non-linear the system becomes (Gilchrist & Nijhout, 2001). This might be a situation where there are many interacting partners for gene regulators such as *sd* and *vg* and genes involved in signalling pathways such as *sevenless* and *ellipse* but not for *miniature* (Chandler et al., 2017; Polaczyk et al., 1998).

6.7 Scalloped Discussion

        Initially we observe that we have successfully captured the extent of the *sd* allelic effects through an observed increase in the differences of gene expression as the severity of the mutation increases (Figure 5.24). Intuitively this makes sense as the alleles in this cross are hypomorphic alleles that result in decreased gene expression levels (Daley, 2019). These patterns resemble the expected non-linear relationship of gene expression and phenotypic expression previously observed in *D. melanogaster* wing development, mouse craniofacial shape and *C. elegans* vulva cell fate (Barkoulas et al., 2013; Chandler et al., 2017; Daley, 2019; Green et al., 2017). Furthermore, we can observe that we see different starting amounts of gene activity among DGRP backgrounds as the levels of *sd* gene expression for wild-type (sd^+) alleles differs by background (Figure 5.28). As well, there are observed different sensitivities in these backgrounds to *scalloped* mutational expressivity that can be seen by line crossing and shifts away from linearity in the reaction norm plots (Figure 5.28, Figure 5.29). This is indicative of model 3 (Figure 3.3) which hypothesizes each genetic background differs with respect to mutational robustness and starting gene activity levels. Further, regarding gene expression levels the Chandler et al. (2017) model seems to hold true as sd^{ETX4} and to lesser extend sd^{E3} appear to show an increase in among line variance in comparison to the weak and severe phenotypic effect *sd* alleles (Figure 5.28, Figure 5.29).

The limitation of the current dataset is one of sample size and noise. Currently due to the multitude of steps involved in staging and dissecting discs there is a large amount of noise involved in the dataset. One of the levels of noise include the employment of wing discs that vary in their developmental timing of +/- 1 hour. Further, due to the chosen experimental design we are observing a large amount of variation due to plate level effects that before publishing, will need to be resolved. Another caveat to the current experimental design is the inclusion of ~30 discs per sample. Due to this, a limitation in our results is that it is impossible to examine within line variation as we cannot disentangle individual wing discs.

A possible method that could mitigate some of these confounding effects is single molecule fluorescent in-situ hybridization (smFISH) (Raj et al., 2008). This method employs short oligonucleotide probes to label individual RNA molecules which can be quantified through fluorescence microscopy (Raj et al., 2008, 2010). This method would allow for information on gene expression levels both among-line and within-line. Furthermore, exploiting this method would allow for understanding of spatial-temporal contexts of genetic background effects. This can be achieved through imaging wing discs at different developmental timepoints as well as the creation of a grid through co-staining with *dpp* and *wg* to give spatial context to gene expression levels (Raj et al., 2008). Finally, this method would allow for the normalization of expression through quantification of wing pouch size as outlined by Chandler et al. (2017). Overall, these results largely corroborate previous results of a non-linear relationships between gene expression and phenotypic trait expression, and exemplify the Chandler et al. (2017) mechanistic model at a gene expression level (Barkoulas et al., 2013; Daley, 2019; Green et al., 2017).

7. References

Abdi, H., & Williams, L. J. (2010). Principal component analysis. *Wiley Interdisciplinary Reviews: Computational Statistics*, *2*(4), 433–459. https://doi.org/10.1002/wics.101

Adams, D. C., & Otárola-Castillo, E. (2013). Geomorph: An r package for the collection and analysis of geometric morphometric shape data. *Methods in Ecology and Evolution*, *4*(4), 393–399. https://doi.org/10.1111/2041-210X.12035

Adler, P. N., Sobala, L. F., Thom, D. S., & Nagaraj, R. (2013). Dusky-like is required to maintain the integrity and planar cell polarity of hairs during the development of the Drosophila wing. *Developmental Biology*, *379*(1), 76–91. https://doi.org/10.1016/j.ydbio.2013.04.012

Attanasio, C., Nord, A. S., Zhu, Y., Blow, M. J., Li, Z., Liberton, D. K., Morrison, H., Plajzer-Frick, I., Holt, A., Hosseini, R., Phouanenavong, S., Akiyama, J. A., Shoukry, M., Afzal, V., Rubin, E. M., FitzPatrick, D. R., Ren, B., Hallgrímsson, B., Pennacchio, L. A., & Visel, A. (2013). Fine tuning of craniofacial morphology by distant-acting enhancers. *Science*, *342*(6157). https://doi.org/10.1126/science.1241006

Baena-Lopez, L. A., & García-Bellido, A. (2006). Control of growth and positional information by the graded vestigial expression pattern in the wing of Drosophila melanogaster. *Proceedings of the National Academy of Sciences of the United States of America*, *103*(37), 13734–13739. https://doi.org/10.1073/pnas.0606092103

Baken, E. K., Collyer, M. L., Kaliontzopoulou, A., & Adams, D. C. (2021). geomorph v4.0 and gmShiny: Enhanced analytics and a new graphical interface for a comprehensive morphometric experience. *Methods in Ecology and Evolution*, *12*(12), 2355–2363. https://doi.org/10.1111/2041-210X.13723

Barkoulas, M., van Zon, J. S., Milloz, J., van Oudenaarden, A., & Félix, M. A. (2013). Robustness and Epistasis in the C. elegans Vulval Signaling Network Revealed by Pathway Dosage Modulation. *Developmental Cell*, *24*(1), 64–75. https://doi.org/10.1016/j.devcel.2012.12.001

Bate, M., & Martinez Arias, A. (1991). The embryonic origin of imaginal discs in Drosophila. *Development*, *112*(3), 755–761. https://doi.org/10.1242/dev.112.3.755

Bates, D., Mächler, M., Bolker, B. M., & Walker, S. C. (2015). Fitting linear mixed-effects models using lme4. *Journal of Statistical Software*, *67*(1). https://doi.org/10.18637/jss.v067.i01

Bilousov, O. O., Kozeretska, I. A., & Katanaev, V. L. (2012). Role of the gene Miniature in Drosophila wing maturation. *Genesis*, *50*(7), 525–533. https://doi.org/10.1002/dvg.22016

Böhni, R., Riesgo-Escovar, J., Oldham, S., Brogiolo, W., Stocker, H., Andruss, B. F., Beckingham, K., & Hafen, E. (1999). Autonomous control of cell and organ size by CHICO, a Drosophila homolog of vertebrate IRS1-4. *Cell*, *97*(7), 865–875. https://doi.org/10.1016/S0092-8674(00)80799-0

Boj, S. F., Petrov, D., & Ferrer, J. (2010). Epistasis of transcriptomes reveals synergism between transcriptional activators Hnf1α and Hnf4α. *PLoS Genetics*, *6*(5), 5.

https://doi.org/10.1371/journal.pgen.1000970

Boyle, E. A., Li, Y. I., & Pritchard, J. K. (2017). An Expanded View of Complex Traits: From Polygenic to Omnigenic. *Cell*, *169*(7), 1177–1186. https://doi.org/10.1016/j.cell.2017.05.038

Bray, S. (1999). Drosophila development: Scalloped and vestigial take wing. *Current Biology*, *9*(7), 245–247. https://doi.org/10.1016/S0960-9822(99)80154-7

Brooks, M. E., Kristensen, K., van Benthem, K. J., Magnusson, A., Berg, C. W., Nielsen, A., Skaug, H. J., Mächler, M., & Bolker, B. M. (2017). glmmTMB balances speed and flexibility among packages for zero-inflated generalized linear mixed modeling. *R Journal*, *9*(2), 378–400. https://doi.org/10.32614/rj-2017-066

Buccitelli, C., & Selbach, M. (2020). mRNAs, proteins and the emerging principles of gene expression control. *Nature Reviews Genetics*, *21*(10), 630–644. https://doi.org/10.1038/s41576-020-0258-4

Chandler, C. H., Chari, S., & Dworkin, I. (2013). Does your gene need a background check? How genetic background impacts the analysis of mutations, genes, and evolution. *Trends in Genetics*, *29*(6), 358–366. https://doi.org/10.1016/j.tig.2013.01.009

Chandler, C. H., Chari, S., Kowalski, A., Choi, L., Tack, D., DeNieu, M., Pitchers, W., Sonnenschein, A., Marvin, L., Hummel, K., Marier, C., Victory, A., Porter, C., Mammel, A., Holms, J., Sivaratnam, G., & Dworkin, I. (2017). How well do you know your mutation? Complex effects of genetic background on expressivity, complementation, and ordering of allelic effects. *PLoS Genetics*, *13*(11), 1–25. https://doi.org/10.1371/journal.pgen.1007075

Chandler, C. H., Chari, S., Tack, D., & Dworkin, I. (2014). Causes and consequences of genetic background effects illuminated by integrative genomic analysis. *Genetics*, *196*(4), 1321–1336. https://doi.org/10.1534/genetics.113.159426

Chanut-Delalande, H., Fernandes, I., Roch, F., Payre, F., & Plaza, S. (2006). Shavenbaby couples patterning to epidermal cell shape control. *PLoS Biology*, *4*(9), 1549–1561. https://doi.org/10.1371/journal.pbio.0040290

Chen, R., Shi, L., Hakenberg, J., Naughton, B., Sklar, P., Zhang, J., Zhou, H., Tian, L., Prakash, O., Lemire, M., Sleiman, P., Cheng, W. Y., Chen, W., Shah, H., Shen, Y., Fromer, M., Omberg, L., Deardorff, M. A., Zackai, E., … Friend, S. H. (2016). Analysis of 589,306 genomes identifies individuals resilient to severe Mendelian childhood diseases. *Nature Biotechnology*, *34*(5), 531–538. https://doi.org/10.1038/nbt.3514

Cooper, D. N., Krawczak, M., Polychronakos, C., Tyler-Smith, C., & Kehrer-Sawatzki, H. (2013). Where genotype is not predictive of phenotype: Towards an understanding of the molecular basis of reduced penetrance in human inherited disease. In *Human Genetics* (Vol. 132, Issue 10). https://doi.org/10.1007/s00439-013-1331-2

Crews, D., & Gore, A. C. (2014). Transgenerational Epigenetics. In *Transgenerational Epigenetics*. https://doi.org/10.1016/b978-0-12-405944-3.00026-x

Crickmore, M. A., Ranade, V., & Mann, R. S. (2009). Regulation of Ubx expression by

epigenetic enhancer silencing in response to Ubx levels and genetic variation. *PLoS Genetics*, *5*(9). https://doi.org/10.1371/journal.pgen.1000633

Daley, C. (2019). *Examining The Predictability of Genetic Background Effects in The Drosophila wing*. McMaster University.

De Belle, J. S., & Heisenberg, M. (1996). Expression of Drosophila mushroom body mutations in alternative genetic backgrounds: A case study of the mushroom body miniature gene (mbm). *Proceedings of the National Academy of Sciences of the United States of America*, *93*(18), 9875–9880. https://doi.org/10.1073/pnas.93.18.9875

De Celis, J. F. (1999). The function of vestigial in Drosophila wing development: How are tissue-specific responses to signalling pathways specified? *BioEssays*, *21*(7), 542–545. https://doi.org/10.1002/(SICI)1521-1878(199907)21:7<542::AID-BIES2>3.0.CO;2-5

De Celis, J. F., Barrio, R., & Kafatos, F. C. (1996). A gene complex acting downstream of dpp in Drosophila wing morphogenesis. *Nature*, *381*(6581), 421–424. https://doi.org/10.1038/381421a0

De Celis, J. F., Garcia-Bellido, A., & Bray, S. J. (1996). Activation and function of Notch at the dorsal-ventral boundary of the wing imaginai disc. *Development*, *122*(1), 359–369. https://doi.org/10.1242/dev.122.1.359

De La Cova, C., Abril, M., Bellosta, P., Gallant, P., & Johnston, L. A. (2004). Drosophila myc regulates organ size by inducing cell competition. *Cell*, *117*(1), 107–116. https://doi.org/10.1016/S0092-8674(04)00214-4

Delanoue, R., Legent, K., Godefroy, N., Flagiello, D., Dutriaux, A., Vaudin, P., Becker, J. L., & Silber, J. (2004). The Drosophila wing differentiation factor vestigial-scalloped is required for cell proliferation and cell survival at the dorso-ventral boundary of the wing imaginal disc. *Cell Death and Differentiation*, *11*(1), 110–122. https://doi.org/10.1038/sj.cdd.4401321

Dobzhansky, T. (1929). The influence of the quantity and quality of chromosomal material on the size of the cells in drosophila melanogaster. *Wilhelm Roux' Archiv Für Entwicklungsmechanik Der Organismen*, *115*(3), 363–379. https://doi.org/10.1007/BF02078996

Domingo, J., Baeza-Centurion, P., & Lehner, B. (2019). The Causes and Consequences of Genetic Interactions (Epistasis). *Annual Review of Genomics and Human Genetics*, *20*, 433–460. https://doi.org/10.1146/annurev-genom-083118-014857

Dorman, A., Baer, D., Tomlinson, I., Mott, R., & Iraqi, F. A. (2016). Genetic analysis of intestinal polyp development in Collaborative Cross mice carrying the Apc Min/+ mutation. *BMC Genetics*, *17*(1), 1–11. https://doi.org/10.1186/s12863-016-0349-6

Dowell, R. D., Ryan, O., Jansen, A., Cheung, D., Agarwala, S., Danford, T., Bernstein, D. A., Alexander Rolfe, P., Heisler, L. E., Chin, B., Nislow, C., Giaever, G., Phillips, P. C., Fink, G. R., Gifford, D. K., & Boone, C. (2010). Genotype to phenotype: A Complex problem. *Science*, *328*(5977), 469. https://doi.org/10.1126/science.1189015

Duronio, R. J., O'Farrell, P. H., Xie, J. E., Brook, A., & Dyson, N. (1995). The transcription

factor E2F is required for S phase during Drosophila embryogenesis. *Genes and Development*, *9*(12), 1445–1455. https://doi.org/10.1101/gad.9.12.1445

Dworkin, I. (2005a). A study of canalization and developmental stability in the sternopleural bristle system of Drosophila melanogaster. *Evolution*, *59*(7), 1500–1509. https://doi.org/10.1111/j.0014-3820.2005.tb01799.x

Dworkin, I. (2005b). Canalization, cryptic variation, and developmental buffering: A critical examination and analytical perspective. In B. & H. K. B. Hallgrímsson (Ed.), *Variation* (pp. 131–158). Academic Press. https://doi.org/10.1016/B978-012088777-4/50010-7

Dworkin, I., & Gibson, G. (2006). Epidermal growth factor receptor and transforming growth factor-β signaling contributes to variation for wing shape in Drosophila melanogaster. *Genetics*, *173*(3), 1417–1431. https://doi.org/10.1534/genetics.105.053868

Dworkin, I., Kennerly, E., Tack, D., Hutchinson, J., Brown, J., Mahaffey, J., & Gibson, G. (2009). Genomic consequences of background effects on scalloped mutant expressivity in the wing of drosophila melamogaster. *Genetics*, *181*(3), 1065–1076. https://doi.org/10.1534/genetics.108.096453

Félix, M. A., & Wagner, A. (2008). Robustness and evolution: Concepts, insights and challenges from a developmental model system. *Heredity*, *100*(2), 132–140. https://doi.org/10.1038/sj.hdy.6800915

Félix, Marie Anne, & Barkoulas, M. (2015). Pervasive robustness in biological systems. *Nature Reviews Genetics*, *16*(8), 483–496. https://doi.org/10.1038/nrg3949

Fernandes, I., Chanut-Delalande, H., Ferrer, P., Latapie, Y., Waltzer, L., Affolter, M., Payre, F., & Plaza, S. (2010). Zona Pellucida Domain Proteins Remodel the Apical Compartment for Localized Cell Shape Changes. *Developmental Cell*, *18*(1), 64–76. https://doi.org/10.1016/j.devcel.2009.11.009

Frankel, N., Davis, G. K., Vargas, D., Wang, S., Payre, F., & Stern, D. L. (2010). Phenotypic robustness conferred by apparently redundant transcriptional enhancers. *Nature*, *466*(7305), 490–493. https://doi.org/10.1038/nature09158

Fristrom, D. (1988). The cellular basis of epithelial morphogenesis. A Review. *Tissue and Cell*, *20*(5), 645–690. https://doi.org/10.1016/0160-9327(94)90114-7

Fromer, M., Pocklington, A. J., Kavanagh, D. H., Williams, H. J., Dwyer, S., Gormley, P., Georgieva, L., Rees, E., Palta, P., Ruderfer, D. M., Carrera, N., Humphreys, I., Johnson, J. S., Roussos, P., Barker, D. D., Banks, E., Milanova, V., Grant, S. G., Hannon, E., … O'Donovan, M. C. (2014). De novo mutations in schizophrenia implicate synaptic networks. *Nature*, *506*(7487), 179–184. https://doi.org/10.1038/nature12929

García-Bellido, A., Ripoll, P., & Morata, G. (1973). Developmental Compartmentalisation of the Wing Disk of Drosophila. *Nat. Phys. Sci.*, *245*, 251–253.

Gibson, G., & Van Helden, S. (1997). Is function of the Drosophila homeotic gene Ultrabithorax canalized? *Genetics*, *147*(3), 1155–1168. https://doi.org/10.1093/genetics/147.3.1155

Gilchrist, M. A., & Nijhout, H. F. (2001). Nonlinear developmental processes as sources of

dominance. *Genetics*, *159*(1), 423–432. https://doi.org/10.1093/genetics/159.1.423

Green, R. M., Fish, J. L., Young, N. M., Smith, F. J., Roberts, B., Dolan, K., Choi, I., Leach, C. L., Gordon, P., Cheverud, J. M., Roseman, C. C., Williams, T. J., Marcucio, R. S., & Hallgrímsson, B. (2017). Developmental nonlinearity drives phenotypic robustness. *Nature Communications*, *8*(1). https://doi.org/10.1038/s41467-017-02037-7

Haber, A. (2011). A Comparative Analysis of Integration Indices. *Evolutionary Biology*, *38*(4), 476–488. https://doi.org/10.1007/s11692-011-9137-4

Haber, A., & Dworkin, I. (2017). Disintegrating the fly: A mutational perspective on phenotypic integration and covariation. *Evolution*, *71*(1), 66–80. https://doi.org/10.1111/evo.13100

Hadfield, J. D. (2010). MCMC methods for multi-response generalized linear mixed models: The MCMCglmm R package. *Journal of Statistical Software*, *33*(2), 1–22. https://doi.org/10.18637/jss.v033.i02

Halder, G., Polaczyk, P., Kraus, M. E., Hudson, A., Kim, J., Laughon, A., & Carroll, S. (1998). The Vestigial and Scalloped proteins act together to directly regulate wing-specific gene expression in Drosophila. *Genes and Development*, *12*(24), 3900–3909. https://doi.org/10.1101/gad.12.24.3900

Halpern, M. E., Rhee, J., Goll, M. G., Akitake, C. M., Parsons, M., & Leach, S. D. (2008). Gal4/UAS Transgenic Tools and Their Application to Zebrafish. *Zebrafish*, *5*(2), 97–110. https://doi.org/10.1089/zeb.2008.0530

Hong, J. W., Hendrix, D. A., & Levine, M. S. (2008). Shadow enhancers as a source of evolutionary novelty. *Science*, *321*(5894), 1314. https://doi.org/10.1126/science.1160631

Houle, D., Govindaraju, D. R., & Omholt, S. (2010). Phenomics: The next challenge. *Nature Reviews Genetics*, *11*(12), 855–866. https://doi.org/10.1038/nrg2897

Houlston, R. S., & Tomlinson, I. P. M. (1998). Modifier genes in humans: Strategies for identification. *European Journal of Human Genetics*, *6*(1), 80–88. https://doi.org/10.1038/sj.ejhg.5200156

Huang, J., Wu, S., Barrera, J., Matthews, K., & Pan, D. (2005). The Hippo signaling pathway coordinately regulates cell proliferation and apoptosis by inactivating Yorkie, the Drosophila homolog of YAP. *Cell*, *122*(3), 421–434. https://doi.org/10.1016/j.cell.2005.06.007

Jack, J., Dorsett, D., Delotto, Y., & Liu, S. (1991). Expression of the cut locus in the Drosophila wing margin is required for cell type specification and is regulated by a distant enhancer. *Development*, *113*(3), 735–747. https://doi.org/10.1242/dev.113.3.735

Jin, S. C., Homsy, J., Zaidi, S., Lu, Q., Morton, S., DePalma, S. R., Zeng, X., Qi, H., Chang, W., Sierant, M. C., Hung, W.-C., Haider, S., Zhang, J., Knight, J., Bjornson, R. D., Castaldi, C., Tikhonoa, I. R., Bilguvar, K., Mane, S. M., … Brueckner, M. (2017). Contribution of rare inherited and de novo variants in 2,871 congenital heart disease probands. *Nature Genetics*, *49*(11), 1593–1601. https://doi.org/10.1038/ng.3970

Jovine, L., Darie, C. C., Litscher, E. S., & Wassarman, P. M. (2005). Zona pellucida domain

proteins. *Annual Review of Biochemistry*, *74*, 83–114. https://doi.org/10.1146/annurev.biochem.74.082803.133039

Kacser, H., & Burns, J. a. (1981). The Molecular Basis of Dominance. *Genetics*, *97*(3–4), 639–666.

Kammenga, J. E. (2017). The background puzzle: how identical mutations in the same gene lead to different disease symptoms. *FEBS Journal*, *284*(20), 3362–3373. https://doi.org/10.1111/febs.14080

Kandasamy, S., Couto, K., & Thackeray, J. (2021). A docked mutation phenocopies dumpy oblique alleles via altered vesicle trafficking. *PeerJ*, *9*, 1–21. https://doi.org/10.7717/peerj.12175

Kiger, J. A., Natzle, J. E., Kimbrell, D. A., Paddy, M. R., Kleinhesselink, K., & Green, M. M. (2007). Tissue remodeling during maturation of the Drosophila wing. *Developmental Biology*, *301*(1), 178–191. https://doi.org/10.1016/j.ydbio.2006.08.011

Kim, J., Sebring, A., Esch, J. J., Kraus, M. E., Vorwerk, K., Magee, J., & Carroll, S. B. (1996). Integration of positional signals and regulation of wing formation and identity by Drosophila vestigial gene. *Nature*, *382*(6587), 133–138. https://doi.org/10.1038/382133a0

Kimura, K. I., Kodama, A., Hayasaka, Y., & Ohta, T. (2004). Activation of the cAMP/PKA signaling pathway is required for postecdysial cell death in wing epidermal cells of Drosophila melanogaster. *Development*, *131*(7), 1597–1606. https://doi.org/10.1242/dev.01049

Klein, T., & Arias, A. M. (1999). The Vestigial gene product provides a molecular context for the interpretation of signals during the development of the wing in Drosophila. *Development*, *126*(5), 913–925. https://doi.org/10.1242/dev.126.5.913

Kozera, B., & Rapacz, M. (2013). Reference genes in real-time PCR. *Journal of Applied Genetics*, *54*(4), 391–406. https://doi.org/10.1007/s13353-013-0173-x

Lachowiec, J., Queitsch, C., & Kliebenstein, D. J. (2016). Molecular mechanisms governing differential robustness of development and environmental responses in plants. *Annals of Botany*, *117*(5), 795–809. https://doi.org/10.1093/aob/mcv151

Lewontin, R. C. (1974). *The genetic basis of evolutionary change*. Columbia University Press.

Liu, H., Zhang, J. J., Wang, S. J., Zhang, X. E., & Zhou, N. Y. (2005). Plasmid-borne catabolism of methyl parathion and p-nitrophenol in Pseudomonas sp. strain WBC-3. *Biochemical and Biophysical Research Communications*, *334*(4), 1107–1114. https://doi.org/10.1016/j.bbrc.2005.07.006

Livak, K. J., & Schmittgen, T. D. (2001). Analysis of relative gene expression data using real-time quantitative PCR and the 2-ΔΔCT method. *Methods*, *25*(4), 402–408. https://doi.org/10.1006/meth.2001.1262

Mandaravally Madhavan, M., & Schneiderman, H. A. (1977). Histological analysis of the dynamics of growth of imaginal discs and histoblast nests during the larval development of Drosophila melanogaster. *Wilhelm Roux's Archives of Developmental Biology*, *183*(4), 269–

305. https://doi.org/10.1007/BF00848459

Martin, F. A., Herrera, S. C., & Morata, G. (2009). Cell competition, growth and size control in the Drosophila wing imaginal disc. *Development*, *136*(22), 3747–3756. https://doi.org/10.1242/dev.038406

Masel, J., & Siegal, M. L. (2009). Robustness: mechanisms and consequences. *Trends in Genetics*, *25*(9), 395–403. https://doi.org/10.1016/j.tig.2009.07.005

Matamoro-Vidal, A., Salazar-Ciudad, I., & Houle, D. (2015). Making quantitative morphological variation from basic developmental processes: Where are we? The case of the Drosophila wing. *Developmental Dynamics*, *244*(9), 1058–1073. https://doi.org/10.1002/dvdy.24255

Matta, B. P., Bitner-Mathé, B. C., & Alves-Ferreira, M. (2011). Getting real with real-time qPCR: A case study of reference gene selection for morphological variation in Drosophila melanogaster wings. *Development Genes and Evolution*, *221*(1), 49–57. https://doi.org/10.1007/s00427-011-0356-6

Melo, D., Garcia, G., Hubbe, A., Assis, A. P., & Marroig, G. (2016). EvolQG - An R package for evolutionary quantitative genetics. *F1000Research*, *4*, 1–27. https://doi.org/10.12688/F1000RESEARCH.7082.2

Milloz, J., Duveau, F., Nuez, I., & Félix, M. A. (2008). Intraspecific evolution of the intercellular signaling network underlying a robust developmental system. *Genes and Development*, *22*(21), 3064–3075. https://doi.org/10.1101/gad.495308

Montagne, J., Groppe, J., Guillemin, K., Krasnow, M. A., Gehring, W. J., & Affolter, M. (1996). The Drosophila Serum Response Factor gene is required for the formation of intervein tissue of the wing and is allelic to blistered. *Development*, *122*(9), 2589–2597. https://doi.org/10.1242/dev.122.9.2589

Montagutelli, X. (2000). Effect of the genetic background on the phenotype of mouse mutations. *Journal of the American Society of Nephrology*, *11*(SUPPL. 16), 101–105.

Morata, G., & Ripoll, P. (1975). Minutes: Mutants of Drosophila autonomously affecting cell division rate. *Developmental Biology*, *42*(2), 211–221. https://doi.org/10.1016/0012-1606(75)90330-9

Moreno, E., & Basler, K. (2004). dMyc transforms cells into super-competitors. *Cell*, *117*(1), 117–129. https://doi.org/10.1016/S0092-8674(04)00262-4

Mullis, M. N., Matsui, T., Schell, R., Foree, R., & Ehrenreich, I. M. (2018). The complex underpinnings of genetic background effects. *Nature Communications*, *9*(1), 1–10. https://doi.org/10.1038/s41467-018-06023-5

Nadeau, J. H. (2001). Modifier genes in mice and humans. *Nature Reviews Genetics*, *2*(3), 165–174. https://doi.org/10.1038/35056009

Neto-Silva, R. M., Wells, B. S., & Johnston, L. A. (2009). Mechanisms of growth and homeostasis in the Drosophila wing. *Annual Review of Cell and Developmental Biology*, *25*, 197–220. https://doi.org/10.1146/annurev.cellbio.24.110707.175242

Neufeld, T. P., De La Cruz, A. F. A., Johnston, L. A., & Edgar, B. A. (1998). Coordination of growth and cell division in the Drosophila wing. *Cell*, *93*(7), 1183–1193. https://doi.org/10.1016/S0092-8674(00)81462-2

Neumann, C. J., & Cohen, S. M. (1997). Long-range action of Wingless organizes the dorsal-ventral axis of the Drosophila wing. *Development*, *124*(4), 871–880. https://doi.org/10.1242/dev.124.4.871

Newby, L. M., White, L., DiBartolomeis, S. M., Walker, B. J., Dowse, H. B., Ringo, J. M., Khuda, N., & Jackson, F. R. (1991). Mutational analysis of the Drosophila miniature-dusky (m-dy) locus: effects on cell size and circadian rhythms. *Genetics*, *128*(3), 571–582. https://doi.org/10.1530/acta.0.0840485

Noben-Trauth, K., Zheng, Q. Y., Johnson, K. R., & Nishina, P. M. (1997). mdfw: A deafness susceptibility locus that interacts with deaf waddler (dfw). *Genomics*, *44*(3), 266–272. https://doi.org/10.1006/geno.1997.4869

O'Neill, J. S. (2009). Circadian clocks can take a few transcriptional knocks. *EMBO Journal*, *28*(2), 84–85. https://doi.org/10.1038/emboj.2008.272

Orgogozo, V., Morizot, B., & Martin, A. (2015). The differential view of genotype-phenotype relationships. *Frontiers in Genetics*, *6*(MAY), 1–14. https://doi.org/10.3389/fgene.2015.00179

Osterwalder, M., Barozzi, I., Tissiéres, V., Fukuda-Yuzawa, Y., Mannion, B. J., Afzal, S. Y., Lee, E. A., Zhu, Y., Plajzer-Frick, I., Pickle, C. S., Kato, M., Garvin, T. H., Pham, Q. T., Harrington, A. N., Akiyama, J. A., Afzal, V., Lopez-Rios, J., Dickel, D. E., Visel, A., & Pennacchio, L. A. (2018). Enhancer redundancy provides phenotypic robustness in mammalian development. *Nature*, *554*(7691), 239–243. https://doi.org/10.1038/nature25461

Osterwalder, M., Speziale, D., Shoukry, M., Mohan, R., Ivanek, R., Kohler, M., Beisel, C., Wen, X., Scales, S. J., Christoffels, V. M., Visel, A., Lopez-Rios, J., & Zeller, R. (2014). HAND2 targets define a network of transcriptional regulators that compartmentalize the early limb bud mesenchyme. *Developmental Cell*, *31*(3), 345–357. https://doi.org/10.1016/j.devcel.2014.09.018

Parker, J., & Struhl, G. (2020). Control of drosophila wing size by morphogen range and hormonal gating. *Proceedings of the National Academy of Sciences of the United States of America*, *117*(50), 31935–31944. https://doi.org/10.1073/pnas.2018196117

Paumard-Rigal, S., Zider, A., Vaudin, P., & Silber, J. (1998). Specific interactions between vestigial and scalloped are required to promote wing tissue proliferation in Drosophila melanogaster. *Development Genes and Evolution*, *208*(8), 440–446. https://doi.org/10.1007/s004270050201

Payre, F., Vincent, A., & Carreno, S. (1999). ovo/svb Integrates Wingless and DER pathways to control epidermis differentiation. *Nature*, *400*(6741), 271–275. https://doi.org/10.1038/22330

Pennacchio, L. A., Ahituv, N., Moses, A. M., Prabhakar, S., Nobrega, M. A., Shoukry, M.,

Minovitsky, S., Dubchak, I., Holt, A., Lewis, K. D., Plajzer-Frick, I., Akiyama, J., De Val, S., Afzal, V., Black, B. L., Couronne, O., Eisen, M. B., Visel, A., & Rubin, E. M. (2006). In vivo enhancer analysis of human conserved non-coding sequences. *Nature*, *444*(7118), 499–502. https://doi.org/10.1038/nature05295

Percival, C. J., Marangoni, P., Tapaltsyan, V., Klein, O., & Hallgrímsson, B. (2017). The interaction of genetic background and mutational effects in regulation of mouse craniofacial shape. *G3: Genes, Genomes, Genetics*, *7*(5), 1439–1450. https://doi.org/10.1534/g3.117.040659

Pesevski, M., & Dworkin, I. (2020). Genetic and environmental canalization are not associated among altitudinally varying populations of Drosophila melanogaster. *Evolution*, *74*(8), 1755–1771. https://doi.org/10.1111/evo.14039

Pettersson, M., Besnier, F., & Siegel, P. B. (2011). *Replication and Explorations of High-Order Epistasis Using a Large Advanced Intercross Line Pedigree*. *7*(7). https://doi.org/10.1371/journal.pgen.1002180

Pigliucci, M. (2003). Phenotypic integration: Studying the ecology and evolution of complex phenotypes. *Ecology Letters*, *6*(3), 265–272. https://doi.org/10.1046/j.1461-0248.2003.00428.x

Polaczyk, P. J., Gasperini, R., & Gibson, G. (1998). Naturally occurring genetic variation affects Drosophila photoreceptor determination. *Development Genes and Evolution*, *207*(7), 462–470. https://doi.org/10.1007/s004270050137

Raj, A., Rifkin, S. A., Andersen, E., & Van Oudenaarden, A. (2010). Variability in gene expression underlies incomplete penetrance. *Nature*, *463*(7283), 913–918. https://doi.org/10.1038/nature08781

Raj, A., van den Bogaard, P., Rifkin, S. A., van Oudenaarden, A., & Tyagi, S. (2008). Imaging individual mRNA molecules using multiple singly labeled probes. *Nature Methods*, *5*(10), 877–879. https://doi.org/10.1038/nmeth.1253

Rau, C. D., Gonzales, N. M., Bloom, J. S., Park, D., Ayroles, J., Palmer, A. A., Lusis, A. J., & Zaitlen, N. (2020). Modeling epistasis in mice and yeast using the proportion of two or more distinct genetic backgrounds: Evidence for "polygenic epistasis." *PLoS Genetics*, *16*(10), 1–18. https://doi.org/10.1371/journal.pgen.1009165

Ray, R. P., Matamoro-Vidal, A., Ribeiro, P. S., Tapon, N., Houle, D., Salazar-Ciudad, I., & Thompson, B. J. (2015). Patterned Anchorage to the Apical Extracellular Matrix Defines Tissue Shape in the Developing Appendages of Drosophila. *Developmental Cell*, *34*(3), 310–322. https://doi.org/10.1016/j.devcel.2015.06.019

Roch, F., Alonso, C. R., & Akam, M. (2003). Drosophila miniature and dusky encode ZP proteins required for cytoskeletal reorganisation during wing morphogenesis. *Journal of Cell Science*, *116*(7), 1199–1207. https://doi.org/10.1242/jcs.00298

Rosin, J. M., Abassah-Oppong, S., & Cobb, J. (2013). Comparative transgenic analysis of enhancers from the human SHOX and mouse Shox2 genomic regions. *Human Molecular Genetics*, *22*(15), 3063–3076. https://doi.org/10.1093/hmg/ddt163

Rzezniczak, T. Z., Rzezniczak, M. T., Reed, B. H., Dworkin, I., & Merritt, T. J. S. (2022). Regulation at Drosophila 's Malic Enzyme highlights the complexity of transvection and its sensitivity to genetic background. *Genetics*, 37. https://doi.org/10.1093/genetics/iyac181

Sanders, S. J., Murtha, M. T., Gupta, A. R., Murdoch, J. D., Raubeson, M. J., Willsey, a J., Ercan-Sencicek, A. G., DiLullo, N. M., Parikshak, N. N., Stein, J. L., Walker, M. F., Ober, G. T., Teran, N. A., Song, Y., El-Fishawy, P., Murtha, R. C., Choi, M., Overton, J. D., Bjornson, R. D., … State, M. W. (2012). De novo mutations revealed by whole-exome sequencing are strongly associated with autism. *Nature*, *485*(7397), 237–241. https://doi.org/10.1038/nature10945

Schell, R., Mullis, M., & Ehrenreich, I. M. (2016). Modifiers of the Genotype–Phenotype Map: Hsp90 and Beyond. *PLoS Biology*, *14*(11), 1–8. https://doi.org/10.1371/journal.pbio.2001015

Schultz, B. B. (1985). Levene's Test for Relative Variation. *Systematic Zoology*, *34*(4), 449. https://doi.org/10.2307/2413207

Sebastiano, M., Lassandro, F., & Bazzicalupo, P. (1991). cut-1 a Caenorhabditis elegans gene coding for a dauer-specific noncollagenous component of the cuticle. *Developmental Biology*, *146*(2), 519–530. https://doi.org/10.1016/0012-1606(91)90253-Y

Siegal, M. L., & Leu, J. Y. (2014). On the nature and evolutionary impact of phenotypic robustness mechanisms. *Annual Review of Ecology, Evolution, and Systematics*, *45*, 495–517. https://doi.org/10.1146/annurev-ecolsys-120213-091705

Simmonds, A. J., Liu, X., Soanes, K. H., Krause, H. M., Irvine, K. D., & Bell, J. B. (1998). Molecular interactions between Vestigial and Scalloped promote wing formation in Drosophila. *Genes and Development*, *12*(24), 3815–3820. https://doi.org/10.1101/gad.12.24.3815

Sobala, L. F., & Adler, P. N. (2016). The Gene Expression Program for the Formation of Wing Cuticle in Drosophila. *PLoS Genetics*, *12*(5), 1–29. https://doi.org/10.1371/journal.pgen.1006100

Srivastava, A., Simmonds, A. J., Garg, A., Fossheim, L., Campbell, S. D., & Bell, J. B. (2004). Molecular and Functional Analysis of scalloped Recessive Lethal Alleles in Drosophila melanogaster. *Genetics*, *166*(April), 1833–1843.

Street, V. A., Robinson, L. C., Erford, S. K., & Tempel, B. L. (1995). Molecular genetic analysis of distal mouse chromosome 6 defines gene order and positions of the deafwaddler and opisthotonos mutations. *Genomics*, *29*(1), 123–130. https://doi.org/10.1006/geno.1995.1222

Sun, L., Dong, Y., Zhou, Y., Yang, M., Zhang, C., Rao, Z., & Zhang, X. E. (2004). Crystallization and preliminary X-ray studies of methyl parathion hydrolase from Pseudomonas sp. WBC-3. *Acta Crystallographica Section D: Biological Crystallography*, *60*(5), 954–956. https://doi.org/10.1107/S0907444904005669

Testa, N. D., & Dworkin, I. (2016). The sex-limited effects of mutations in the EGFR and TGF-β signaling pathways on shape and size sexual dimorphism and allometry in the Drosophila wing. *Development Genes and Evolution*, *226*(3), 159–171. https://doi.org/10.1007/s00427-

016-0534-7

Thompson, B. J., & Cohen, S. M. (2006). The Hippo Pathway Regulates the bantam microRNA to Control Cell Proliferation and Apoptosis in Drosophila. *Cell*, *126*(4), 767–774. https://doi.org/10.1016/j.cell.2006.07.013

van Neerven, S. M., & Vermeulen, L. (2022). Cell competition in development, homeostasis and cancer. *Nature Reviews Molecular Cell Biology*, *0123456789*. https://doi.org/10.1038/s41580-022-00538-y

Visel, A., Minovitsky, S., Dubchak, I., & Pennacchio, L. A. (2007). VISTA Enhancer Browser - A database of tissue-specific human enhancers. *Nucleic Acids Research*, *35*(SUPPL. 1), 88–92. https://doi.org/10.1093/nar/gkl822

Vu, V., Verster, A. J., Schertzberg, M., Chuluunbaatar, T., Spensley, M., Pajkic, D., Hart, G. T., Moffat, J., & Fraser, A. G. (2015). Natural Variation in Gene Expression Modulates the Severity of Mutant Phenotypes. *Cell*, *162*(2), 391–402. https://doi.org/10.1016/j.cell.2015.06.037

Waddington, C. H. (1942). Canalization of Development and the Inheritance of Aquired Characters. *Nature Publishing Group*, *150*, 563–565.

Waddington, C. H. (1952). Selection of the Genetic Basis for an Aquired Character. *Nature*, *169*, 278.

Williams, J. A., Paddock, S. W., & Carroll, S. B. (1993). Pattern formation in a secondary field: A hierarchy of regulatory genes subdivides the developing Drosophila wing disc into discrete subregions. *Development*, *117*(2), 571–584. https://doi.org/10.1242/dev.117.2.571

Williams, Jim A., Paddock, S. W., Vorwerk, K., & Carroll, S. B. (1994). Organization of wing formation and induction of a wing-patterning gene at the dorsal/ventral compartment boundary. *Nature*, *368*(6469), 299–305. https://doi.org/10.1038/368299a0

Williams, N. (1997). PHILOSOPHY OF SCIENCE: Biologists Cut Reductionist Approach Down to Size. *Science*, *277*(5325), 476–477. https://doi.org/10.1126/science.277.5325.476

Wright, S. (1934). Physiological and Evolutionary Theories of Dominance. *The American Naturalist*, *68*(714), 24–53. https://doi.org/10.1086/280521

Yang, G., Anderson, D. W., Baier, F., Dohmen, E., Hong, N., Carr, P. D., Kamerlin, S. C. L., Jackson, C. J., Bornberg-Bauer, E., & Tokuriki, N. (2019). Higher-order epistasis shapes the fitness landscape of a xenobiotic-degrading enzyme. *Nature Chemical Biology*, *15*(11), 1120–1128. https://doi.org/10.1038/s41589-019-0386-3

Yoshiki, A., & Moriwaki, K. (2006). Mouse phenome research: Implications of genetic background. *ILAR Journal*, *47*(2), 94–102. https://doi.org/10.1093/ilar.47.2.94

Zecca, M., Basler, K., & Struhl, G. (1996). Direct and long-range action of a wingless morphogen gradient. *Cell*, *87*(5), 833–844. https://doi.org/10.1016/S0092-8674(00)81991-1

Zecca, M., & Struhl, G. (2010). A feed-forward circuit linking wingless, Fat-Dachsous signaling, and the warts-hippo pathway to drosophila wing growth. *PLoS Biology*, *8*(6).

https://doi.org/10.1371/journal.pbio.1000386

Zhang, L., Ren, F., Zhang, Q., Chen, Y., Wang, B., & Jiang, J. (2008). The TEAD/TEF Family of Transcription Factor Scalloped Mediates Hippo Signaling in Organ Size Control. *Developmental Cell*, *14*(3), 377–387. https://doi.org/10.1016/j.devcel.2008.01.006

8. Appendix

Supplemental Table 8.1: List of drosophila genetics reference panel genotype numbers and their respective Bloomington stock numbers utilized in experiment 1.

DGRP Genotype	DGRP Bloomington stock number
DGRP028	28124
DGRP038	28125
DGRP048	55016
DGRP075	28132
DGRP083	28134
DGRP088	28135
DGRP229	29653
DGRP239	28161
DGRP301	25175
DGRP315	25181
DGRP319	55018
DGRP371	28183
DGRP385	28191
DGRP391	25191
DGRP392	28194
DGRP443	28199
DGRP491	28202
DGRP492	28203
DGRP517	25197
DGRP757	28226
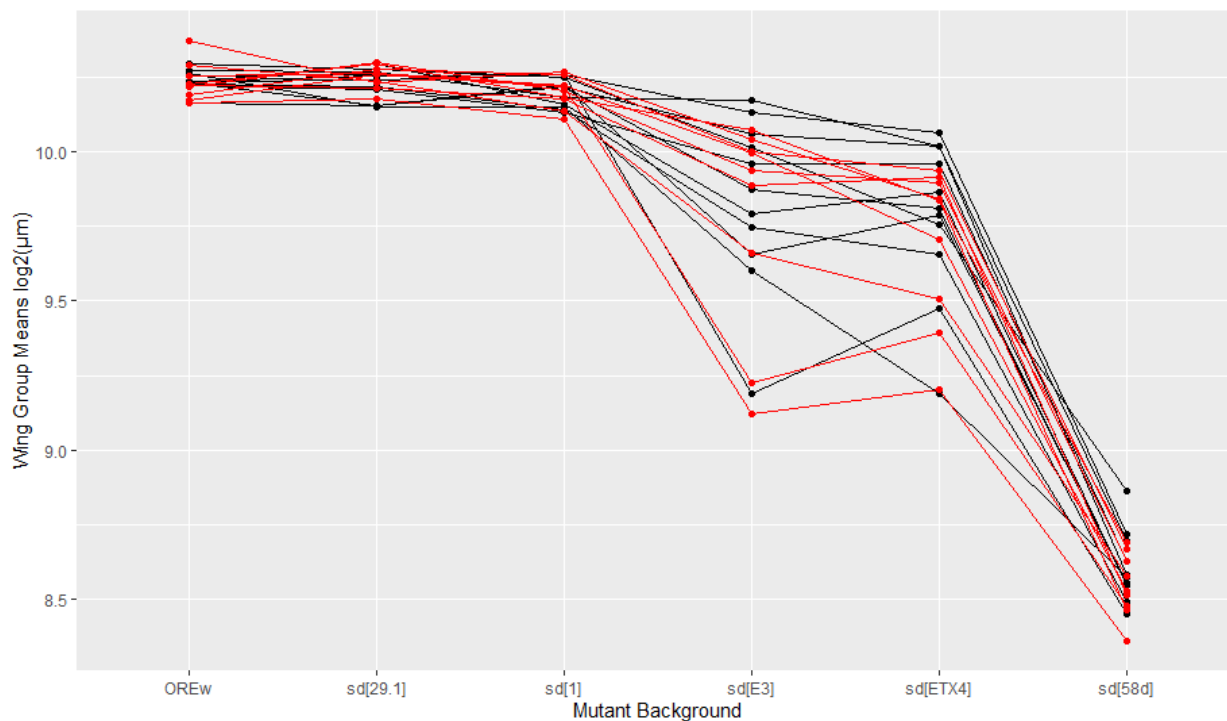
Supplementary Figure 8.1: A reaction norm of the mean plot displaying wing group means in log2(μm). Each line represents a distinct DGRP strain with each dot representing group averages in wing size. The originally proposed DGRP lines for experiment 2 are highlighted in red.

Supplemental Table 8.2: List of DGRP genotype numbers and their respective Bloomington stock numbers originally to be utilized in experiment 2. Lines that experienced hybrid dysgenesis are highlighted in red.

DGRP Genotype	DGRP Bloomington stock number
DGRP038	28125
DGRP075	28132
DGRP229	29653
DGRP239	28161
DGRP301	25175
DGRP385	28191
DGRP391	25191
DGRP517	25197
DGRP757	28226
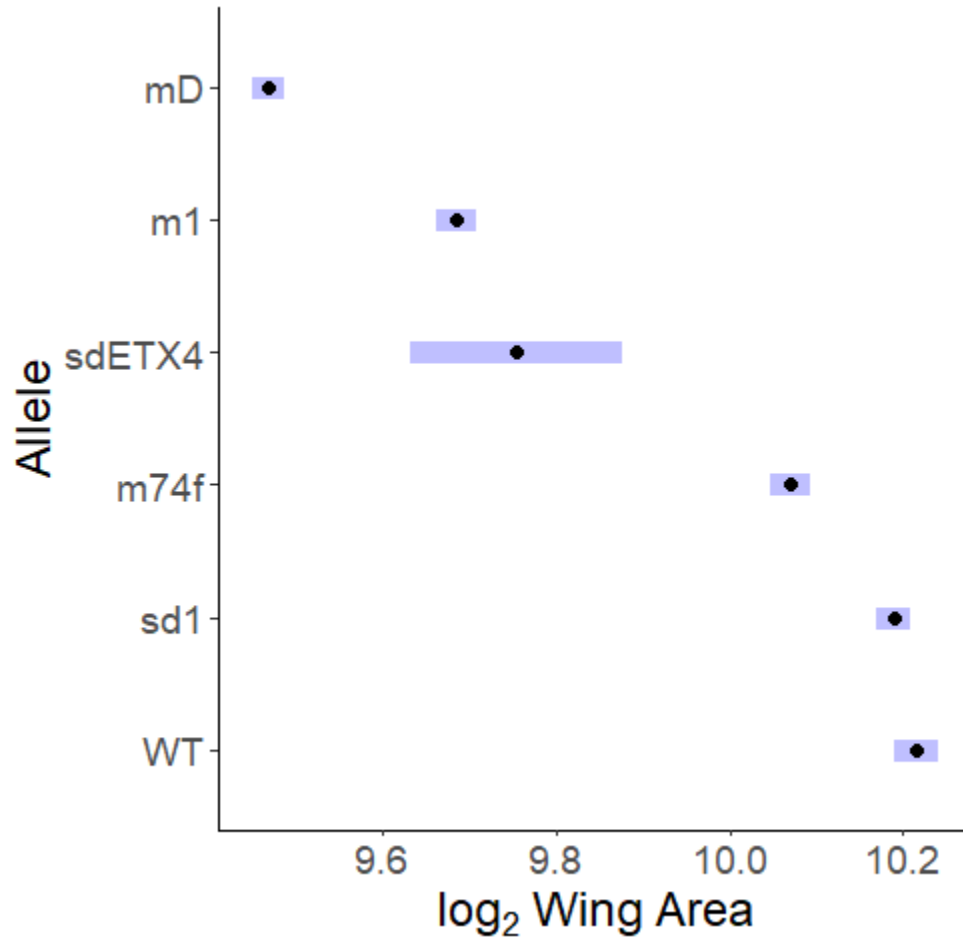
Supplementary Figure 8.2: Estimated marginal means of scalloped and miniature alleles log2 wing area. Each of these are grouped means across 19 distinct DGRP backgrounds from wild-type (WT) to *miniature*[D] regarding mutational severity on wing morphology. With the black dots representing means and blue bars representing 95% confidence intervals.
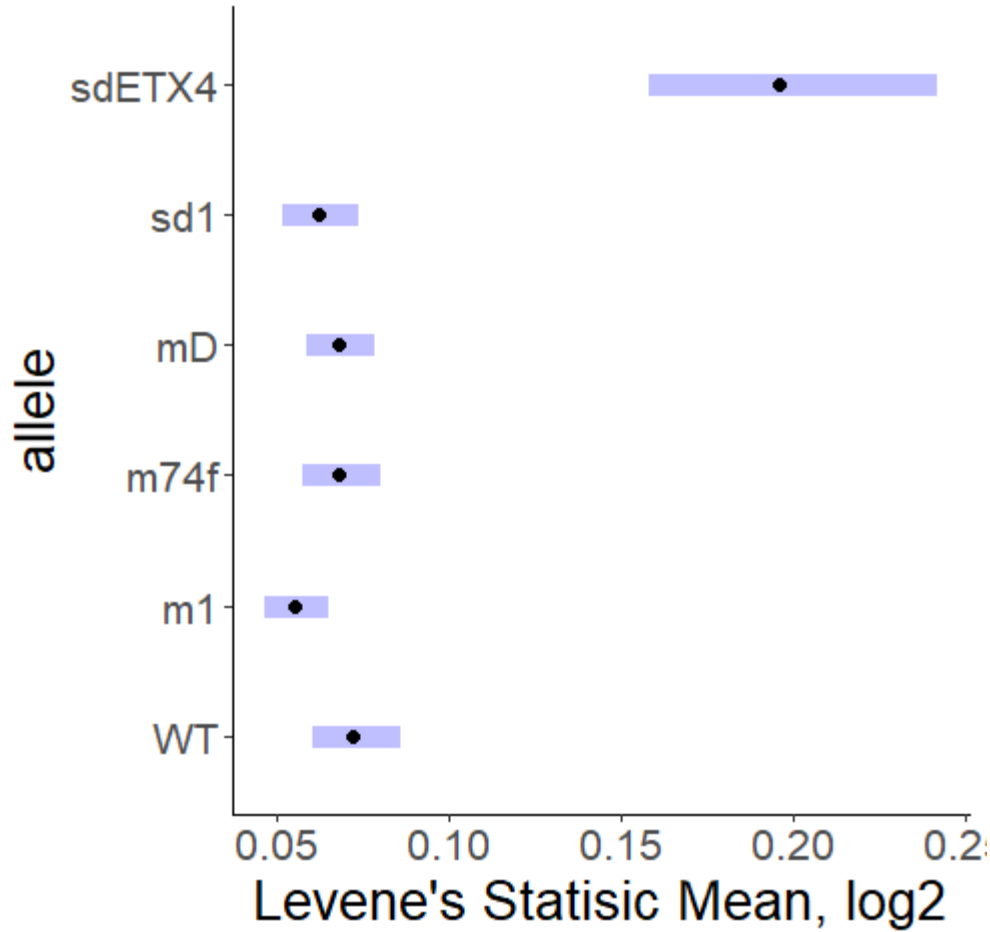
Supplementary Figure 8.3: Estimated marginal means of *scalloped* and *miniature alleles* log₂ Levene's Statistic. Each of these are grouped means across 19 distinct DGRP backgrounds from wild-type (WT) to *miniature^D* regarding mutational severity on wing morphology. With the black dots representing means and blue bars representing 95% confidence intervals.